Dissertation zur Erlangung des Doktorgrades
der Fakultät für Chemie und Pharmazie
der Ludwig–Maximilians–Universität München

Role of *S. pombe* nucleophosmins in ribosome biogenesis and the negative genetic interaction with RNAi

Ilaria Ugolini
aus
Bologna, Italien

2020

Erklärung

Diese Dissertation wurde im Sinne von §7 der Promotionsordnung vom 28. November 2011 von Herrn Dr. Mario Halic betreut.

Eidesstattliche Versicherung

Diese Dissertation wurde eigenständig und ohne unerlaubte Hilfe erarbeitet.

München, 28.09.2020

.....

Ilaria Ugolini

Dissertation eingereicht am 30.09.2020

1. Gutachterin / 1. Gutachter: Dr. Mario Halic

2. Gutachterin / 2. Gutachter: Prof. Dr. Klaus Förstermann

Mündlichen Prüfung am 25.11.2020

Contents

List of Figures

List of Tables

Summary

Eukaryotic ribosome biogenesis starts in the nucleolus, a membrane-less compartment assembled via liquid-liquid phase separation of its constituent molecules. It organizes around tandem rDNA repeats and is divided into functionally distinct compartments. As ribosome biogenesis proceeds, early intermediates move from central rDNA repeats towards outer nucleolar phases, where later maturation takes place. The earliest steps of ribosome biogenesis, which take place on chromatin, are not very well characterized. This work shows that yeast nucleophosmins, main constituents of the external nucleolar compartment, localize to rDNA repeats, mainly over the sites that encode for the large subunit RNAs, and interact specifically with nascent 60S subunits. In our model, nucleophosmin, initially associated with nucleosomes, binds emerging nascent 60S subunits and separates them from chromatin. Self-association of nucleophosmin via liquid-liquid phase separation organizes the nucleolar sub-compartment where later maturation occurs, and from which nascent 40S subunits are mainly excluded. In absence of nucleophosmin, nascent 60S subunits are retained on chromatin, with a consequent delay in the kinetic of ribosome assembly.

S. pombe nucleophosmin proteins may have other functions in addition to the previously mentioned role in ribosome biogenesis. Indeed Fkbp39 contributes to the silencing of centromeric and subtelomeric heterochromatic transcripts. Unexpectedly, while investigating the molecular basis of the negative genetic interaction between Fkbp39 and RNAi, we observed a transcription defect for *ago1* deletion cells, which still requires further investigation.

Overall this work highlights the role of chromatin in ribosome biogenesis and provides a connection between compartment organization via phase separation and the biological process hosted within the compartment itself. Moreover, it opens further line of investigation by presenting interesting observations about argonaute proteins role in transcription regulation.

Chapter 1

Introduction

1.1 The nucleoplasmin/nucleophosmin family of proteins

The nucleoplasmin/nucleophosmin (NPM) family of metazoan nuclear chaperones is composed by nucleophosmin (NPM1), nucleoplasmin (NPM2), NPM3, and invertebrate NPM proteins. This family is involved in several fundamental processes such as chromatin remodelling, DNA duplication and ribosome biogenesis [1]. Chaperones assist the folding of other proteins and their assembly into the correct oligomeric state, preventing the formation of inappropriate complexes and eventually disrupting the wrong interactions that may have occurred [2, 3]. Nuclear chaperones, in particular, assist the interaction between proteins and nucleic acids, preventing non-specific electrostatic interactions, which could lead to aggregation, facilitating the formation and maintenance of the chromatin structure and ribonucleoprotein complexes [4]. In these processes the substrates are normally highly charged, proteins tend to be small and basic to interact with nucleic acids, and both are prone to aggregation [5].

Characteristic of this family is the nucleophosmin fold: a pentamer, in which each monomer is an eight-stranded β barrel, followed by an intrinsically disordered domain, also called tail domain [6, 7, 8]. Three less conserved acidic tracts are interspersed in the domain: the first protrudes from the β barrel and the other two are within the disordered region. NPM1 has an additional C-terminal domain responsible for nucleic acids binding, the RRM domain [9]. NPM1 and NPM2 have both proved *in vitro* histone chaperone activity, whereas, even though it can bind histones, NPM3 seems to mainly regulate NPM1 activity [10, 8, 11, 12, 13, 14]. Histone chaperones participate in different aspects of nucleosome assembly, from histone nuclear import and storage to their deposition onto or eviction from DNA and even transfer to modifying enzymes

[15]. NPM2 is expressed only in the oocyte nucleus, where it promotes nucleosomes assembly and paternal chromatin decondensation. On the contrary, NPM1 and NPM3 have mainly a nucleolar localization and are found in many different cell types.

NPM1 is a multifunctional protein involved in ribosome biogenesis, chromatin remodeling, apoptosis and genome stability maintenance [16]. Phosphorylation regulates the monomer-pentamer equilibrium and the nucleolar localization, promoting pentamer disassemble into unfolded monomers involved in the DNA damage and apoptosis response [17]. In general, NPM1 down-regulation sensitizes cells to apoptosis, whereas overexpression has the opposite effect. NPM1 associates with unduplicated centrosomes, as a consequence, loss of function mutations cause genome instability. Moreover, NPM1 is directly involved in DNA repair, with a reported role in homologous recombination, in the translesion synthesis pathway and nucleotide excision repair [16]. However, NPM1 is a key regulator of the nucleolus structure via liquid-liquid phase separation (LLPS, discussed later) and is necessary for the structural integrity of both nucleolus and nucleus [18]. NPM1 localizes to the ribosomal DNA (rDNA) chromatin and associates with nascent 60S subunits [19, 20, 21]. It is reported to function in ribosomal RNA (rRNA) processing and ribosome export [22, 23, 24, 25]. Due to its role in such fundamental processes, it is not surprising that NPM1 mutations, also due to chromosome translocation events, are associated with cancer development, especially with hematopoietic malignancies [16].

The nucleophosmin fold is present also in non-metazoan proteins (nucleophosmin like domain, NPL). In these proteins, the NPL domain is generally combined with other functions [26]. NPL-FKBP proteins, present in plants, arthropods and yeasts, are members of one of these families characterized by the N-terminal NPL domain and a C-terminal prolyl isomerase domain (FKBP). Despite the weak sequence similarity with nucleoplasmin, these proteins maintain the characteristic pentameric fold of the family [26].

1.2 NPL-FKBP proteins

The peptide bond connecting prolines to the preceding amino acid is peculiar, being the only one with a relatively small free energy difference between the *trans* and *cis* conformation. A fraction of these bonds is indeed in the *cis* conformation, though the majority is in *trans*. This conformational switch regulates protein foldings and functions, playing a role in many processes such as cell cycle regulation, signaling and gene expression. Due to the high energy of the transition state, the timescale of intrinsic prolyl isomerization is slow relative to the timing of biological processes, so prolyl isomerase enzymes (PPIase) catalyze the pro-

cess. There are four structurally non-related families of PPIase: cyclophilin, FKBP (FK506 binding proteins), parvulin and PTPA (Ser/Thr phosphatase 2A activator). The first threes act as monomers, whereas PTPAs form a substrate-induced dimer [27]. The family of FKBPs is quite heterogeneous, with the PPIase function often combined with other domains. This confers target specificity and directs these enzymes to distinct cellular compartments [28].

Saccharomyces cerevisiae encodes two nuclear NPL-FKBP proteins, Fpr3 and Fpr4, the best characterized within the family. These proteins have been reported to regulate the chromatin structure in different ways. Both Fpr3 and Fpr4 N terminal domains have *in vitro* histone chaperone activity [29, 30]. Surprisingly, not only the NPL domain binds to nucleosomes, but also the FKBP domain contributes to this binding. A comparison between the FKBP present in NPL-FKBP proteins and other FKBP domains reveals how the formers are characterized by the presence of basic residues, which organize into basic patches fundamental for nucleosomes binding [31]. Fpr4 associates *in vivo* with the rDNA locus, though its role in rDNA regulation is controversial [29, 30]. Fpr4 was also found interacting with nucleolar precursors of 60S ribosomal subunits [32]. These proteins are reported to regulate transcription via the PPIase domain, in particular, Fpr4 prolin isomerization of H3 histone tail regulates histone methylation and so transcription [30, 33]. Fpr3 regulates the CenpA^{Cse4} H3 centromeric variant protein stability through prolyl isomerization, targeting Cse4 for degradation [34]. *fpr3*Δ and *fpr4*Δ cells exhibit a moderate chromosome mis-segregation defect [34].

Similar to *S. cerevisiae*, *Schizosaccharomyces pombe* encodes two nucleolar NPL-FKBP proteins, SPBC1347.02 (Fkbp39) and SPAC27F1.06c (Fkbp41) [35]. Analogous functions were reported for these proteins. Fkbp39 N terminal domain has indeed *in vitro* histone chaperone activity [29] and these proteins were implicated in CenpA^{Cnp1} proline isomerization, important for precise chromosome segregation [36]. Fkbp39 was also identified by screening of a library of deletion mutants as a new factor involved in heterochromatin maintenance at the mating-type locus [37], and was reported to have a negative genetic interaction with the RNA interference silencing pathway (RNAi) [38].

1.3 The nucleolus

As mentioned before, NPM1 is a key regulator of the nucleolus structure. The nucleolus is a compartmentalized membrane-less organelle, with a primary function in ribosome biogenesis. Inside cells exist other membrane-less organelles as Cajal bodies and P-bodies. These organelles organize into defined space fundamental processes, often related to RNA metabolism, and can react readily to environmental changes since

macromolecules can freely diffuse. Indeed photobleaching recovery experiments showed that components within these organelles are continuously exchanged with the surrounding medium [39]. These structures are highly dynamic and exhibit liquid-like properties such as diffusion, condensation and the capacity to dissolve, as initially described for *Caenorhabditis elegans* P-granules in 2009 [40, 41].

These organelles form through liquid-liquid phase separation (LLPS): after reaching a critical concentration (higher than the solubility limit) some components form a concentrated phase, which is physically different from the diluted one [42]. For this to happen, the interactions between the phase-separated components have to be energetically favorable than the interactions with the solvent [43]. Key for this process is the establishment of multiple weak interactions within the condensate, that create a network, in which each molecule interacts with several other components simultaneously [43]. This is normally referred to as multivalency and is granted by the alternation between folded domains and disordered segments, highly enriched in constituents of membrane-less organelles [44, 45]. Folded domains organize the scaffold of these organelles, often through self-oligomerization, and disordered segments provide dynamic interactions with several partners [46]. The *scaffold-client* model divides the constituents of condensates into *scaffolds* and *clients* [47]. The formers are essential for the condensate structure whereas the latter is often present only under some circumstances and diffuse more rapidly.

Condensation of biomolecules via LLPS is believed to highly concentrate specific macromolecules and so to increase reactions rate or to confer specificity to reactions by limiting the availability of possible substrates [46, 39]. Indeed, the biochemical environment within biomolecules condensates may be extremely different from that in the surroundings, but at the same time, the formation and dissolution of a condensed phase can be controlled very rapidly [39].

First observations of the nucleolus were already reported in the 19th century, but only more than 100 years later our knowledge on this organelle significantly improved. As mentioned before, the nucleolus is the organelle where ribosome biogenesis begins, and for a long time this was regarded as its sole function. Over time several observations led to the formulation of the “plurifunctional nucleolus” hypothesis, and nowadays it is granted that the nucleolus plays a role also in other processes. The nucleolus regulates the cell cycles beyond its direct role in ribosome biogenesis. These two processes are indeed intimately connected. In yeast, almost 60% of the transcriptional activity accounts for the synthesis of ribosomal RNA (rRNA), with almost half of the remaining transcription devoted to the production of ribosomal proteins mRNAs. Moreover, ribosomes account for half of the cell protein mass [48]. The nucleolus can also sense and rapidly react to changing conditions, for example adapting ribosome production to nutrients availability, which in

turn influence cell growth. The nucleolus is also involved in the production of other types of ribonucleoprotein complexes (such as the signal recognition particle, SRP) and the nucleolar stress response [49, 50]. Recently, the nucleolus function as a protein quality control compartment was described [51]. After stress, misfolded proteins enter the nucleolus and associate with nucleolar proteins, such as NPM1, in an Hsp70 regulated manner. The storage of misfolded proteins inside the nucleolus prevents their irreversible aggregation, although it temporarily alters its liquid-like properties. Indeed, the capacity of the nucleolus to store misfolded proteins is limited.

Nucleoli form around stretches of tandem rDNA repeats, called nucleolar organizer regions. Human nucleoli are organized into three compartments: the fibrillar center (FC); the dense fibrillar component (DFC); and the granular component (GC), fig. 1.1(a). The FC contains chromatin, rDNA repeats competent for transcription and transcription factors; the DFC is enriched in fibrillarin and nascent rRNAs whereas the GC, which accounts for the vast majority of the nucleolar mass, is characterized by the presence of nucleophosmin and ribosome assembling intermediates. The FC is surrounded by the DFC and they are embedded in the GC. This architecture results in the vectorial movement of nascent ribosomes subunits from the internal fibrillar center to the outer granular component as their biogenesis proceeds. Indeed, rRNA is transcribed at the interface between the FC and DFC, and since ribosome biogenesis starts co-transcriptionally, early factors associate with the nascent transcript as soon as it emerges. Early rRNA processing takes place in the DFC whereas maturation of the assembly particle in the GC. Yeast nucleoli have a simpler structure with only two compartments: the central fibrillar strand (F), that contains rDNA repeats and has characteristics of both the FC and DFC; and granules (G), fig. 1.1(b). It was suggested that during evolution the initial fibrillar compartment present in bipartite nucleoli specialized into FC and DFC as the rDNA intergenic region expanded [52]. This is not the only difference between human and yeast nucleoli: in yeast, neither the nucleus nor the nucleolus disassembles during mitosis (closed mitosis) differently from what happens in humans [48]. Despite these differences, yeast has been extensively used as a model organism to investigate ribosome biogenesis and cell cycle regulation.

The nucleolus organization in compartments arises due to differences in miscibility between the liquid-like phases generated by the main constituents of each compartment, fibrillarin and nucleophosmin. The different physical properties of these condensed phases, such as viscosity and surface tension, keep the compartment separated and allow the nucleolus layered organization, in which the GC, enriched in NPM1, surrounds the DFC, enriched in fibrillarin [54]. NPM1 can be considered as a ”model” phase separating protein, containing both folded domains (the nucleophosmin domain that mediates the pentameric oligomer-

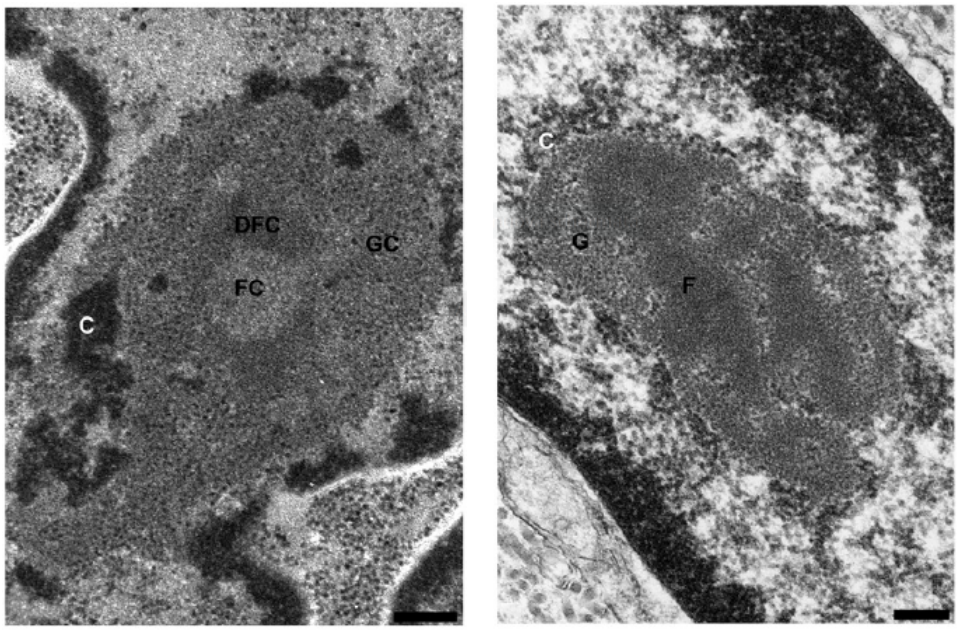

(a) (b)

Figure 1.1: Tripartite e bipartite nucleoli Electron microscopy images of tripartite and bipartite nucleoli, scale bars represent 0.25 μm. (a), tripartite nucleolus from a bovine cell. FC, DFC and GC are labeled. (b), bipartite nucleolus from *Pleurodeles waltlii*. F and G are highlighted. Figure from [53].

ization and the nucleic acid RRM binding domain), and the intrinsically disordered region highly charged, fig. 1.2. Weak and transient electrostatic interactions allow NPM1 phase transition, either alone (homotypic phase transition) or with rRNA and ribosomal proteins (heterotypic phase transition). The interaction between the acidic tracts, present both in the oligomerization domain and in the disordered region, with arginine motifs are responsible for the heterotypic phase separation with ribosomal proteins. The heterotypic phase separation with rRNA relies instead on the interaction between the positive charges of basic tracts and the RRM domain, with the negative charges of the RNA. At the same time, NPM1 homotypic phase separation is based on the interactions between its acidic and basic tracts. This generates competition between homotypic and heterotypic phase separation, creating a network considered important for the organization and regulation of the vectorial assembly of ribosomes [55]. Disruption of NPM1 phase separation with either ribosomal proteins or rRNA prevents its accumulation in the nucleoli [56].

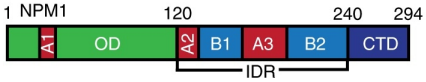

Figure 1.2: NPM1 domain organization NPM1 oligomerization domain (OD), the nucleophosmin domain responsible for the organization into pentamers, is represented in green. It is followed by the highly charged intrinsically disordered region (IDR), with acidic and basic tracts in red and blue respectively. The C-terminal nucleotide binding domain (CTD), is in dark blue. Figure adapted from [57].

Fibrillarin (Nop1 in yeast) also consists of a low sequence complexity disordered region (an N terminal arginine/glycine domain, GAR), followed by a structured domain (the methyltransferase domain). *In vitro*, the full-length protein requires either rRNA or heparin to phase separate, probably because electrostatic interactions contribute to droplet condensation. The GAR domain alone does phase separate *in vitro*, without the need for rRNA, but *in vivo*, it localizes to the entire nucleolus. The methyltransferase domain, on the other hand, does not phase separate *in vitro*, but *in vivo* partitions to the DFC, probably thanks to interactions that it establishes with the full-length protein. These observations suggest that the disordered GAR domain drives fibrillarin phase separation while the methyltransferase domain confers the peculiar viscoelastic properties and the specific localization to the DFC compartment [54].

1.4 Ribosomes

Ribosomes are the ribonucleoprotein complexes that decode the information stored in messenger RNAs (mRNAs) and synthesise polypeptide chains, during translation. The eukaryotic ribosome, named 80S ribosome (where ”S” is the Svedberg coefficient, used to define particle’s size based on sedimentation properties), consists of a small 40S subunit, containing the 18S rRNA and 33 ribosomal proteins, and a 60S large subunit, comprising the 25S, 5.8S and 5S rRNAs together with 47 ribosomal proteins (46 in yeast).

Translation can be roughly divided into four steps: initiation, elongation, termination and recycling. Each step requires assistance from several eukaryotic regulatory factors and is energy-consuming. mRNA decoding takes place in the small subunit, where tRNAs base-pare with mRNA, while peptide bond formation is catalyzed in the large subunit, in the peptidyl transferase center. The two ribosome subunits associate only during translation, awaiting separate in the pool of translating competent cytoplasmic subunits. Very briefly, for the vast majority of the transcripts, the small subunit binds the mRNA at the 5’-7-methyl-guanosine cap proximal region and scans it up to the first start codon, assisted by several eukaryotic translation initiation factors. After binding of the initiation tRNA to the start codon and release of the eukaryotic translation initiation factors, the 60S subunit can be recruited [58]. Elongation can now take place. Base pairing between the mRNA codon and the corresponding aminoacyl-tRNA anticodon allows for its accommodation within the A site. Now, the peptide bond between the peptidyl-tRNA at the P site and the aminoacyl-tRNA within the A site is formed. To proceed with the catalysis of a new peptide bond, the A site has to be empty and the following mRNA codon be exposed. This is achieved through ribosomal subunits translocation, which results in the presence of a deacylated-tRNA at the E site, which can be released, the peptidyl-tRNA in the P site and an empty A site, with the following mRNA codon available for base-pairing with its corresponding aminoacyl-tRNA. When a stop codon enters the A site, termination takes place. The stop codon is recognized by specific release factors, which causes peptidyl-tRNA hydrolysis. After the polypeptide chain is released, the 80S ribosome is still associated with the mRNA, the deacylated-tRNA and the release factors. Recycling, which is the dissociation of these factors and separation of the two subunits, allows the re-use of ribosome subunits and translation factors in further rounds of translation [59].

1.5 Ribosome biogenesis

Ribosome biogenesis is a particularly complex process, in which the coordinated activity of all three RNA polymerases is required. Transcription of rRNAs, small nucleolar RNAs (snoRNAs), mRNA encoding for ribosomal proteins and ribosome biogenesis factors, needs to be coordinated. All these components are required for the synthesis of this huge ribonucleoprotein complex. Ribosome biogenesis factors associate with pre-ribosomes during biogenesis but are not present in the mature subunits. Some biogenesis factors have enzymatic activities, but others are chaperones that assist the folding. The consume of energy assures a directional assembly.

Ribosome biogenesis starts as early as the nascent rRNA emerges from the transcribing polymerase, but only after complex processing steps in the nucleolus, nucleoplasm and cytoplasm and final quality controls, the mature subunits are added to the pool of translating competent cytoplasmic subunits [42, 60]. In the nucleolus, the co-transcriptional association of biogenesis factors with the nascent rRNA reduces its conformational freedom and supports the formation of subdomains. The mature organization of these subdomains is achieved in the nucleus, even though local remodeling is still necessary. Finally, in the cytoplasm, the last steps of processing take place, alongside with quality control. Nucleus-cytoplasmatic trafficking is therefore particularly relevant, in both directions. Indeed, ribosomal proteins and biogenesis factors required for ribosomes assembling in the nucleolus are produced in the cytoplasm, and ribosome intermediates have to be exported to the cytoplasm, through nuclear pore complexes, for final maturation. Importins, nucleoporins, Ran-GTPases, exportins and karyopherins are all necessary for these trafficking and so for ribosome biogenesis.

The eukaryotic rDNA organization is similar in all organisms. One polycistronic rDNA transcript unit contains the sequences for the 18S, 5.8S and 25S rRNA (28S in higher eukaryotes) separated by two internal transcribed spacer, ITS1 and ITS2, flanked by two external transcribed spacer (the 5' ETS and the 3' ETS). This unit is transcribed by the RNA polymerase I (Pol I). The 5S rRNA is encoded separately and is transcribed by the RNA polymerase III [61]. rRNA maturation requires both endonucleolytic and exonucleolytic processing to eliminate the spacer sequences. In general, cleavage within the ITS1 separates the small subunit rRNA from the ones for the large subunit. These are themselves separated with a cleavage within the ITS2. Exonucleolytic processing is then required for the formation of the mature rRNA termini. The 5S rRNA is extremely peculiar because it binds a ribosomal protein before its incorporation into the ribosome. Indeed, after transcription, which does not happen in the nucleolus, and processing (the 3' end

is trimmed by exonucleases), the 5S rRNA is exported to the cytoplasm. There it associates with Rpl5 and only the resulting ribonucleoprotein particle can shuttle back to the nucleolus, where it assembles with the nascent 60S subunit [62]. This general framework applies to all eukaryotes, but significant differences exist between organisms, also between yeast (a very important model system for ribosome biogenesis) and humans [63]. Although rRNA processing starts in the nucleolus, the final maturation steps happen in the cytoplasm.

In yeast, rRNA cleavage can happen both co-transcriptionally (nascent transcript cleavage, NTC), the main processing pathway in exponentially growing cells, or post-transcriptionally (released transcript cleavage, RTC) [64, 65]. Both pathways exist, and their relative equilibrium shifts depending on growth conditions. In other eukaryotes, it seems that only the RTC pathway exists. rRNA transcription has been extensively visualized by electron microscopy, in the so-called Miller chromatin spreads. In these images several nascent rRNAs (of different lengths because at different stages of transcription) emerge from one rDNA transcriptional unit, resembling a ”Christmas tree”. The ”pearl” at the end of each transcript, a 5’ terminal knob, contains the nascent rRNA as well as RNA processing factors. As transcription proceeds these structures, initially extended, condense into compact larger knobs, the small subunit processome (a stable intermediate in the 40S subunit biogenesis, see later). In exponentially growing yeasts cells, Miller spreads show that the transcripts towards the end of the rDNA unit are shorter than they should be considered their position, and that most of them do not have the 5’ terminal knob, fig. 1.3. This suggested that, at least on some nascent transcripts, large terminal knobs are cleaved before transcription is completed, proving that rRNA cleavage can happen co-transcriptionally [64]. Because rRNA modification happens before rRNA cleavage, this also proved that modification happens co-transcriptionally as well. Indeed, modification of the 18S rRNA mainly happens co-transcriptionally, whereas the 25S rRNA may be modified either co- or post-transcriptionally, probably depending on the processing pathway [65]. On the cleaved transcripts a new 5’ terminal knob forms, which grows as transcription proceeds. This second terminal knob corresponds to the first intermediates of the large subunit. Pol I is not distributed uniformly over the rDNA unit, with a higher density in the proximity of the sites where the terminal knobs compact. Probably, Pol I pauses or slows down due to the interaction with the assembling particles, and this may facilitate co-transcriptional assembly [66].

During NTC, the nascent rRNA is cleaved at site A0, A1 (within the 5’ETS) and A2 (in the ITS1) before the transcription of the rDNA polycistronic unit is completed, fig. 1.3, 1.4. The cleavage at site A2 happens when Pol I has already transcribed a further 1-1.5 kb, so it is over the 25S rDNA [65]. In this way the transcript corresponding to the whole rDNA unit, the 35S rRNA, is not produced, the opposite to what happens

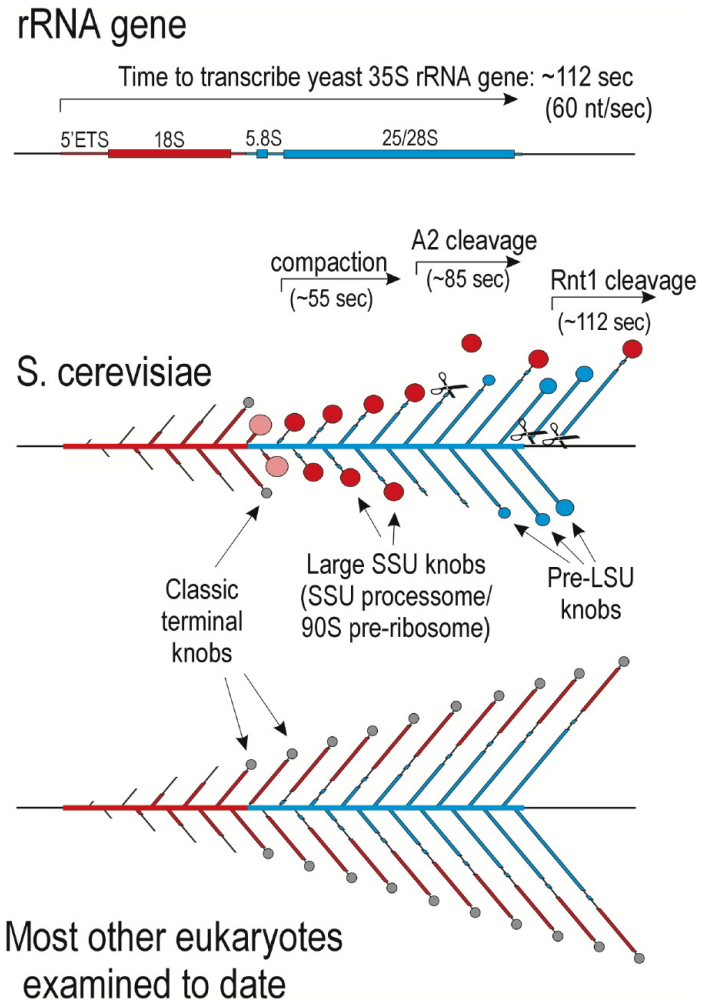

Figure 1.3: Model of rRNA co-transcriptional processing At the top the organization of a polycistronic rDNA transcript unit is shown, with the rRNA sequences incorporated in the nascent 40S subunit colored in red and the ones for the 60S subunit in blue. The middle panel shows the schematic model of yeast nascent transcript cleavage, whereas the lower panel the released transcript cleavage in other eukaryotes. In yeast both processing pathways exist, and even during exponential growth some transcripts are processed via RTC, as depicted in the model. In both pathways Miller chromatin spreads reveal the presence of terminal knobs, which indicate co-transcriptional association of biogenesis factors with rRNA and processing steps. Figure from [64].

during RTC. The cleavage at the 3' end that releases the 35S rRNA, mediated by the endonuclease Rnt1, happens in any case co-transcriptionally. The mature 3' end is generated in a successive step by the exonuclease Rex1. It is important to underline that, even though in eukaryotes other than yeast NTC does not happen, terminal knobs are visible on Miller chromatin spreads. This suggests that during RTC, even though co-transcriptional cleavage does not happen, co-transcriptional assembling and compaction of ribosome subunits take place, fig. 1.3. Also during RTC, the terminal knob corresponds to the small subunit processome, which in this case is associated with the 35S rRNA (a very unstable RNA). This structure was alternatively named 90S pre-ribosome. Most of the factors in the 90S pre-ribosome are involved in the biogenesis of the 40S subunit, and associate with and assist the folding of the nascent 18S rRNA, whereas the 25S rRNA is devoid of biogenesis factors [67]. After cleavage of the 35S rRNA at sites A0, A1 and A2 the two nascent subunits are separated. Independently on the pathway, the resulting 20S rRNA is converted into the mature 18S rRNA in the cytoplasm by cleavage at site D, fig. 1.4. After A2 cleavage, the resulting 27SA2 rRNA is cleaved at A3 by the RNA component of mitochondrial RNA processing endoribonuclease (RMRP), which releases the 27SA3 rRNA. The large ribosome subunit contains a long (L) and a short (S) form of 5.8S rRNA, which are the result of different processing of its 5' terminus (by the exoribonucleases Rat1 and Rrp17). The 5.8S 3' terminus is initially determined by an endonucleolytic cleavage within the ITS2 at site C2, which releases the 7S and 26S pre-rRNA. The 7S rRNA is trimmed to 6S rRNA by the exosome and to the mature 5.8S in the cytoplasm by Eri1, in *S. pombe*. The 26S pre-rRNA 5' is trimmed by Rat1, fig. 1.4.

The rRNA is highly modified but not all molecules have the same amount of modification. As a consequence, there are populations of ribosomes with differently modified RNA, but the functional implications are currently unclear. rRNA modifications are normally clustered and are important either for rRNA structure or function. snoRNAs play a key role in rRNA modification. They are grouped into two classes: C/D box snoRNAs associated with fibrillarin and H/ACA box snoRNAs. Most of C/D box snoRNAs are involved in 2'-*O*-ribose methylation catalyzed by the methyltransferase fibrillarin (associated with Nop56 and Nop58), whereas H/ACA box snoRNAs take part in rRNA pseudo-uridylation. In both these processes, the target is selected due to base pairing between the snoRNA and the rRNA itself. As this requires access to single-stranded rRNA, these modifications occur co-transcriptionally, before nascent rRNA folding. Not all small nucleolar ribonucleoprotein particles (snoRNPs) are involved in rRNA modification, some indeed associate with the rRNA to prevent wrong conformations and assist assembly of the nascent subunits. For example, the U3 snoRNP is essential for the structural organization of the small subunit, it is required for rRNA

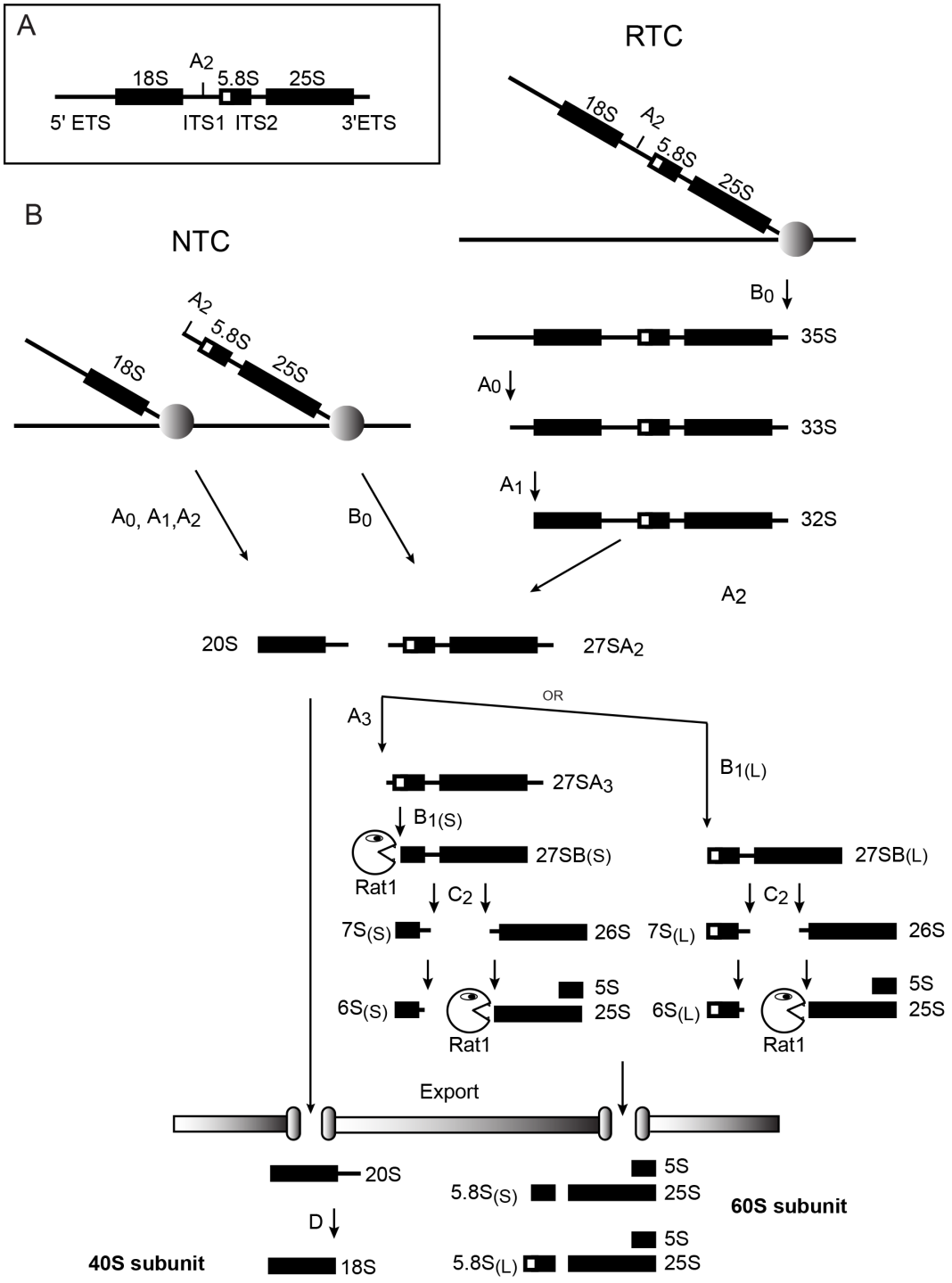

Figure 1.4: Model of rRNA processing pathway in yeast (A), Representation of the 35S rRNA. (B), rRNA processing via the nascent transcript cleavage or the released transcript cleavage pathways. Figure from [68].

cleavage but is not involved in 2'-*O*-ribose methylation.

During small subunit biogenesis, RNAs and biogenesis proteins that associate with the nascent rRNA reduce its conformational freedom so that each rRNA domain, four within the 18S rRNA, is assembled separately in a protective environment. As the 5' ETS emerges from Pol I, the UtpA, UtpB and Mpp10 protein complexes and the U3 snoRNP associate with it, forming the 5' ETS particle, which constitutes the first scaffold for the small subunit assembly, fig. 1.5. The U3 snoRNA base pairs both with the 5' ETS and the nascent 18S rRNA, introducing spatial constrictions that shape the organization of the nascent particle. As transcription proceeds, more factors associate resulting in the small subunit processome (SSU processome), the first intermediate for which a structure is available, fig. 1.5. As this particle grows, more factors provide structural support: while the 18S rRNA domains assemble the premature formation of the central pseudoknot (an RNA motif at the interface of the domains, which is required to set up the decoding center) is prevented. For further processing, which triggers the transition from the SSU processome to pre-40S particle, several assembling factors and the 5'ETS particle are released from the SSU processome, fig. 1.5. This requires two coordinated rRNA cleavages, one for the release of the 5'ETS (cleavage at site A1) and one for the separation of the premature 18S and 25S rRNA (cleavage at site A2). The 5' ETS RNA is degraded by the nuclear exosome within the assembly particle [69], which results in 5' ETS particle disassembly and recycling of its biogenesis factors. The resulting 40S particle associates with exporting factors and is exported to the cytoplasm, fig. 1.5. For quality control, it associates with a mature 60S subunit. This event triggers the last 18S rRNA cleavage and dissociation of the remaining biogenesis factor. A mature 40S subunit is released [70, 60].

The rRNA cleavage (at site A2) that separates the nascent 18S rRNA from the nascent 25S rRNA, and so the two subunits, takes place only when Pol I is already more than 1 kb downstream of it, already transcribing the 25S rDNA. Appropriate RNA folding, which signals for a correct initial assembly of the large subunit, creates the substrate for this cleavage, coordinating the assembly of the two subunits. Indeed, depletion of early 60S biogenesis factors, for example the exonuclease Rat1 involved in 27SA3 trimming, delays the 40S subunit processing without reducing the synthesis of 18S rRNA. This could be explained by a switch from NTC to RTC [66, 68]. The large subunit is structurally more complex than the small one, and so it is the assembly. The 25S rRNA organizes into six domains, which are not incorporated into the nascent 60S subunit following the order in which they are transcribed. Moreover, these domains are extensively interconnected, with assembling factors and ribosomal proteins creating bridges and extensive interactions between them. First, the 5.8S rRNA folds with the ITS2 and domains I and II resulting in the

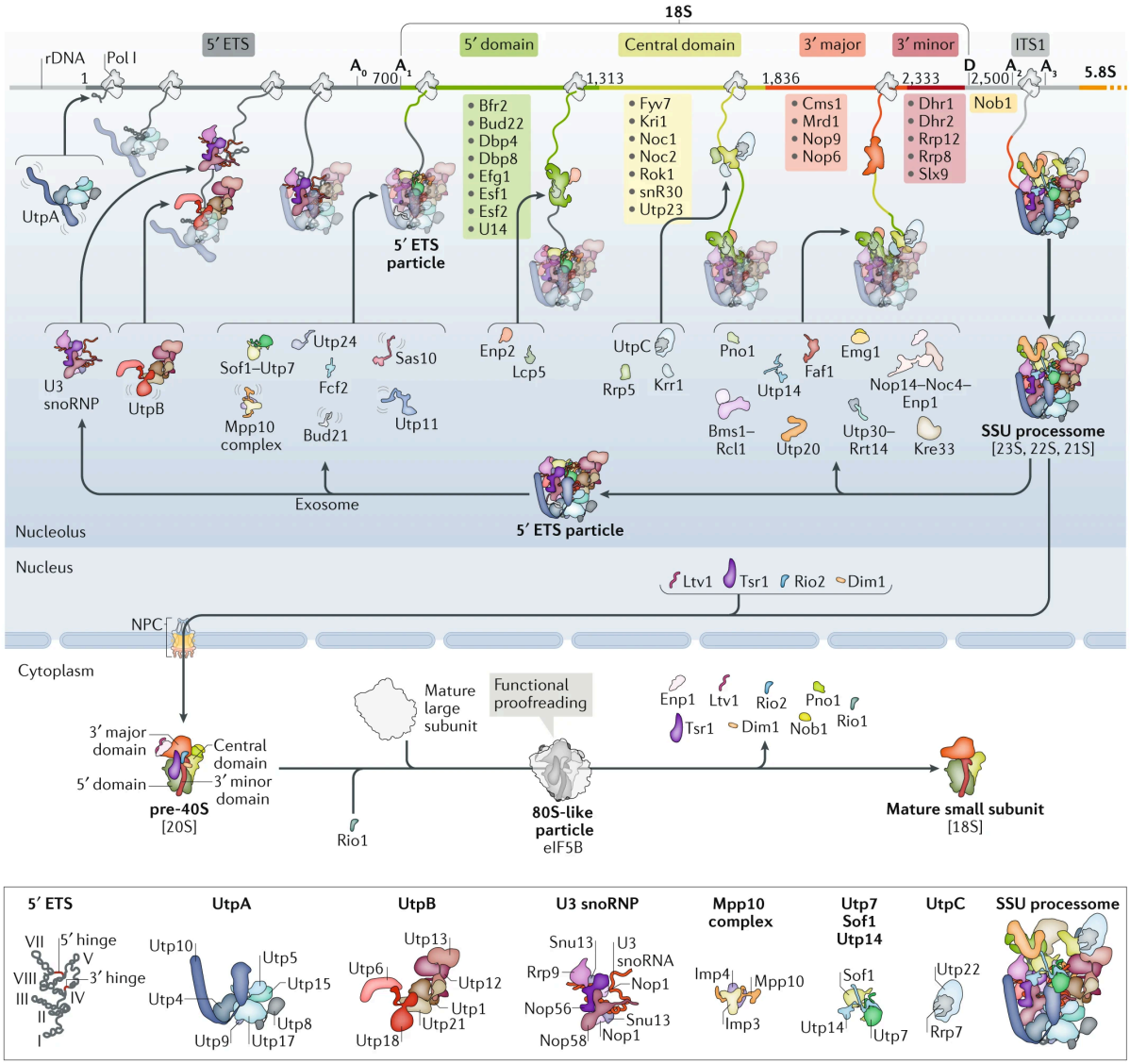

Figure 1.5: Small ribosomal subunit assembly Schematic representation of the maturation of the small subunit, from the earliest co-transcriptional events in the nucleolus to the final maturation in the cytoplasm. rRNA subdomains are represented in different colors, and the consequential association and dissociation of biogenesis factors to and from the assembly subunit is shown. Biogenesis factors and complexes for which a structure is available are represented as cartoons. At the bottom the composition and structural organization of key processing complexes is illustrated. Figure from [70].

earliest intermediate for which a structure was solved, state 1/A in fig. 1.6. The ITS2 RNA, together with the associated biogenesis factors, supports the hybridization between the 5.8S rRNA and domain I, playing an important structural role, acting as a scaffold for the large subunit in a similar way as the U3 snoRNP does for the small subunit. Then, the ITS1 and the 3'ETS are removed and domain VI folds resulting in a ring-like intermediate (again a stable assembly particle, in which the 5' and 3' end of rRNA are connected), state 2/B in fig. 1.6. Later, domains III, IV and V associate stably with these intermediates and result visible in the Cryo-EM structures, state E in fig. 1.6. Already within the nucleolus, several fundamental structures of the large subunit are recognizable, like the GTPase activating center (where GTPases involved in initiation and elongation are located), the peptidyl transferase centre and the polypeptide exit tunnel (the tunnel that connects the peptidyl transferase centre with the solvent, mostly constituted by rRNA, through which nascent polypeptides leave the peptidyl transferase centre). The 5S RNP, imported from the cytoplasm, associates early with the assembling particle but is not visible up to late nucleolar stages. Exchange of biogenesis factors mark the migration to the nucleus, where the peptidyl transferase centre and the polypeptide exit tunnel are further processed, the ITS2 is cleaved (then degraded by the exosome) and the 5S rRNA rotates for 180°, fig. 1.6. The structural organization of both the peptidyl transferase centre and the polypeptide exit tunnel is checked before nuclear export. In the cytoplasm, remaining biogenesis factors dissociate while the last ribosomal proteins are incorporated. The key functional centers are associated with biogenesis factors until the last stages of biogenesis, to be functionally tested prior to the release of the assembled subunit [70, 60].

1.6 Phase separation in ribosome biogenesis

Even though phase separation in biological systems has been extensively characterized since the first report in 2009, a connection with the underlying biological processes is often missing. This in part is because phase separation is a way molecules interact one with each other, organizing the environments where biological processes take place. However, the alteration of these structures has consequences. Moreover, the dynamic organization of these compartments and the movement within them is important in the contest of biological processes. Recent publications started to reveal the connection between the phase-separated nature of the nucleolus with the biological process of ribosome biogenesis, shedding light on the very beginning and very end of the nucleolar transition.

During ribosome biogenesis, a high amount of nascent rRNA are rapidly transcribed at the FC/DFC

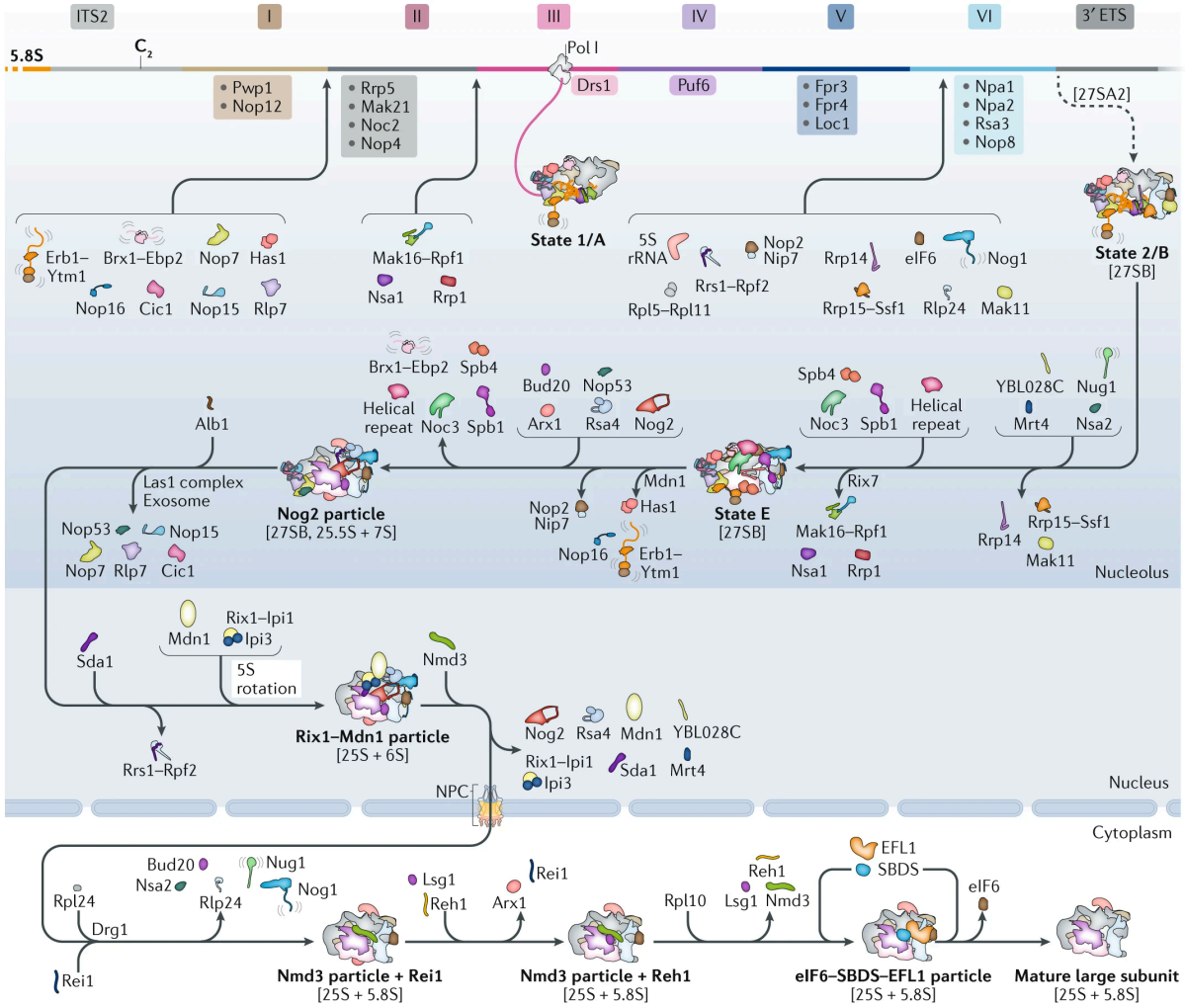

Figure 1.6: Large ribosomal subunit assembly Schematic representation of the maturation of the large subunit, from the earliest co-transcriptional events in the nucleolus, through the remodeling in the nucleoplasm, to the final maturation in the cytoplasm. rRNA subdomains are represented in different colors, and the consequential association and dissociation of biogenesis factors to and from the assembly subunit is shown. Biogenesis factors and complexes for which a structure is available are represented as cartoons. Figure from [70].

border and need to be efficiently processed in the DFC. Recently it was shown in human cells, that rRNA translocation from the FC/DFC border to the DFC starts immediately: while Pol I is still transcribing, the 5' ETS already localizes to the DFC [71]. Fibrillarin is responsible for this translocation, and to a lower extent also components of the UtpA complex are involved. As previously described, the U3 snoRNP complex binds the nascent rRNA as soon as it emerges from Pol I. *In vivo* experiments showed that fibrillarin methyltransferase domain is necessary to constrain nascent rRNA localization at the FC/DFC border but is not able to mediate its translocation to the DFC, in agreement with what previously shown [54]. This suggests that the GAR domain is responsible for that. In the proposed model, the methyltransferase domain initially binds the nascent rRNA at the 5' ETS, then fibrillarin self-association via phase separation through the GAR domain mediates the translocation to the DFC [71]. Moreover, since processing factors within the DFC are organized in clusters rather than being uniform, the authors of this study suggest that rRNA translocation originates these clusters that would later fuse in one DFC [71]. This suggests that nascent pre-rRNA sorting is involved in DFC assembly. This model is supported by the *in vitro* observation that the folded 5' ETS RNA partitions very efficiently into fibrillarin condensates, which *in vivo* would result in its fast localization into the fibrillarin organized compartment.

In vitro and *in vivo* studies showed that within multicomponent phase-separated organelles the parameters governing phase separation, such as the concentration at which phase separation happens, are dynamic and depend on the composition/concentration of the different molecules. As a consequence, in multicomponent NPM1 organized condensates, increasing only NPM1 concentration results in a destabilization of the system. This suggests that heterotypic interactions stabilize these condensates, rather than homotypic interactions within the *scaffold* as proposed by the *scaffold-client* model [72, 47]. This provides the framework necessary to understand the dynamics of biological processes within phase-separated organelle and the type of interactions that support them. During ribosome biogenesis, the nascent ribosomes move from the internal nucleolar compartments toward the external GC and finally to the nucleus. As ribosome biogenesis proceeds, the nature of the assembly particle changes, from an immature rRNA bound co-transcriptionally by biogenesis factors to an almost structurally mature ribosomal subunit. As a consequence, the number of sites available for interactions with NPM1, the *scaffold* of the GC, decreases as maturation proceeds. This is supported by the observation that NPM1 *in vitro* phase separates weaker with ribosomal subunits than with rRNA [72]. So as ribosome biogenesis proceeds, phase separation of the assembling particles with NPM1 becomes progressively less energetically favourable, which results in their exit from the phase-separated nucleolus [72].

1.7 Chromatin

Inside cells, the genetic information stored in the DNA molecules needs to be highly organized and packed due to spatial constraints. In prokaryotes, DNA is not segregated into a membrane separate compartment but is highly condensed through supercoiling, so that it forms a pseudo-compartment within the cytoplasm, called nucleoid [73]. In eukaryotic cells, DNA is stored within the nucleus and organized into chromatin, composed by an equal mass of proteins and DNA. The fundamental unit of this structure is the nucleosome, formed by two copies of each histone proteins (with two H2A-H2B dimers and an H3-H4 tetramer) and 146 base pairs of DNA wrapped around it [74]. The linker histone H1 (not present in *S. pombe* [75]) binds to the DNA that connects two consecutive nucleosomes, called linker DNA. Chromatin can compact to different extents, from more accessible conformation to the highly condensed chromosomes at cell division. Histones chaperones assist nucleosomes assembly onto the newly synthesized DNA during replication and histone deposition that takes place outside of S phase, for example during DNA repair. Remodellers are macromolecular complexes that use the energy from ATP hydrolysis to change the chromatin structure, for example by sliding or disassembling nucleosomes. Thanks to the activity of remodellers, to the incorporation of different histone variants and post-translational modifications (PTMs, mainly on histone tails), nucleosomes not only pack the eukaryotic DNA but also regulate the expression of the genome. Histone tail modifications change as cell physiology requires, have a deep impact on the chromatin structure and DNA metabolism providing a further level of information and regulation [76, 77]. Histone modifications, such as acetylation, methylation and phosphorylation, are deposited and removed by histone-modifying enzymes (also called *writers* and *erasers*) and affect the activity of chromatin-binding proteins (also called *readers*). Together with DNA modification, such as methylation, histones variants and PMTs stably affect gene expression without changing the underlying DNA sequence, providing stable and inheritable information, commonly defined as ”epigenetic” information [78, 79]. However, not all chromatin modifications contribute to the transmission of epigenetic information.

Already in 1928, cytological staining of chromosomes revealed regions that do not decondense after mitosis. These regions, darker than the others during interphase, were named heterochromatin and the others euchromatin [80, 81]. Heterochromatin, which corresponds to chromatin in the repressed compact state, is divided into constitutive (present in every cell) and facultative heterochromatin. Facultative heterochromatin is present only in certain cells and can switch to euchromatin under particular conditions. Constitutive heterochromatin assembles at repetitive sequences, such as satellite repeats and transposable elements, which

are highly enriched at centromeres and telomeres. Because of this, constitutive heterochromatin contributes to genome stability, both as a chromosome structural component and by suppressing the expression and recombination or mobilization of these repetitive elements [82]. Heterochromatin also determines cell-type-specific transcription in multicellular organisms. Euchromatin, instead, corresponds to gene-rich transcribed regions. The open and close chromatin conformations characteristic of euchromatin and heterochromatin arise from the presence of different histone post-translational modifications. Constitutive heterochromatin is normally hypoacetylated and marked by the presence of methyl groups, from one to three, on H3 lysine 9 (H3K9me) catalyzed by orthologues of the *Drosophila melanogaster* methyl-transferase suppressor of variegation 3-9 (Su(var)3-9), and recognized by the chromodomain of proteins orthologues of the heterochromatin protein 1 (HP1) [83]. In some organisms, these histone modifications are coupled with the repressive DNA 5-methylcytosine mark (not present in *S. pombe*). However, not in all organisms constitutive heterochromatin is characterized by the H3K9 methylation mark, a notably exception is the yeast *S. cerevisiae* [84].

Constitutive heterochromatin and the silencing pathways necessary for its establishment and maintenance share common features in the different organisms, from *S. pombe* to humans [83]. For example, the enzymes that catalyze H3K9me normally can also *read* this modification. This is very important because by binding to pre-existing H3K9me, they can propagate and maintain this silencing mark. Moreover, factors that are required for heterochromatin establishment might differ from those required for maintenance. This, together with the PTMs *reader-writer* coupling strategy, allows heterochromatin spreading: once established it can propagate to the neighboring regions independently of the DNA sequence. To balance this, different mechanisms constrain this expansion and avoid deleterious gene silencing. Even though heterochromatin is silenced and compact during most of the cell cycle, during DNA replication it becomes accessible. This allows the transcription of these normally silenced loci. The resulting transcripts, which are often noncoding RNAs, are necessary for the re-establishment of the repressed state because support the recruitment of silencing factors.

1.8 Heterochromatin in *S. pombe*

S. pombe genome is composed of three chromosomes for a total of 13.8 Mb [85]. Constitutive heterochromatin is assembled at centromeres and subtelomeres and at the mating-type locus, on chromosome 2. The heterochromatin present at centromeres and subtelomeres has mainly a structural role, whereas regulation

of the mating-type locus is important for cell identity specification [86].

At centromeres, heterochromatin is fundamental for the deposition of the centromeric histone H3 variant CenpA^{Cnp1}, which is required for kinetochore assembly [87]. Moreover, centromeric heterochromatin allows a tight interaction between sister chromatids by trapping high level of cohesin, which associates with HP1^{Swi6}. As a consequence, in absence of centromeric heterochromatin, chromosome segregation is impaired [83]. Surprisingly, the specific role of subtelomeric heterochromatin is elusive, but, as centromeric heterochromatin does, it prevents recombination between repetitive elements, which could result in chromosome rearrangement [88]. At the mating-type locus, heterochromatin silences two transcription factors that determine the alternative mating-type (plus or minus), after being integrated at the expression site. Heterochromatin also regulates the directionality of the recombination that allows the switching between the two mating-types [83].

Heterochromatin at centromeres is established and maintained through the RNA interference pathway (RNAi), whereas at subtelomeres and the mating-type locus RNAi acts redundantly with other mechanisms. RNAi is targeted both to the mating-type locus and to subtelomeres thanks to the presence at these loci of sequences with high homology to centromeric repeats (*cenH* at the mating-type locus and *tlh* at subtelomeres [89, 90]). RNAi pathways are present in several organisms, though profound differences exist, and are involved in gene expression regulation, defense against foreign genetic material and genome stability [91]. As common features, these pathways achieve silencing, either at the transcriptional or post-transcriptional level, through the action of a single strand small RNAs loaded onto a member of the argonaute family of proteins. The argonaute-bound small RNA confers target specificity to the complex, which is recognized by base-pairing interactions between the small RNA and the target itself. RNAi pathways differ mainly in the source of the small RNA and the mechanism of silencing [92].

S. pombe centromeric heterochromatin silencing can be divided conceptually into two phases: establishment and maintenance. After DNA duplication, centromeric regions are accessible and heterochromatin needs to be re-established. *S. pombe* centromeres contain a central core region (*cnt*) where the histone CenpA^{Cnp1} is located, flanked by innermost (*imr*) and outermost (*otr*) repeats. Outermost repeats are further composed by *dh* and *dg* repeats. The current model for centromeric heterochromatin establishment suggests that the *S. pombe* argonaute protein (Ago1) carries out general transcriptome surveillance by binding the degradation products of abundant transcripts, called primal small RNAs (priRNAs) [93, 94]. Due to the de-repression of centromeres, RNA polymerase II transcribes *dh* and *dg* repeats, generating sense and antisense transcripts, which are processed into sense and antisense priRNAs. Through base-pairing in-

teractions between the Ago1-bound priRNAs and non-coding centromeric transcripts, Ago1 is recruited to centromeric repeats, fig. 1.7. This step exemplifies the so-called ”nascent transcript model” for heterochromatin assembly, in which the chromatin-associated RNA acts as a scaffold for the recruitment of the silencing complexes [91]. Ago1 is a member of the RNA induced transcriptional gene silencing (RITS) complex, together with Tas3, a GW (glycine-tryptophan) domain protein, and Chp1 (one of *S. pombe* HP1 proteins) [95]. The RITS complex interacts and recruits to chromatin other two complexes required for heterochromatin establishment and maintenance, the Clr4-Rik1-Cul4 (CLRC) and the RNA-directed RNA polymerase (RDRC) complexes [96, 97]. Clr4 is responsible for dimethylation or trimethylation of H3K9, being homologous of *Drosophila melanogaster* Su(var)3-9 [98]. H3K9me is recognized by *S. pombe* HP1 proteins, Swi6 and Chp2, which induce the silenced state (defined as transcriptional gene silencing, TGS) [99]. Both proteins recruit the Snf2–histone deacetylase repressor complex, SHREC, which shuts down the transcription of the repeats [100]. Chp1 within the RITS complex also binds to H3K9me, stabilizing RITS localization to heterochromatin [101]. The activity of the RDRC complex allows the establishment of a positive feedback loop that enforces silencing. The RNA-dependent RNA polymerase (RdRP, Rdp1 in *S. pombe*) within the RDRC complex synthesizes a single strand RNA, complementary to the non-coding centromeric transcript targeted by RISC [102]. The resulting dsRNA is processed by Dicer, Dcr1 an RNase III class ribonuclease, into double-stranded small interfering RNAs (siRNAs) that are loaded onto Ago1 (via the argonaute chaperone, ARC, complex). Argonaute slicing and release of the siRNA passenger strand results in an active RITS complex [103]. Thanks to base-pairing interactions between the Ago1 bound single-stranded siRNA and centromeric non-coding transcripts, the RITS complex is targeted to centromeres. Silencing takes place also co-transcriptionally (CTGS), as nascent non-coding centromeric transcripts are targeted by TRAMP to degradation by the exosome, and the dsRNA generated by Rdp1 is cleaved by Dcr1 into siRNAs [104].

1.9 rDNA chromatin

rDNA is organized similarly in all eukaryotes, with arrays of tandem head-to-tail repeats, either on one or more chromosomes. In *S. cerevisiae*, about 200 repeats are located on chromosome XII, whereas in *S. pombe* they are at both ends of chromosome 3. In humans, 400 rDNA repeats are distributed on the short arms of acrocentric chromosomes [105]. As previously mentioned, each repeat encodes the 18S, 5.8S, and 25S rRNA sequences, separated by ITS1 and ITS2, and flanked by the 5’ ETS and 3’ ETS, fig. 1.8. Repeats are separated themselves by non-transcribed spacers (NTS), which contain an origin of

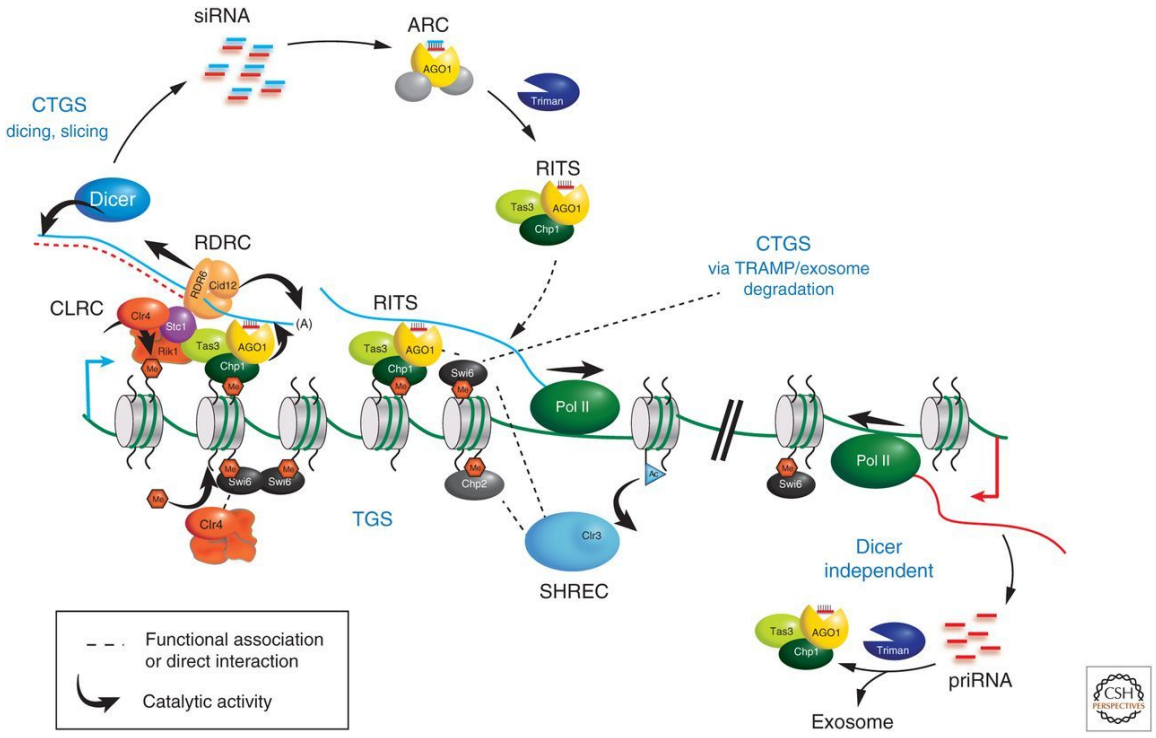

Figure 1.7: RNAi mediated heterochromatin assembly and maintenance in *S. pombe* Schematic representation of centromeric heterochromatin establishment and maintenance. On the right, transcription of centromeric repeats generates non coding RNAs, that, processed into priRNAs, guide low level of centromeric H3K9me deposition. On the left, the positive feedback loop through which high level of H3K9me are established and maintained. Centromeric silencing is achieved through both transcritpional and co-transcriptional gene silencing. Figure modified from [86].

replication, a replication fork blocking site (to avoid the collision between the transcription and replication machinery), and the promoter [106]. Of all these repeats, only a fraction is transcriptionally active, and this correlates with the underlying chromatin structure. rDNA repeats can be either in a nucleosome-depleted transcriptionally competent state, or devoid of Pol I and occupied by nucleosomes [107, 108]. Likely, the nucleosome-depleted state of active repeats is at least partially due to the high level of Pol I transcription [109]. Yeast regulates rRNA transcription depending on its requirement for ribosomes, by changing both the number of active repeats and their transcription rate [110]. Repeats in the active and silenced states are characterized by the presence of euchromatic (hypomethylation and acetylation) and heterochromatic epigenetic marks (H3K9 di- and trimethylation, DNA methylation) respectively [111, 112]. In *S. pombe*, Clr4, Swi6, Chp1, and Chp2 are indeed required for rDNA silencing [113].

The rDNA locus is very unstable, being a hot spot for double-strand breaks. This is due to its high transcription rate and the general difficulty of replicating repetitive elements [114]. Because there are so many rDNA repeats, depending on which substrate is used as a template for homologous recombination, required to repair double-strand breaks, rDNA repeats can expand, contract, or being preserved [115, 116]. Even maintaining such a high number of rDNA repeats, of which only a fraction is active, seems to be necessary to allow proper DNA repair. Condensin indeed binds silent rDNA repeats, allowing the association between sister-chromatids and facilitating homologous recombination [117]. Anyway rDNA recombination is normally counterbalanced by rDNA silencing, especially at the level of NTS and loss of silencing correlates with rDNA instability.

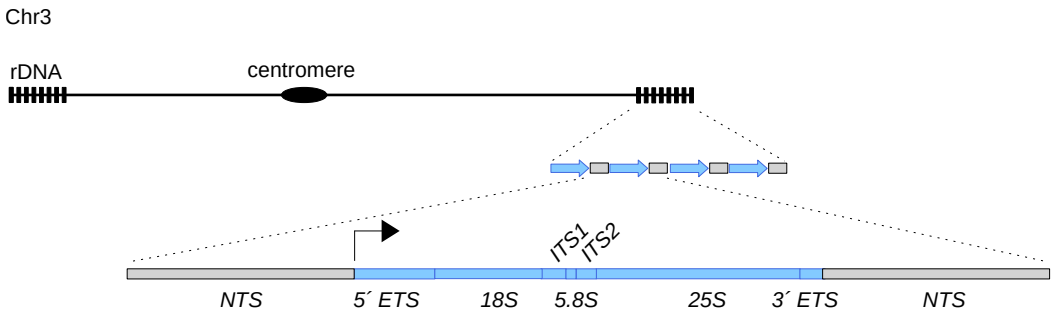

Figure 1.8: Schematic representation of rDNA in *S. pombe* In *S. pombe*, rDNA is located at both ends of chromosome 3. In the upper panel, rDNA repeats and the centromeric region are indicated. In middle and lower panels, progressive zoom-in of the rDNA unit. The direction of Pol I transcription is indicated by the arrow.

Chapter 2

Aim of the study

The published data about yeast (both *S. cerevisiae* and *S. pombe*) NPL-FKBP proteins are very confusing and partially contradictory, even though a leitmotif can be found in their connection with chromatin. Indeed yeast NPL-FKBP proteins are *in vitro* histone chaperone, that maybe regulate genome wide transcription or/and the rDNA locus or/and the deposition or degradation of the histone H3 centromeric variant [29, 31, 30, 33, 29, 34]. In addition, *S. pombe* Fkbp39 has a negative genetic interaction with RNAi [38]. Even more confusing is the fact that these proteins are homologous to NPM1, a widely studied protein involved in all important cell processes, from ribosome biogenesis to DNA repair and, in particular, in the nucleolus organization via phase separation [26, 5, 54]. Nowadays, phase separation is considered a trend topic in the molecular biology field. Nevertheless, despite the increasing number of publication, the connection with cell physiology is often underestimated.

This premises arise many questions: what is the real role of NPL-FKBPs proteins? Do they have a similar function in *S. pombe* as NPM1 in human? If so, what is the role of chromatin in ribosome biogenesis? And what is the contribution of phase separation to the process? What are the molecular basis for the negative genetic interaction with RNAi? Is there a connection between RNAi and ribosomes in *S. pombe*? The aim of this work is to address these questions, with the use of *in vitro* assays, yeast genetics and genome wide data analysis.

Chapter 3

Materials and methods

3.1 Materials

3.1.1 *S. pombe* strains and plasmids used in this study

strain number	genotype
63	h+ *otrR*(SphI)::*ura4 ura4 DS/E leu1-32 ade6-M210*
65	h+ *otrR*(SphI)::*ura4 ura4 DS/E leu1-32 ade6-M210 natMx6::*3xFLAG-*ago1*
860	h+ *leu1-32 ade6-M216 ura4-D18 his3 fkbp39*-HA::*kanMX6*
1164	h+ *otrR(SphI)::ura4 ura4 DS/E leu1-32 ade6-M210 fkbp41*-3HA::*kanMX6*
1315	h- *leu1-32 fkbp39*-1xFLAG6His::*hphMX6*
1323	h- *leu1-32 1-768fkbp39*-1xFLAG6His::*hphMX6*
1331	*leu1-32 fkbp41-3HA::kanMX6 fkbp39*-1xFLAG6His::*hphMX6*
1333	*leu1-32 fkbp41*-3HA::*kanMX6 fkbp39F301CW314CY337K*-1xFLAG6His::*hphMX6*
1334	*leu1-32 fkbp41*-3HA::kanMX6 *1-768fkbp39*-1xFLAG6His::*hphMX6*
1340	*leu1-32 fkbp41*-3HA::*kanMX6 fkbp39*Δ*::natMX6*
776	h+ *otrR*(SphI)::*ura4 ura4 DS/E leu1-32 ade6-M210 natMx6::*3xFLAG-*ago1 fkbp39*Δ*::kanMX6*
986	h+ *otrR*(SphI)::*ura4 ura4 DS/E leu1-32 ade6-M210 fkbp39*-2XFLAG6His::*hphMx6*
1172	h+ *otrR*(SphI)::*ura4 ura4 DS/E leu1-32 ade6-M210 fkbp41*Δ*::hphMx6*
1173	h+ *otrR*(SphI)::*ura4 ura4 DS/E leu1-32 ade6-M210 fkbp41*Δ*::hphMx6 natMx6::*3xFLAG-*ago1 fkbp39*Δ*::kanMX6*
1314	h+ textitotrR(SphI)::*ura4 ura4 DS/E leu1-32 ade6-M210 natMx6::*1xFLAG-*ytm1*
1318	h- *leu1-32 natMx6::*1xFLAG-*ytm1 fkbp39*Δ*::kanMx6*
1319	h- *leu1-32 fkbp39F301CW314CY337K*-3xHA::*kanMX6*
1329	h- *leu1-32 1-768fkbp39*-3xHA::*kanMX6*
1335	h+ *leu1-32 natMx6::*1xFLAG-*ytm1 fkbp39*-HA::*kanMX6*

strain number	genotype
1338	*leu1-32 natMx6::*1xFLAG-*ytm1 1-768fkbp39*-3xHA::*kanMX6*
1341	h+ *otrR*(SphI)::*ura4 ura4 DS/E leu1-32 ade6-M210 hphMx6::*1xFLAG-*ytm1*
1342	h+ *otrR*(SphI)::*ura4 ura4 DS/E leu1-32 ade6-M210 hphMx6::*1xFLAG-*ytm1 fkbp41*-3HA::*kanMX6*
1343	*leu1-32 hphMx6::*1xFLAG-*ytm1 fkbp41*-3HA::*kanMX6 fkbp39Δ::natMx6*
1435	h+ *leu1-32 natMx6::*1xFLAG-*ytm1 fkbp39*-HA::*kanMX6 fkbp41Δ::hphMx6*
1436	*leu1-32 natMx6::*1xFLAG-*ytm1 1-768fkbp39*-3xHA::*kanMX6 fkbp41Δ::hphMx6*
1447	h+ *otrR*(SphI)::*ura4 ura4 DS/E leu1-32 ade6-M210 natMx6::*1xFLAG-*nop1*
1349	h+ *otrR*(SphI)::*ura4 ura4 DS/E leu1-32 ade6-M210 fkbp41Δ::hphMx6 natMx6::*1xFLAG-*ytm1*
1346	h- *leu1-32 natMx6::*1xFLAG-*ytm1 fkbp39Δ::kanMx6 fkbp41Δ::hphMx6*
80	h+ *leu1-32 ade6-210 ura4DS/E otrR*(SPhI)::*ura4+ clr4Δ::Kanr*
207	h- *ago1Δ::hph*
209	h- *chp1Δ::nat imr1::ura4 ura4-D18 ade- leu-*
288	h+ *otrR*(SphI)::*ura4 ura4 DS/E leu1-32 ade6-M210 swi6Δ::natR*
638	h+ *otrR*(SphI)::*ura4 ura4 DS/E leu1-32 ade6-M210 ago1Δ::kanr*
930	*fkbp39Δ::kan ago1Δ::hph lys1::cnp1*-GFP
1321	h- *ago1Δ::hph natMx6::*1xFLAG-*ytm1*
810	h-*lys1::cnp1*-GFP *leu1-32 ura4-D18*
914	*lys1::cnp1*-GFP *leu1-32 clr4Δ::Kanr*
928	*leu1-32 natMx6::*3xFLAG-*ago1 fkbp39Δ::kanMX6 lys1::cnp1*-GFP
922	*leu1-32 ago1Δ::kanr lys1::cnp1*-GFP
1160	*ade6-704 arg3-D4 his3-D1 leu1-32 ura4-D18/DSE cnt1:ura4 cnt3:arg3arg3* + pH-icc3i-H
1162	*ago1Δ::hph* + pH-icc3i-H
1166	*natMx6::*3xFLAG-*ago1 fkbp39Δ::kanMX6* + pH-icc3i-H
1232	*fkbp39Δ::kanMX6 ago1Δ::hph* + pH-icc3i-H
1233	*fkbp39Δ::kanMX6 ago1Δ::hph* + pH-icc3i-H
1174	h+ *otrR*(SphI)::*ura4 ura4 DS/E leu1-32 ade6-M210 fkbp41Δ::hphMx6 ago1Δ::kanr*

Table 3.1: *S. pombe* strains used in this study

strain number	genotype
106	h+ *otrR*(SphI)::*ura4 ura4 DS/E leu1-32 ade6-M210* + p379
109	h+ *otrR*(SphI)::*ura4 ura4 DS/E leu1-32 ade6-M210 ago1Δ::kanr* + p379
114	h- *leu1-32 ade6-M210 fkbp39Δ::kanMX6* + p379
115	*fkbp39Δ::kan ago1Δ::hph lys1::cnp1*-GFP + p379

Table 3.2: *S. pombe* strains + plasmid used in this study

plasmid number	description
p822	pET Duet 6His-Sumo-Fkbp39
p1300	pET Duet 6His-Sumo-Fkbp39_cys
p1322	pET Duet 6His-Sumo-Fkbp39_1-198
p1323	pET Duet 6His-Sumo-Fkbp39_199-361
p1331	pET Duet 6His-Sumo-Fkbp39_1-256
p379	pREP1*nmt1*promoter-3XFLAGTriman

Table 3.3: Plasmids used in this study

3.1.2 Media

	composition
LB (*E. coli*)	10 g/l tryptone, 5 g/l Yeast extract, 10 g/l NaCl, pH 7.0
YES (*S. pombe*)	5 g/l Yeast extract, 30 g/l glucose 0.226 g/l each: leucine, adenine, histidine, lysine, uracil
YEA (*S. pombe*)	5 g/l Yeast extract, 30 g/l glucose, 0.226 g/l each: leucine, histidine, lysine, uracil and 0.0075 g/ adenine
EMMC-LEU (*S. pombe*)	20 g/l glucose, 12.4 g/l EMM without dextrose 0.226 g/l adenine, 0.226 g/l uracil

Table 3.4: List of media used in this study

3.1.3 Oligonucleotides

	target	sequence	use
113C	25S rDNA	TTTTCTCCTTCTCGGGGATT	qPCR
113D	25S rDNA	AACACCACTTTCTGGCCATC	qPCR
1371	25S rRNA	GATTTGAGGTCAA-Atto488	probe
1372	25S rRNA	ACGTTGCCGTGTTGATT-Atto488	probe
1373	25S rRNA	TTTCTGGTGTCTGAT-Atto488	probe
110a F	*tdh1*	CCAAGCCTACCAACTACGA	qPCR
110a R	*tdh1*	AGAGACGAGCTTGACGAA	RT qPCR
153QF	*tri1*	TCGAGCGAGTTGTCACATTC	qPCR
153QR	*tri1*	TGGCAGAGCATTGAGTTGTC	RT qPCR

Table 3.5: Primers used in this study Probe, fluorescent probe used for nascent 60S subunits labeling; RT, primers used for gene-specific retrotranscription; qPCR, primer used for qPCR quantification.

3.1.4 Sequencing data

ChIP sequencing	RNA sequencing
wild type (63)_Fkbp ChIP seq	wild type (63)_total RNA seq
Fkbp39-HA (860)_Fkbp ChIP seq	wild type (65)_total RNA seq
Fkbp41-3xHA (1164)_Fkbp ChIP seq	*fkbp39*Δ (776)_total RNA seq
wild type (63)_Ytm1 ChIP seq	wild type (63)_nascent RNA seq
1xFLAG-Ytm1 (1314)_Ytm1 ChIP seq	*fkbp39*Δ (776)_nascent RNA seq
ago1Δ (638)_Pol II ChIP seq	*swi6*Δ (288)_nascent RNA seq
wild type (63)_Nop1 ChIP seq	wild type (65)_Ago1-bound sRNA seq
1xFLAG-Nop1 (1447)_Nop1 ChIP seq	*fkbp39*Δ (776)_Ago1-bound sRNA seq
1xFLAG-Ytm1 *fkbp41*Δ (1349)_Ytm1 ChIP seq	wild type (63)_total RNA seq from void
1xFLAG-Ytm1 *fkbp39*Δ*fkbp41*Δ (1346)_Ytm1 ChIP seq	*fkbp39*Δ (776)_total RNA seq from void
wild type (63)_H3 ChIP seq	*ago1*Δ (207)_total RNA seq
fkbp39Δ (776)_H3 ChIP seq	*fkbp39*Δ*ago1*Δ (930)_total RNA seq
wild type (63)_H3K92me ChIP seq	*ago1*Δ (638)_nascent RNA seq
fkbp39Δ (776)_H3K92me ChIP seq	*clr4*Δ (80)_nascent RNA seq
wild type (63)_Pol II ChIP seq	*chp1*Δ (209)_nascent RNA seq
fkbp39Δ (776)_Pol II ChIP seq	
fkbp39Δ (1318)_Pol II ChIP seq	
ago1Δ (1321)_Pol II ChIP seq	
1xFLAG-Ytm1 *fkbp39*Δ (1318)_Ytm1 ChIP seq	

Table 3.6: Sequencing data List of sequencing data, which support this study. For each sequencing, both the strain and the type of experiment is indicated.

3.2 Methods

3.2.1 Strain construction and plasmid generation

All *S. pombe* strained used in this study are listed in table 3.1 and 3.2. The strains were generated by electroporation (Biorad MicroPulser) with plasmids or PCR products for specific gene targeting as described in [94]. *fkbp39_1-256* was designed based on [29], *fkbp39*^{F301CW314CY337K} on [118]. All the plasmids used in this study are listed in table 3.3. Plasmids were generated via enzymatic digestion of the plasmid backbone and the insert, followed by DNA-ligation. For bacterial over expression, *fkbp39* was cloned in pET Duet with 6His-SUMO N terminal tag followed by a HRV-3C recognition site, *fkbp39* mutant constructs were generated from this plasmid via inverse PCR [119].

3.2.2 Over expressed protein purification

Fkbp39 constructs were overexpressed in *E. coli* Rosetta with 0.2 mM IPTG at 18°C overnight. Pelleted cells were resuspended in lysis buffer (500 mM NaCl, 20 mM imidazole, 50 mM Hepes pH 7.5) supplemented with 3 mM β-mercaptoethanol, 1 mM PMSF and lysozyme and lysed by sonication. The clear supernatant was incubated with Ni Sepharose 6 Fast Flow resin (GE Healthcare) for 30 minutes at 4°C. The resin was washed with lysis buffer and with 4 bed volumes of washing buffer (500 mM NaCl, 40 mM imidazole, 50 mM Hepes pH 7.5, 3 mM β-mercaptoethanol). The bound protein was eluted with 5 bed volumes of elution buffer (350 mM NaCl, 300 mM imidazole, 35 mM Hepes pH 7.5, 3 mM b-mercaptoethanol). The protein tag was proteolytically removed during overnight dialysis at 4°C against 300 mM NaCl, 30 mM Hepes pH 7.5, 3 mM β-mercaptoethanol. To remove the tag, the protein was incubated again with Ni Sepharose 6 Fast Flow resin (GE Healthcare) for 25 minutes at 4°C (imidazole was adjusted to 20 mM). For phase separation studies (turbidity assays and fluorescence microscopy), the protein was further purified via ion exchange (SP column, GE Healthcare) using a linear gradient of salt starting from 250 mM NaCl in 30 mM Hepes pH 7.5 1 mM DTT (ion exchange was performed with the assistance of Dr. Silvija Bilokapic Halic).

3.2.3 Turbidity assay

Fkbp39, purified from *E. coli* over-expression culture via ion exchange, was dialyzed against 300 mM NaCl, 10 mM Tris pH 7.5, 1 mM DTT and concentrated to 90 μM. Serial dilutions of the protein were prepared in 125 mM NaCl, 10 mM Tris pH 7.5 with or without crowder (15% PEG), in a final volume of 10 μl. Alternatively serial dilutions of Fkbp39 were prepared in 125 mM NaCl, 10 mM Tris pH 7.5 with 50 ng/μl of nucleosomalDNA or 50 ng/μl of S. pombe rRNA (enriched from total RNA by 30% ethanol precipitation). Dilutions were incubated for 10 minutes at room temperature. Turbidity was determined by measuring UV-Vis absorbance at 340 nm using CLARIOstar microplate reader (BMG LabTech; NC, USA). Samples were prepared in triplicate.

3.2.4 Fluorescence microscopy

Fkbp39_cys was purified as described above, with the only difference that 0.5 mM TCEP replaced DTT during ion exchange. For fluorescent cysteine labeling the protein was concentrated to 50 μM and incubated either with Alexa Fluor™ 546 C5 Maleimid (Thermo Fisher) or CF®405 dye (Biotium, Fremont, CA) for two

hours at room temperature following the manufacturer instructions. The labeling reaction was quenched with excess DTT. The protein was dialyzed 4 times against 300 mM NaCl, 10 mM Tris pH 7.5, 1 mM DTT to completely remove the unreacted dye. A mixture of labeled and non labeled Fkbp39 was concentrated for fluorescence microscopy experiments.

Fkbp39-546 serial dilutions were prepared with 15% PEG or without, in 150 mM NaCl, 10 mM Tris pH 7.5, 1 mM DTT and allowed to equilibrate before imaging with a 3i marianas spinning disk confocal microscope with SlideBook 6.0 software (Intelligent Imaging Innovations, Inc., Denver, CO). Alternatively, Fkbp39-546 serial dilutions were prepared either with 50 ng/μl nucleosomal DNA or with 50 ng/μl *S. pombe* rRNA in 150 mM NaCl, 10 mM Tris pH 7.5, 1 mM DTT, 10% PEG and 500 nM SYTO40^{TM} (Thermo Fisher).

Fkbp39:nucleosomes condensates were formed by mixing 5 μM Fkbp39-405 with 1.3 pmole of labeled nucleosomes (alexa 647 dye) in 7.5 mM Tris, 12.5 mM sodium phosphate, 137.5 mM NaCl, 2 mM MgCl2, pH 8.0. Fkbp39:nascent 60S subunits condensates were formed by mixing 5 μM Fkbp39-405 with 1.3 pmole of labeled nascent 60S subunits (atto 488 dye). Condensates were transferred to a 16-well CultureWell chambered slide (Grace BioLabs, Bend, OR) coated with PlusOne Repel Silane ES (GE Healthcare,Pittsburgh,PA) and Pluronic F-127 (Sigma-Aldrich, St. Louis, MO) and allowed to equilibrate for an hour at room temperature. To test the competition between nucleosomes and nascent 60S subunits for binding to Fkbp39, either 1.3 pmole of labeled nascent 60S subunits were added to pre-equilibrated Fkbp39:nucleosomes condensates, or 1.3 pmole of labeled nucleosomes were added to pre-equilibrated Fkbp39:nascent 60S subunits condensates. Condensates were let to incubate for an additional hour. As control for dilution, buffer was added to both pre-equilibrates Fkbp39:nucleosomes and Fkbp39:nascent 60S subunits condensates. Condensates were imaged using a 780 NLO point scanning confocal microscope (Carl Zeiss Microscopy GmbH, Jena, Germany) with 63x Plan Apochromat (N.A. 1.4) objective. Imaging parameters were adjusted to offset any fluorescence signals from buffer alone. Partition coefficients were calculated for each component using the equation: $(I^{dense}/I^{light})/C.F.$, where I^{dense} is the mean intensity inside condensates, I^{light} is the mean intensity outside the condensates and C.F. is the correction factor for the differences in quantum yields of the each dye in highly viscous environments [55]. Partition coefficients for each component were measured from more than 300 condensates and averaged over four imaging fields per condition. Since nascent 60S subunits are bigger than nucleosomes, we normalized nascent 60S subunits and nucleosomes partition coefficients with respect to their masses. We estimated nascent 60S subunits to be about 9.7 times bigger in mass than nucleosomes. Moles and mass for nascent 60S subunits are approximate, they should be considered with at least 1.5 fold uncertainty.

3.2.5 *S. pombe* endogenous protein purification

Yeast cultures OD 1 were pelleted and resuspended in lysis buffer (100 mM NaCl, 7.5 mM MgCl2, Na Phosphate pH 8, 0.1% Nonidet P40, 5% glycerol) supplemented with 1 mM DTT, 1 mM PMSF and Complete EDTA-free Protease Inhibitor Cocktail (Roche) in a 1:5 buffer:pellet ratio. The suspension was dripped in liquid nitrogen to create small frozen drops suitable for cryogenic grinding by Freezer Mill (SPEXSample Prep), alternatively cells were disrupted by mechanical lysis with BioSpec FastPrep-24 bead beater. The powder pellet was thawed and lysis buffer without glycerol was added to reach a final buffer:pellet ratio of 1:1. The lysate was incubated either with Pierce universal nuclease for Cell lysis (Thermo Fisher) or DNase I (Thermo Scientific, in this case the buffer was supplemented with 130 μM CaCl2) for 30 minutes at 4°C on rotation. Cell debris was removed by centrifugation and the normalized crude lysate was incubated with 100 μl anti-FLAG M2 affinity gel (Sigma) for 3 hours at 4°C on rotation. The beads were extensively washed with lysis buffer without glycerol and with elution buffer (100 mM NaCl, 7.5 mM MgCl2, 100 mM sucrose, Na Phosphate pH 8). Elution was performed three times by adding 150 μl of elution buffer supplemented with 3XFLAG peptide (Sigma, final concentration 150 μg/ml) to the beads, incubated for 20 minutes shaking at 4°C. The protein content was analyzed on denaturing acrylamide gel. Samples were eventually used for mass spectrometry analysis (Proteomics Core Facility, EMBL Heidelberg and Proteomics Facility, St. Jude Children's Research Hospital, Memphis).

3.2.6 Nucleosomes and *S. pombe* nascent 60S subunits labeling

Nucleosomes were assembled by Dr. Silvija Bilokapic Halic as described in [120]. For fluorescence microscopy experiments, nucleosomes were assembled using fluorescent labeled DNA (PCR amplified using alexa 647 labeled primers, IDT).

Nascent 60S subunits purified from *S. pombe* through Fkbp39-FLAG endogenous protein purification, were incubated over night with a 100 fold excess of single stranded atto488 labeled DNA oligos (IDT) complementary to the 25S rRNA at 4°C (oligos are listed in table 3.5). To remove non-bound oligos, the complex was dialyzed against 100 mM NaCl, 7.5 mM MgCl2, 50 mM Na phosphate pH 8.

3.2.7 *In vitro* binding assays

Fkbp39, purified from *E. coli* over-expression culture, was transferred to incubation buffer (100 mM NaCl, 5 mM MgCl2, 50 mM Na phosphate pH 8, 20% glycerol, 1 mM DTT for cysteine mutant) via PD-10 desalting column (GE Healthcare). Increasing amount of Fkbp39 were incubated with either DNA, RNA, nucleosomes, nascent 60S subunits or nascent 40S subunits at 20 °C for 30 minutes in incubation buffer. The complex formation was analyzed on 6% TBE acrylamide gel (Fkbp39:DNA; Fkbp39:RNA; Fkbp39:nucleosome complex) or on 0.8% TBE agarose gel (Fkbp39:nascent 60S subunits complex, Fkbp39:nascent 40S subunits complex). For competition experiments, Fkbp39 was pre-incubated with either nucleosomes or nascent 60S subunits at 20 °C for 20 minutes in incubation buffer, then the other component was added and the reaction incubated for further 20 minutes The reaction was analyzed both on 6% TBE acrylamide gel and 0.8% TBE agarose gel to follow Fkbp39:nucleosome and Fkbp39:nascent 60S subunits complexes formation. All the gels were stained with SYBR Gold (ThermoFisher Scientific). Nascent 60S subunits and nascent 40S subunits mole determination carries a certain degree of uncertainty (estimated from RNA absorbance).

3.2.8 Co-immunoprecipitation

50 ml of pelleted yeast cells were resuspended in lysis buffer (100 mM NaCl, 5 mM MgCl2, 50 mM Tris pH 7.5, 0.1% Nonidet P40, 5% glycerol) supplemented with 1 mM DTT, 1 mM PMSF, complete EDTA-free Protease Inhibitor Cocktail (Roche) and Pierce universal nuclease for Cell lysis (Thermo Fisher), and disrupted by mechanical lysis with BioSpec FastPrep-24 bead beater. Cell debris was removed by centrifugation and the normalized crude lysate was incubated with 10 μl anti-FLAG M2 affinity gel (Sigma) for 3 hours at 4°C on rotation. The beads were extensively washed with lysis buffer. Elution was performed two times adding 15 μl of lysis buffer supplemented with 3XFLAG peptide (Sigma, final concentration 150 μg/ml) to the beads, incubated for 20 minutes shaking at room temperature. The protein content was analyzed by western blot (Monoclonal ANTI-FLAG M2-Peroxidase (HRP) antibody Sigma, HA-probe Santa Cruz Biotechnology, Anti-Mouse IgG-Peroxidase Sigma).

3.2.9 Chromatin immunoprecipitation qPCR and sequencing

Mid-log phase yeast cultures were cross linked with 1% formaldehyde for 15 minutes at room temperature and quenched with 125 mM glycine. The pellet was resuspended in lysis buffer (250 mM KCl, 1X Triton

x-100, 0.1% SDS, 0.1% Na-Desoxycholate, 50 mM Hepes pH 7.5, 2 mM EDTA, 2 mM EGTA, 5 mM MgCl2, 0.1% Nonidet P40, 20% glycerol) with 1 mM PMSF and Complete EDTA-free Protease Inhibitor Cocktail (Roche). Cells were disrupted by mechanical lysis with BioSpec FastPrep-24 bead beater and the DNA sheared via sonication. Cell debris was removed by centrifugation and the normalized crude lysate was incubated over night at 4°C with the immobilized antibody. The resin was extensively washed with lysis buffer and the DNA-protein complex eluted with 150 μl of elution buffer (50 mM Tris HCl pH 8, 10 mM EDTA, 1% SDS) at 65°C for 15 minutes. Both inputs (normalized crude lysate aliquots) and elutions were de-crosslinked (95°C for 15 minutes) and treated with RNase A (Thermo Scientific) and Proteinase K (Roche) at 37°C over night. DNA was recovered by phenole-chloroform-isoamylalcohol (25:24:1, Roth) extraction followed by ethanol precipitation. DNA was analyzed by qPCR with rDNA specific primers (listed in table 3.5), the fold enrichment was normalized to input levels. qPCR was performed using the DyNamo Flash SYBR Green qPCR Master Mix (Thermo Scientific), in the Toptical thermocycler (Biometra), according to the manufacturer's instructions. Alternatively, ChIP-seq libraries were prepared using the NEBNext Ultra II DNA Library Prep Kit for Illumina (NEB) following the manufacturer instructions.

antibody	experiment
HA-probe, Santa Cruz Biotechnology*	Fkbp39 and Fkbp41 ChIP-seq
anti-FLAG M2 Magnetic Beads, Sigma	Nop1 and Ytm1 ChIP-seq
anti-H3K9me2, Abcam (1220)*	H3K9me2 ChIP-seq
anti-H3, Active Motif (61475)*	H3 ChIP-seq
anti-RNA polymerase II CTD repeat phospho S2, Abcam (5095)*	Pol II ChIP-seq

Table 3.7: Antibodies used in ChIP experiments List of antibodies used in ChIP experiments. Antibodies marked with *, were immobilized on Dynabeads Protein A (Invitrogen).

3.2.10 Nascent RNA labeling and RNA library preparation

For nascent RNA labeling, yeast over night cultures were diluted in YEA media and let grow up to OD 600 nm 0.6. 4 Thiouracil (Sigma) was supplemented to 5 mM final concentration, and aliquots for RNA extraction were taken after 2 and 10 minutes (and before 4 Thiouracil addition). Cells were briefly centrifuged and immediately frozen in liquid nitrogen. For RNA isolation (hot phenol method), the pellet was resuspended in 500 μl lysis buffer (300 mM NaOAc pH 5.2, 10 mM EDTA, 1% SDS) and 500 phenol-chloroform-isoamylalcohol (25:24:1, Roth) and incubated at 65°C for 10 minutes, mixing. The aqueous fraction was separated from the organic fraction by centrifugation at 20000 x g for 10 minutes and then ethanol precipitated. Nucleic

acids were treated with DNAse I (Thermo Scientific) for 2 hours at 37°C and the RNA was recovered with a second phenol-chloroform-isoamylalcohol extraction. 30 μg of RNA were treated with EZ-Link HPDP-Biotin (Thermo Scientific) to biotin-label the 4 Thiouracil -SH group. The reaction was carried on in 500 μl of biotinylation buffer (100 mM Tris pH 7.5, 10 mM EDTA) and 300 μg/ml EZ-Link HPDP-Biotin for 2 hours at room temperature shaking in a thermomixer. RNA was recovered by phenol-chloroform-isoamylalcohol extraction followed by ethanol precipitation. The nascent RNA (biotin labeled) was isolated thanks to the interaction biotin-streptavidin. Prior to binding, streptavidin beads (Roche) were blocked with a non specific single stranded DNA sequence (hph cassette sequence) in binding buffer (100 mM NaCl, 10 mM Tris pH 7.5, 1 mM EDTA) for 20 minutes shaking in a thermomixer at room temperature. A spike in DNA sequence (mouse Ahctf1 sequence, coding for ELYS protein) was added to the beads, which were then distributed to the RNA samples and incubated for 15 minutes shaking in a thermomixer at room temperature. The beads were washed 6 times with washing buffer (1 M NaCl, 100 mM Tris pH 7.5, 10 mM EDTA, 0.1% tween), the first 3 performed at 65°C. Biotinylated RNA was eluted twice with 100 mM DTT for 5 minutes shaking in a thermomixer at room temperature and ethanol precipitated. The recovered RNA was used for the preparation of RNA library using the NEBNext Ultra II Directional RNA Library Prep Kit for Illumina (NEB) following the manufacturer instructions. For total RNA libraries, RNA was extracted following the hot phenol method, treated with DNAse I (Thermo Scientific) and used for the preparation of RNA library using the NEBNext Ultra II Directional RNA Library Prep Kit for Illumina (NEB) following the manufacturer instructions.

3.2.11 Polysome profiles

100 ml of yeast cultures OD 1 were pelleted, frozen and then resuspended in lysis buffer (100 mM KOAc, 7.5 mM Mg(OAc)2, 125 mM sucrose, 20 mM Hepes pH 7.5) supplemented with 1 mM DTT, 1 mM PMSF and Complete EDTA-free Protease Inhibitor Cocktail (Roche). Cells were lysed by glass bead disruption using BioSpec FastPrep-24 bead beater and cells debris was removed by centrifugation. Between 5-10 260 nm absorbance unit of the normalized samples were loaded onto a linear 10-50% sucrose gradient (100 mM KOAc, 7.5 mM Mg(OAc)2, 20 mM Hepes pH 7.5, 1 mM DTT) and centrifuged for 3 hours onto SW40 Beckman Coulter rotor at 40K rpm. For cycloheximide treatment, cells were incubated with 0.1 mg/ml cycloheximide for 5 minutes prior to pelleting. All the solutions were then supplemented with 0.1 mg/ml cycloheximide. Gradients were collected on a Gradient Station (Biocomp) with an Econo UV Monitor (Biorad) and a FC203B Fraction Collector (Gilson). For quantification of the 260 nm signal, the polysome profiles

from different strains were aligned and the peaks corresponding to different species identified. For each strain the signal from the void fraction (non ribosome) and the ribosome fractions (everything but the void) were normalized to the signal of the whole gradient.

3.2.12 Growth assay and minichromosome loss assay

Tenfold serial dilutions of cultures were spotted on YES rich media (or YEA low adenine media), so that the highest density point contained 10^5 cells. Plates were incubated at 32° and imaged after 2 days.

For minichromosome loss assay, a single colony containing the minichromosome system (white on low adenine plates) was grown over night in rich media and then plated on YEA low adenine media. When colors were clearly visible, plates were imaged and white/red colonies counted.

3.2.13 Ago1-bound sRNAs sequencing

Endogenous 3xFLAG-tagged Ago1 was purified from *fkbp39*Δ and wild type cells by affinity purification as described in [94]. Cell pellet was resuspended in lysis buffer (50 mM HEPES pH 7.5, 1.5 M NaOAc, 5 mM MgCl2, 2 mM EDTA pH 8, 2 mM EGTA pH 8, 0.1% nonidet P-40, 20% glycerol) supplemented with 1 mM PMSF, 0.8 mM DTT and Complete EDTA free Protease Inhibitor Cocktail (Roche). Cells were lysed by glass bead disruption using BioSpec FastPrep-24 bead beater and cells debris was removed by centrifugation. The cleared supernatant was incubated with 30 μl FLAG-M2 agarose beads (Sigma) at 4°C for 1.5 hour. The resin was washed 5 times with lysis buffer and Ago1 was eluted with 1% SDS, 300 mM NaOAc. The protein-bound RNA was recovered by phenol-chloroform-isoamylalcohol extraction and ethanol precipitation. Small RNAs in the length range 20-30 nt were excised from an 18% polyacrylamide urea gel. 2 pmol of a preadenylated 3' adaptor oligonucleotide (miRNA Cloning Linker-1 from IDT, 5'-App CTG TAG GCA CCA TCA AT/ddC/-3') were ligated in a 10 μl reaction with 5 U T4 RNA ligase (TaKaRa), ligation buffer without ATP and 5 U RNasin (Promega) at 20°C for 2 hours. The 3' ligated products were purified on an 18% acrylamide urea gel. The 5' adaptor ligation was performed in a 10 μl reaction with 2 pmol 5' adaptor oligonucleotide (5'-GUU CAG AGU UCU ACA GUC CGA CGA UC-3'), 5 U RNasin (Promega), 0.06 μg BSA, 5 U T4 RNA ligase (Thermo Fischer Scientific) and 1x ligation buffer with ATP (Thermo Fischer Scientific) at 20°C for 2 hours. The ligated products were gel purified and reverse transcribed with 10 pmol primer (RT primer: 5'- GTG ACT GGA GTT CAG ACG TGT GCT CTT CCG ATC GAT TGA TGG TGC CTA CAG-3') and the SuperScript III First Strand Synthesis System (Thermo Fischer Scientific). The cDNA was PCR-

amplified using the Illumina P5 5' primer and the Illumina P7 3' primer (the P7 primer contains the sample specific barcode).

3.2.14 Analysis of sequencing data

Single end sequencing of libraries was performed on an Illumina GAIIX sequencer at the LAFUGA core facility of the Gene Center, Munich. The Galaxy platform was used to demultiplex the obtained reads with Je-Demultiplex-Illu [121]. Demultiplexed illumina reads were mapped to the *S. pombe* genome, allowing 2 nucleotides mismatch using Novoalign (htttp://www.novocraft.com).

ChIP seq datasets were normalized to regions, which were not changed in the different strains (background). Steady state RNA, RNA from the void fraction of polysome profiles and small RNA datasets were normalized to total reads. For nascent RNA libraries, reads were normalized to total reads and the signal/background factor, defined as the fraction of *hph* background sequences present in each sample relative to its background, T0, for which this parameter was set to 1.

Custom perl scripts were used for reads assignment, extractions and quantification. We used the genome sequence and annotation available from the *S. pombe* Genome Project [85]. The data are displayed using the Integrative Genomics Viewer (IGV) [122]. Sequenced strains are listed in table 3.6.

3.2.15 *In vivo* translation assay

Cells containing the pREP1 plasmid encoding FLAG-Tri1 under the control of the *nmt1* promoter, were grown on EMMC-LEU + 15 μM thiamine solid media. In the evening, cells grown in EMMC-LEU + 15 μM thiamine liquid media were pelleted, washed with sterile water and resuspended in EMMC-LEU to OD600 0.08 (T0). Aliquots for protein and RNA extraction were taken at T0 and after 10-12-14 hours post induction.

For protein extraction, cells were resuspended in lysis buffer (50 mM HEPES pH 7.5, 1.5 M NaOAc, 5 mM MgCl2, 2 mM EDTA pH 8, 2 mM EGTA pH8, 0.1% nonidet P-40, 20% glycerol) supplemented with 1 mM PMSF, 1 mM DTT and Complete EDTA free Protease Inhibitor Cocktail (Roche). Cells were disrupted by mechanical lysis with BioSpec FastPrep-24 bead beater and cell debris was removed by centrifugation. The normalized crude lysate was analyzed by western blot (Monoclonal ANTI-FLAG M2-Peroxidase (HRP) antibody Sigma, equal loading was veryfied by amido black staining). The western blot signal was quantified using Quantity One (BIORAD), with the local background subtraction setting. FLAG-Triman intensity in wild type cells at 14 hours was set to 1.

RNA was extracted following the hot-phenol method previously described. 50 ng of total RNA was reverse transcribed with SuperScript III First Strand Synthesis System (Thermo Scientific) and specific primers (listed in table 3.5). qPCR was performed with 1 ng of cDNA, using the DyNamo Flash SYBR Green qPCR Master Mix (Thermo Scientific), in the Toptical thermocycler (Biometra), according to the manufacturer's instructions (primers listed in table 3.5). Non reverse-transcribed total RNA was used as control for DNA contamination. *tri1* transcript amounts were normalized to *tdh1*, wild type value at 14 hours was set to 1.

Chapter 4

Results

4.1 Fkbp39 and Fkbp41 localize to the rDNA locus

S. pombe encodes two NPL-FKBP proteins, Fkbp39 (SPBC1347.02) and Fkbp41 (SPAC27F1.06c). Proteins belonging to this family have a very conserved domain organization: the N terminal nucleophosmin like domain, responsible for pentamer oligomerization, the intrinsically disordered region, with acidic and basic tracts, and the C terminal FKBP prolyl isomerase domain, fig. 4.1.

Fkbp39 was previously described as a histone chaperone able to load histones on naked DNA [29]. *In vitro* binding assays confirm that Fkbp39 can bind short DNA oligos, fig. 4.2(a). More interesting, Fkbp39 binds nucleosomes, fig. 4.2(b), in agreement with what previously shown for Fpr4 [31]. Binding to DNA is necessary for this interaction since Fkbp39 does not interact with nucleosome core particles, fig. 4.2(c). Fkbp39 residues 1-256, spanning the oligomerization domain and the intrinsically disordered region, were proved to be sufficient for the *in vitro* histone chaperone activity [29]. *In vitro* nucleosomes binding assays confirm that Fkbp39 intrinsically disordered region (residues 120-256) is required for nucleosomes binding, although the prolyl isomerase domain contributes as well, fig. 4.2(d)

ChIP-seq experiments show that Fkbp39 and Fkbp41 bind chromatin *in vivo* and are localized specifically at the rDNA locus, fig. 4.4(a), in agreement with what previously reported for *S. cerevisiae* Fpr4 [29], and human NPM1 [19, 22, 20]. Both proteins show a peak predominantly over the 25S and the 3'ETS, fig. 4.4(b), 4.4(c). ChIP-qPCR experiments show that both Fkbp39 first 256 residues (Fkbp39_1-256) and Fkbp39 prolyl isomerase mutant (Fkbp39_activity*) localize to chromatin *in vivo*, although with a 50% reduction compared to the wild type protein, fig. 4.5(a). Collectively these experiments show that Fkbp39

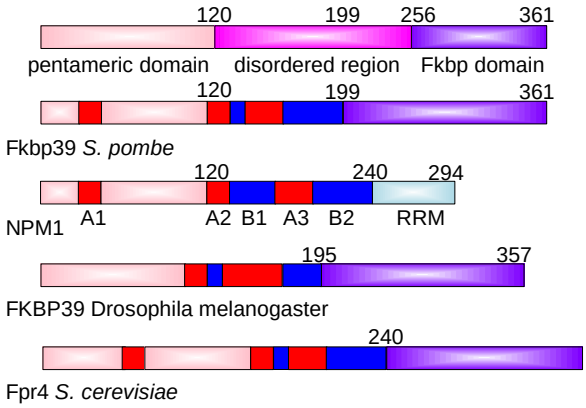

(a)

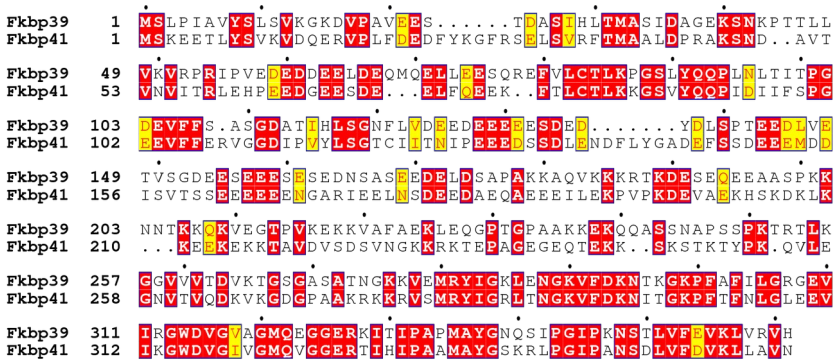

(b)

Figure 4.1: NPL-FKBP proteins domain organization (a), Domain organization of NPL-FKBP proteins relative to NPM1. The N terminal NPL oligomerization domain is in pink, followed by the intrinsically disordered region, depicted in lilac, composed by acidic and basic tracts (in red and blue respectively). NPM1 C terminal nucleic acid binding domain (RRM) is in light blue, whereas the C terminal FKBP prolyl isomerase domains are in violet. (b), Fkbp39 and Fkbp41 alignment generated with the ESPript server [123]. Conserved residues are in red, residues with similar properties in yellow.

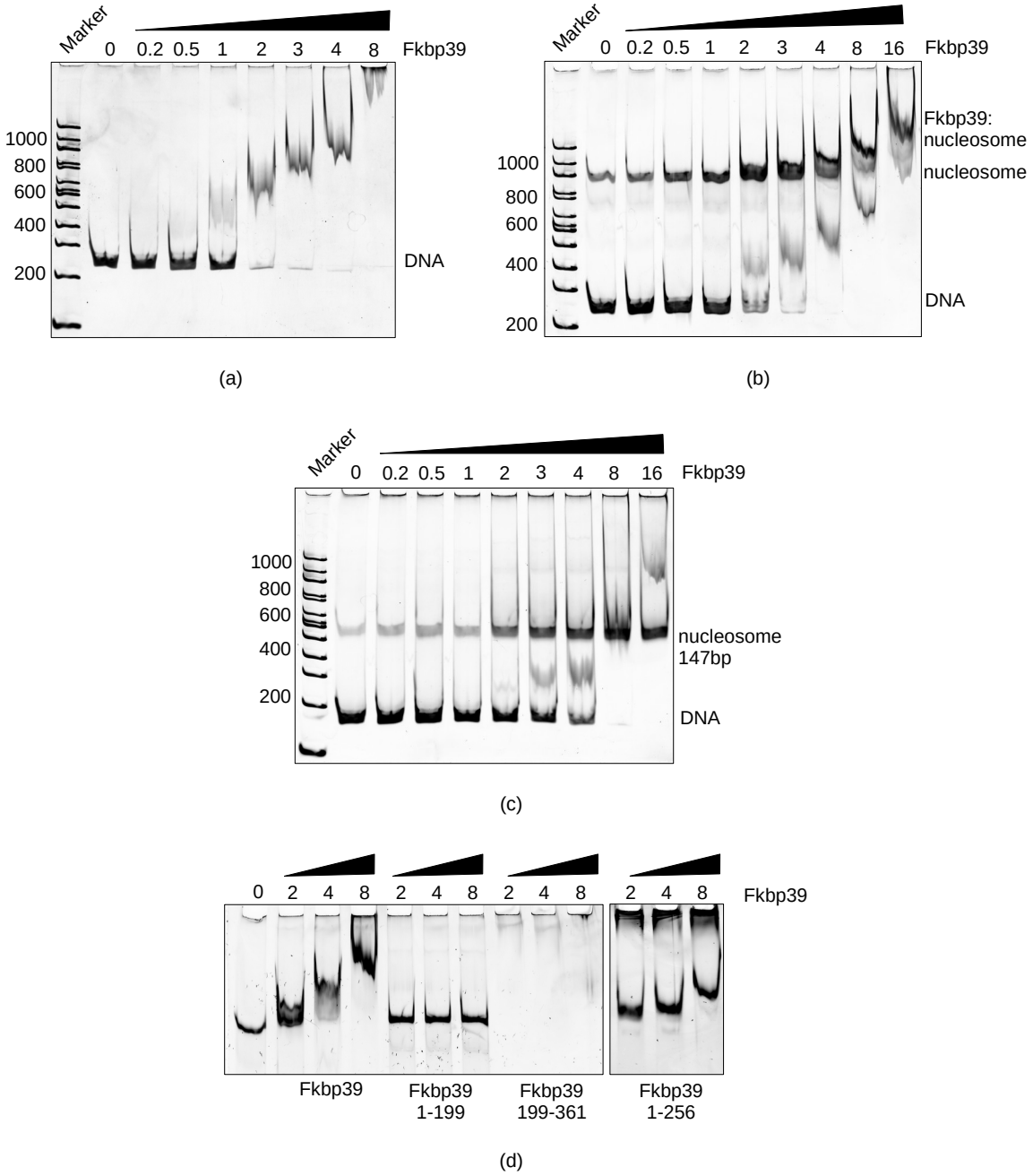

Figure 4.2: Nucleosome binding *In vitro* binding assays. Numbers indicate Fkbp39 molar ratio in respect to the binding parter, with Fkbp39 functional unit being a pentamer. Fkbp39 was incubated with nucleosomal DNA (227 bp) (a), with nucleosomes with 40 bp of symmetric linker DNA (b), with nucleosome core particles (c). (d), Fkbp39 domains binding to nucleosomes. The prolyl isomerization domain (Fkbp39_199-361), lacking the NPL domain, does not form pentamers. Complexes were visualized on 6% TBE acrylamide gel stayned with SYBR gold. (a), (c) and (d) are representative of three independent assays, (b) of two. Nucleosomes were assembled by Dr. Silvija Bilokapic Halic.

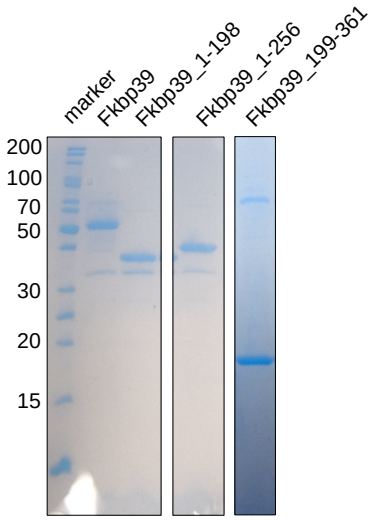

Figure 4.3: Fkbp39 purified constructs used for *in vitro* assays Representative SDS gels of Fkbp39 and the indicated domains used for the *in vitro* binding assays.

intrinsically disordered region is required for rDNA localization but the prolyl isomerase domain also contributes to chromatin binding. Fkbp41 rDNA localization is reduced to 50% upon *fkbp39* deletion and in *fkbp39* mutant backgrounds, fig. 4.5(b). This suggests that the two NPL-Fkbp proteins interact and that Fkbp39 is required for Fkbp41 localization.

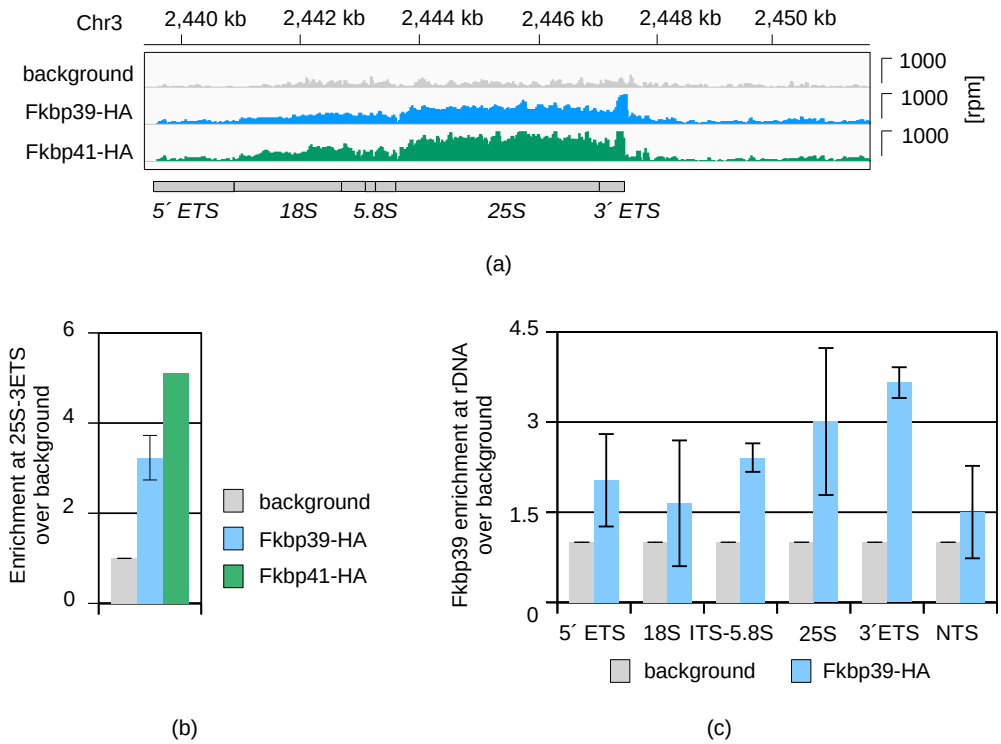

Figure 4.4: NPL-FKBP proteins localize to the rDNA locus (a), NPL-FKBP proteins ChIP-seq. Both proteins localize at rDNA with a peak over the 25S and 3'ETS. Scale bars on the right denote read numbers per million reads (rpm) normalized over background regions. The coordinates of the genomic location are indicated above the chart, the rDNA locus organization is depicted below in gray boxes. (b), Quantification of the reads mapping over the 25S and 3'ETS rDNA locus from ChIP-seq experiments. Reads were normalized to background regions and plotted relative to background. Fkbp39 quantification is the average of two independent ChIP-seq experiments and error bars represent the standard error. (c), Fkbp39 ChIP-seq reads quantification over the rDNA locus from two independent ChIP-seq experiments. Error bars represent standard deviation. Reads were normalized to background regions and plotted relative to background.

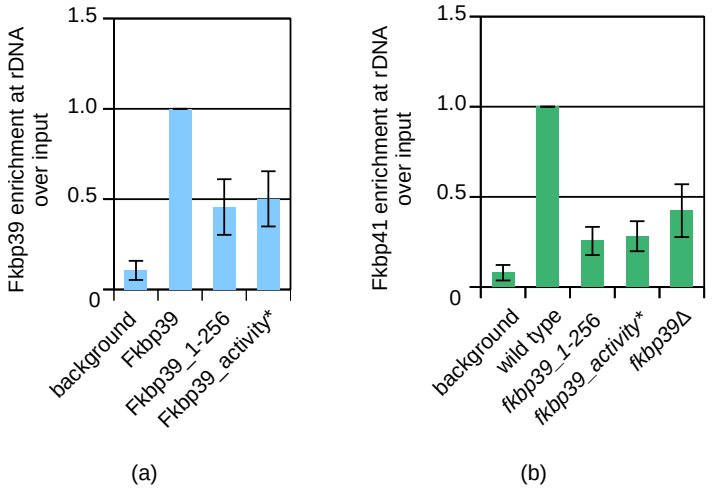

Figure 4.5: The FKBP domain contributes to chromatin binding (a), ChIP-qPCR experiment showing Fkbp39 wild type and prolyl isomerase mutants enrichment at rDNA. Fkbp39_activity* carries three point mutations, F301CW314CY337K. Fkbp39 constructs enrichment at rDNA was calculated over input and the enrichment for Fkbp39 wild type was set to 1. Error bars represent standard error, as an average of three independent experiments. (b), ChIP-qPCR experiment showing Fkbp41 enrichment at rDNA in different background strains: wild type, *fkbp39_1-256*, *fkbp39_activity** and *fkbp39*Δ. Fkbp41 enrichment at rDNA was calculated over input, and the enrichment in wild type background was set to 1. Error bars represent standard error, as an average of three independent experiments.

4.2 Fkbp39 interacts with nascent 60S subunits

NPM1 and Fpr4 co-purify with ribosome biogenesis factors [21, 32], and this strongly suggests they have a role in ribosome biogenesis. Endogenous Fkbp39 purification followed by mass spectrometry confirms that Fkbp39 interacts with ribosomal proteins and ribosome biogenesis factors (almost 30% of the identified interacting proteins), fig. 4.6 and table 4.1. It is important to underline that even if ribosomal proteins are often contaminants in mass spectrometry, this is not true for ribosome biogenesis factors. Moreover, within the identified proteins, there are all the components of a known complex involved in 60S subunit biogenesis (the Ytm1-Erb1-Ppp1 complex composed by Ytm1-Erb1-Nop7 in *S. cerevisiae* [124]), which supports the good quality of the data. The biogenesis factors identified by mass spectrometry are specifically involved in 60S subunit nucleolar maturation, which is in agreement with Fkbp39 localization over the 25S rDNA. The second most abundant protein after Fkbp39 itself is always Fkbp41, suggesting that these two proteins form heteropentamers.

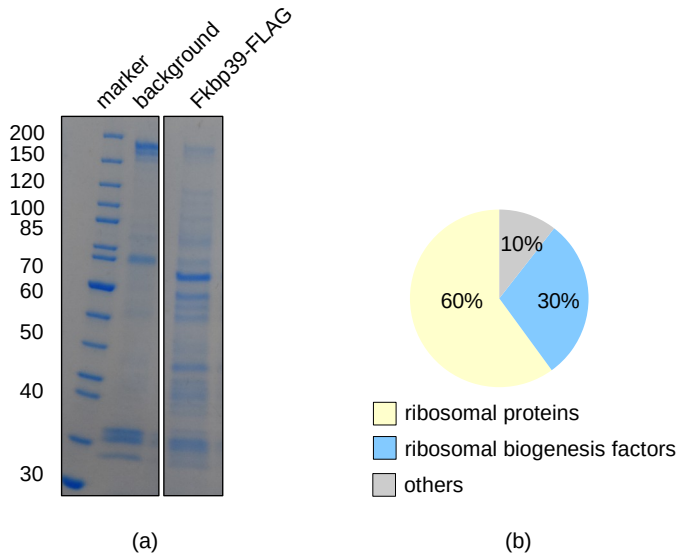

Figure 4.6: Fkbp39 purification (a), Representative SDS gel from Fkbp39 purification used for mass spectometry analysis. (b), Functional classification of the specific Fkbp39 co-immunoprecipitating proteins.

	spectral counts (unique peptides)					
protein	no tag	Fkbp39-FLAG6His	no tag (1)	Fkbp39-FLAG6His (1)	no tag (2)	Fkbp39-FLAG6His (2)
Fkbp39	0(0)	355(22)	3(1)	281(19)	12(6)	597(34)
Fkbp41	0(0)	303(23)	0(0)	231(20)	4(2)	232(26)
Nog1	0(0)	126(29)	0(0)	116(27)	0(0)	31(23)
Ppp1	0(0)	87(21)	0(0)	73(20)	0(0)	14(11)
Nop2	0(0)	79(21)	0(0)	70(21)	0(0)	24(13)
Erb1	0(0)	60(23)	0(0)	60(17)	0(0)	5(5)
Grn1	0(0)	60(20)	0(0)	54(18)	0(0)	4(4)
Ytm1	0(0)	57(17)	0(0)	40(13)	0(0)	9(9)
SPAC8F11.04	0(0)	53(18)	0(0)	52(14)	0(0)	5(4)
Rpf2	0(0)	53(11)	0(0)	54(11)	0(0)	13(10)
Rpl20a	0(0)	47(11)	0(0)	42(8)	0(0)	84(22)
Has1	0(0)	46(15)	0(0)	53(20)	0(0)	11(7)
Brx1	0(0)	45(13)	0(0)	23(7)	0(0)	5(5)
Nsa2	0(0)	45(11)	0(0)	28(10)	0(0)	12(10)

Table 4.1: Fkbp39 interacting proteins Mass spectrometry results, top hits involved in ribosome biogenesis are listed as total peptides count and number of unique peptides per protein (in brackets) for control samples and the endogenously tagged strains. Results from three independent purifications.

Some of the interactions identified through mass spectrometry were confirmed by Co-IP experiments, fig. 4.6. Co-IP proved that Fkbp39 and Fkbp41 interact through the NPL oligomerization domain, supporting the hypothesis of heteropentamers formation, fig. 4.7(a). Fkbp41 also interacts with Ytm1, although this interaction is impaired upon *fkbp39* deletion, fig. 4.7(b). Ytm1 is used as representative for nascent 60S subunits, indeed it is an early 60S subunit-specific biogenesis factor [32], which reproducibly interacts with Fkbp39 (identified in all mass spectrometry experiments). The FKBP prolyl isomerase domain is necessary for the interaction between Fkbp39 and Ytm1, as Fkbp39_1-256 does not interact with Ytm1 in *fkbp41*Δ cells, fig. 4.7(c).

In vitro assays were used to further characterize the interaction between Fkbp39 and nascent 60S subunits. Fkbp39 binds not only DNA but also RNA, fig. 4.8(a). Fkbp39 also binds to purified nascent 60S subunits, fig. 4.8(b). In agreement with *in vivo* Co-IP experiments, the prolyl isomerase domain is necessary for this interaction, fig. 4.8(c). Such an important role for the FKBP domain in binding both to nucleosomes and nascent 60S subunits, fig. 4.2(d), 4.8(c), might sound counterintuitive, especially because the intrinsically disordered region contains both acidic and basic tracts, which could bind via non-specific electrostatic interactions both to nucleic acids and to positively charged proteins. It was anyway suggested

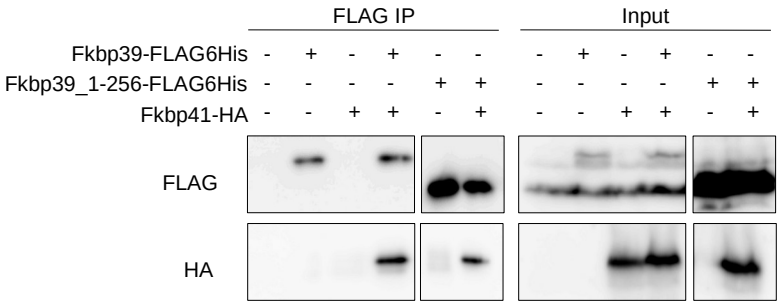

(a)

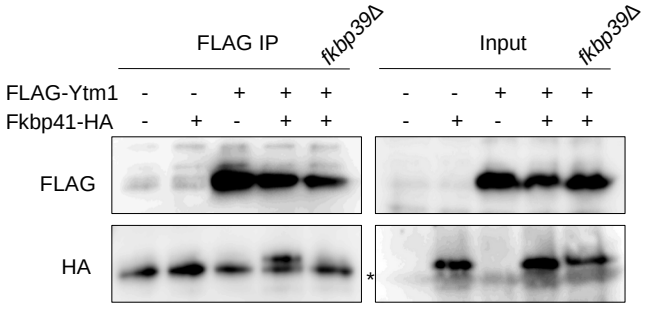

(b)

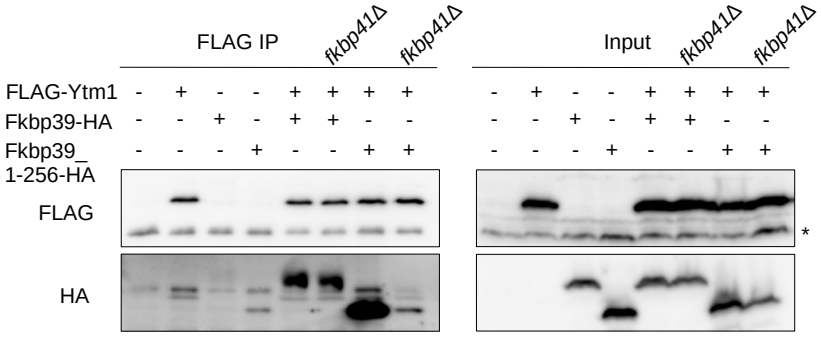

(c)

Figure 4.7: *S. pombe* NPL-FKBP proteins interact with Ytm1 (a), Co-immunoprecipitation experiments between Fkbp39-FLAG6His or Fkbp39_1-256-FLAG6His and Fkbp41-HA; (b), Co-IP between FLAG-Ytm1 and Fkbp41-HA in wild type and *fkbp39Δ* cells; (c), Co-IP between FLAG-Ytm1 and Fkbp39-HA or Fkbp39_1-256-HA in wild type and *fkbp41Δ* cells (c). Immunoprecipitates and inputs were analyzed by anti-FLAG and anti-HA western blot. The asterisks represent antibody non specific signal. These are representative images from independent experiments (two for (a) and (b), three for (c)).

that deletion of the FKBP domain could allow new interactions between the acidic and basic tracts, which are normally restricted, and this, in turn, could mask the contribution of the intrinsically disordered region to the interactions with binding partners [125]. Moreover, the RRM domain is necessary for NPM1 *in vitro* phase separation with rRNA and for its *in vivo* nucleolar localization [56], so the FKBP domain might fulfill a similar function in yeast.

The mass spectrometry result suggests that *in vivo* Fkbp39 binds exclusively to nascent 60S subunits. To test if Fkbp39 can specifically recognize nascent 60S subunits, Fkbp39 binding to both ribosome subunit precursors was tested. Nascent 40S subunits were isolated through endogenous fibrillarin (Nop1 in yeast) purification, as confirmed by mass spectrometry, fig. 4.9(a) and table 4.2. Fibrillarin interacts also with nascent 60S subunits, in agreement with its role in rRNA 2'-*O*-ribose methylation and its localization over the whole rDNA locus, fig. 4.9(b) and 4.9(c). However, this interaction is mediated by RNA and can be disrupted by nuclease treatment. The nascent 40S subunits used for the *in vitro* binding assay were purified from nuclease treated lysates.

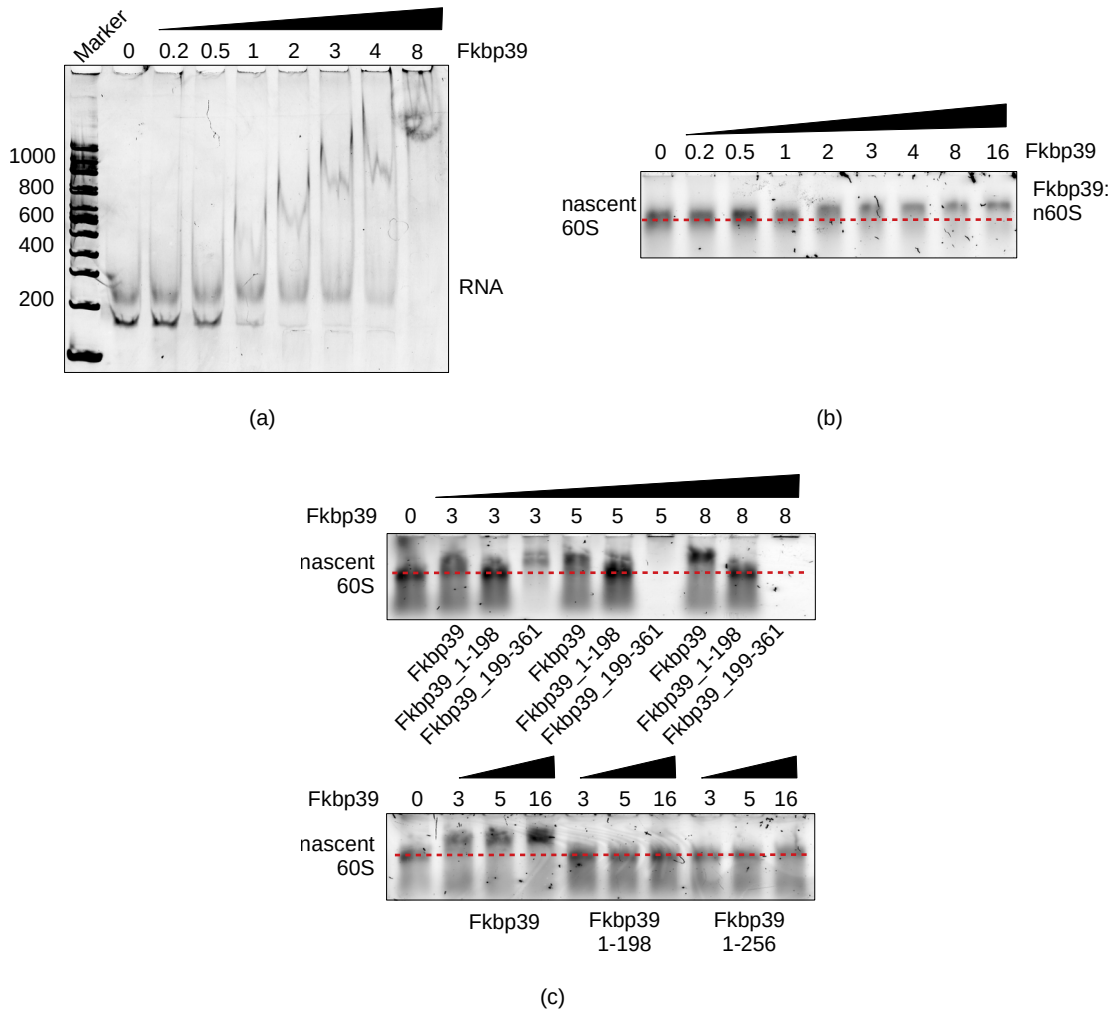

Figure 4.8: The FKBP domain is required for nascent 60S subunits binding *In vitro* binding assays (a), Fkbp39 binding to RNA, the relative molar ratio of Fkbp39 in respect to RNA is indicated, with Fkbp39 functional unit being a pentamer. The formation of the complex was visualized on 6% TBE acrylamide gel stained with SYBR gold. This is a representative experiment of three independent assays. (b), Fkbp39 binding to nascent 60S subunits, the relative molar ratio of Fkbp39 in respect to nascent 60S subunits (n60S) is indicated, with Fkbp39 functional unit being a pentamer. The formation of the complex was visualized on 0.8% TBE agarose gel stained with SYBR gold. The red dash line represents the migration line of n60S. This is a representative experiment of three independent assays. (c), Fkbp39 domains binding to nascent 60S subunits, the relative molar ratio of Fkbp39 mutants in respect to nascent 60S subunits is indicated, with Fkbp39 functional unit being a pentamer, although the prolyl isomerase domain (Fkbp39_199-361) does not form pentamers. The formation of the complex was visualized on 0.8% TBE agarose gel stained with SYBR gold. This is a representative experiment of three independent assays.

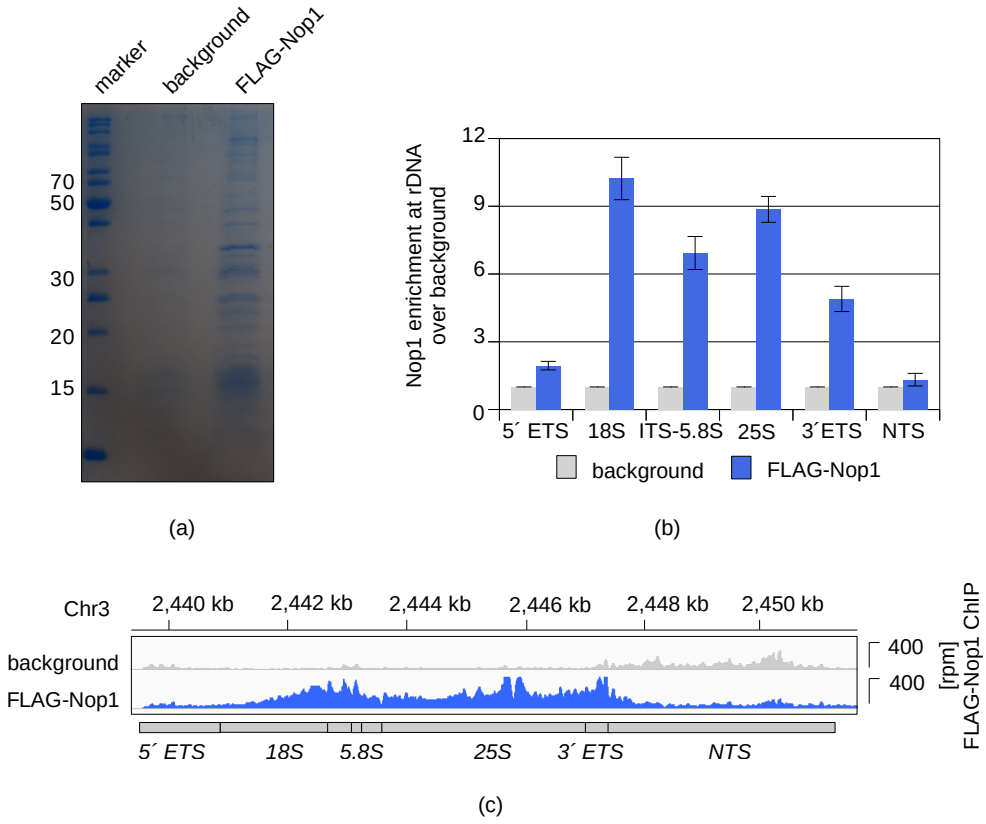

Figure 4.9: Fibrillarin localization at the rDNA locus (a), Representative SDS gel from Nop1 (fibrillarin) purification used for mass spectometry analysis. (b), Nop1 ChIP-seq reads quantification over the rDNA locus from three independent ChIP-seq experiments. Error bars represent the standard error. Reads were normalized to background regions and plotted relative to background. (c), FLAG-Nop1 ChIP-seq. Scale bars on the right denote read numbers per million reads (rpm) normalized over background regions. The coordinates of the genomic location are indicated above the chart, the rDNA locus organization is depicted below in gray boxes.

	spectral counts (unique peptides)					
protein	no tag (DNAse)	FLAG-Nop1 (DNAse)	no tag (nuclease-1)	FLAG-Nop1 (nuclease-1)	no tag (nuclease-2)	FLAG-Nop1 (nuclease-2)
Nop1	0(0)	107(16)	0(0)	194(17)	0(0)	139(15)
Nop56	0(0)	75(17)	0(0)	127(21)	0(0)	88(18)
Dip2	0(0)	84(27)	0(0)	104(27)	0(0)	52(15)
Utp21	0(0)	65(21)	0(0)	95(24)	0(0)	39(14)
Utp13	0(0)	73(24)	0(0)	89(24)	0(0)	43(12)
Utp8	0(0)	54(17)	0(0)	88(21)	0(0)	33(11)
Nop58	0(0)	40(13)	0(0)	81(17)	0(0)	50(13)
Pwp2	0(0)	63(24)	0(0)	78(24)	0(0)	21(12)
Utp4	0(0)	45(16)	0(0)	76(17)	0(0)	47(13)
Nan1 (UTP17)	0(0)	69(19)	0(0)	75(19)	0(0)	31(12)
Utp10	0(0)	67(25)	0(0)	68(27)	0(0)	16(5)
Utp7	0(0)	34(10)	0(0)	64(12)	0(0)	30(9)
Utp18	0(0)	36(12)	0(0)	62(13)	0(0)	17(5)
Sof1	0(0)	28(12)	0(0)	51(11)	0(0)	14(5)
Ytm1*	0(0)	11(5)	0(0)	6(3)	0(0)	0(0)
SPAC8F11.04(Cic1)*	0(0)	15(6)	0(0)	3(3)	0(0)	0(0)
Has1*	0(0)	5(3)	0(0)	0(0)	0(0)	0(0)
Tif6*	0(0)	6(2)	0(0)	0(0)	0(0)	0(0)
Ebp2*	0(0)	6(3)	0(0)	0(0)	0(0)	0(0)

Table 4.2: Fibrillarin interacting proteins Mass spectrometry results, top hits involved in ribosome biogenesis (factors marked with * are involved in 60S biogenesis) are listed as total peptides count and number of unique peptides per protein (in brackets) for control samples and the endogenously tagged strains. Results from three independent purifications, performed with the indicated treatment.

In vitro Fkbp39 binds equally well to nascent 60S and 40S subunits, fig. 4.10. This suggests that Fkbp39 binding to nascent 60S subunits is mediated through non-specific electrostatic interactions and some other factor provides the *in vivo* specificity.

4.3 Nucleosomes and nascent 60S subunits enter Fkbp39-organized condensates

Fkbp39 proved to share several properties with NPM1, for which the role in ribosome biogenesis and nucleolus structure organization is due to its emerging phase separation properties. NPM1 phase separates together with rRNA, ribosomal proteins and alone via heterotypic and homotypic interactions [55]. Similarly, Fkbp39 does phase separates homotypically even without crowder, as shown by turbidity assay in fig. 4.11(a). To test the effects of DNA and RNA on Fkbp39 phase separation properties, the turbidity assay was performed in presence of 50 ng/μl of either nucleosomal DNA or *S. pombe* rRNA. Nucleosomal DNA does not affect Fkbp39 phase separation whereas rRNA seems to slightly impair the process, fig. 4.11(b).

The formation of phase-separated condensates can be visualized through microscopy techniques. These techniques are very powerful when combined with fluorescent labeling, which allows tracing simultaneously different components of the system. Due to the risk of protein mis-folding caused by the big fluorophores, the preferred approach is site-specific labeling. For this, an additional cysteine was cloned at Fkbp39 C terminus and this mutant was used for cysteine labeling and fluorescent microscopy experiments (Fkbp39 only cysteine is buried inside the structured NPL domain and can not be used for labeling). Through *in vitro* binding assays, we confirmed that the C terminal cysteine does not affect Fkbp39 binding either to nucleosomes or to nascent 60S subunits, fig. 4.12.

Using fluorescent microscopy techniques we confirmed that Fkbp39 phase separates alone and together with nucleic acids, which localize inside the condensates, fig. 4.13.

Because Fkbp39 binds both to nucleosomes and to nascent 60S subunits, Fkbp39 condensates forma-

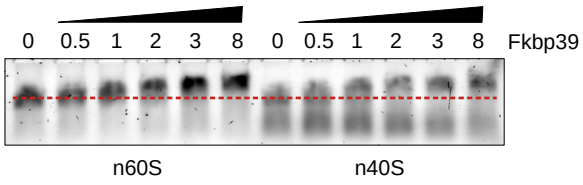

Figure 4.10: Fkbp39 binding to nascent 60S and 40S subunits *In vitro* binding assay. The relative molar ratio of Fkbp39 in respect to nascent subunits (n60S and n40S) is indicated, with Fkbp39 functional unit being a pentamer. The formation of the complexes was visualized on 0.8% TBE agarose gel stained with SYBR gold. The red dash line represents the migration line of nascent subunits. This is a representative experiment of three independent assays.

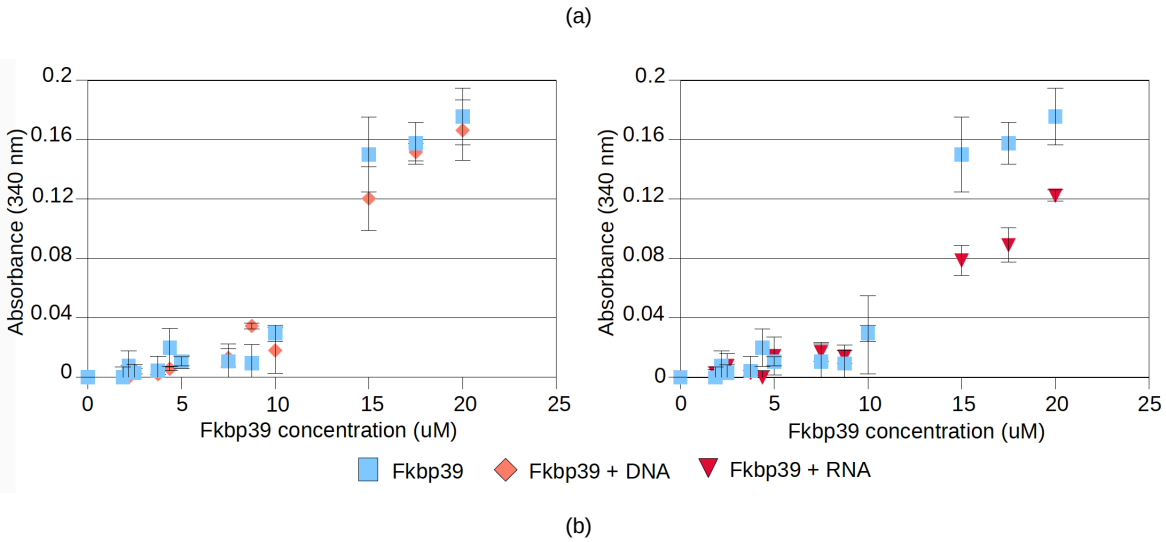

Figure 4.11: Fkbp39 homo- and hetero-typic phase separation Turbidity assays. Serial dilutions of Fkbp39 (on the x axis) were incubated with or without PEG (a), 50 ng/μl of nucleosomal DNA or 50 ng/μl of *S. pombe* rRNA (b) and the light scattering at 340 nm (on the y axis) was measured. Error bars represent standard deviation from measurements of three independent Fkbp39 dilutions.

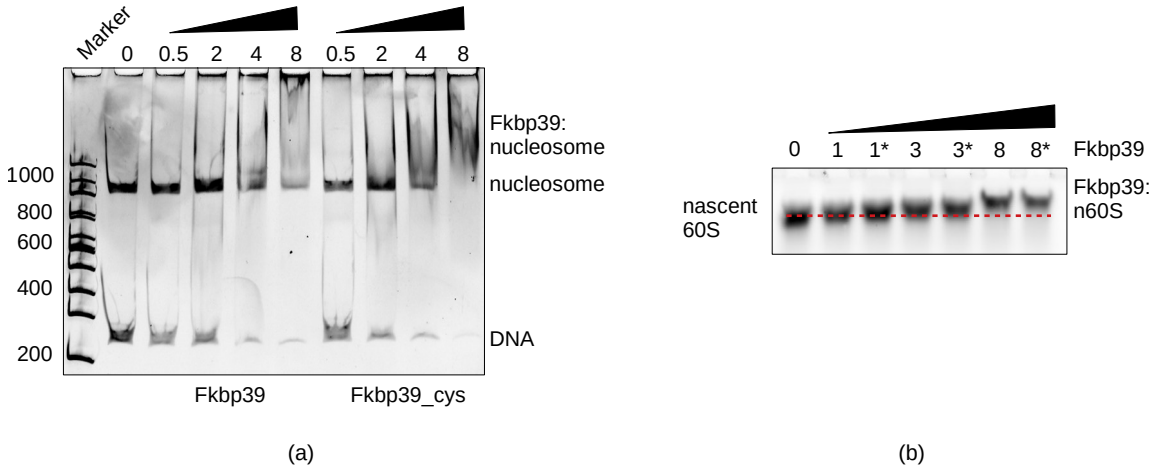

Figure 4.12: Fkbp39_cys binding properties *In vitro* binding assays. Numbers indicate Fkbp39 relative molar ratio in respect to the binding parter, with Fkbp39 functional unit being a pentamer. (a) Fkbp39 or Fkbp39 C terminal cys (Fkbp39_cys) were incubated with nucleosomes with 40 bp of symmetric linker DNA. The formation of the complexes was visualized on 6% TBE acrylamide gel stayned with SYBR gold. This is a representative experiments of three independent assays. Nucleosomes were assembled by Dr. Silvija Bilokapic Halic. (b), Fkbp39 or Fkbp39 C terminal cys (indicated by *) were incubated with nascent 60S subunits (n60S). The formation of the complexes was visualized on 0.8% TBE agarose gel stayned with SYBR gold. The red dash line represents the migration of n60S. This is a representative experiment of two independent assays.

(a)

(b)

(c)

Figure 4.13: Nucleic acids enter Fkbp39-organized condensates Fluorescence microscopy experiments. (a), 15 μM Fkbp39 labeled with alexa 546 were incubated either with or without PEG. (b), 5 μM Fkbp39 labeled with alexa 546 in presence of 10% PEG were incubated with 50 ng/μl nucleosomal DNA and with 50 ng/μl *S. pombe* rRNA (c). Nucleic acids were stained non specifically by addition of 500 nM SYTO40 before imaging. Scale bars represents 10 μm. These microscopy experiments were performed in collaboration with Dr. Michael White.

tion was tested in presence of either nucleosomes or nascent 60S subunits, with each component specifically and differently labeled. Both nucleosomes and nascent 60S subunits enter Fkbp39 condensates, fig. 4.14. From microscopy experiments it is possible to quantify the distribution of the different components in the dense phase (separated phase) in respect to the light phase via the partition coefficient parameter, Kp [55, 47]. The Kp value describes the phase separation properties of the molecule in the analyzed condition and for multicomponent systems is an indirect measure of the interaction between them. Fkbp39 Kp in either nucleosomes or nascent 60S subunits containing condensates is similar, and nucleosomes and nascent 60S subunits Kps are very similar as well. To be able to compare nucleosomes and nascent 60S subunits Kps, these values were normalized in respect to their difference in mass: ribosome precursors are indeed about 9.7 times bigger than nucleosomes (described in details in methods).

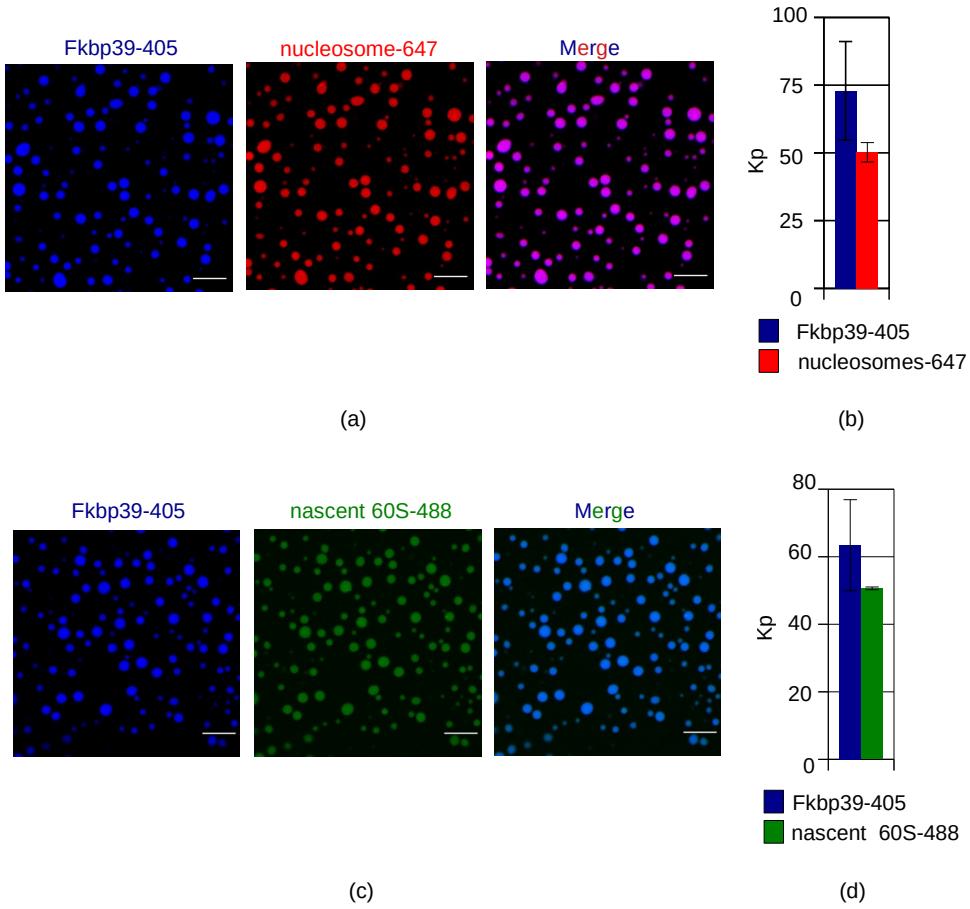

Figure 4.14: Nucleosomes and nascent 60S subunits enter Fkbp39-organized condensates Fluorescence microscopy experiments. Fkbp39 labeled with alexa 405 was incubated either with nucleosomes labeled with alexa 647 (a) or with nascent 60S subunits labeled with atto 488 (c) and droplets were imaged. Scale bars represents 10 μm. In (b) and (d), Kp values were calculated for each component, error bars represent standard deviation. These fluorescent microscopy experiments were performed in collaboration with Dr. Mylene Ferrolino and nucleosomes were assembled by Dr. Silvija Bilokapic Halic.

4.4 Fkbp39 separates nascent 60S subunits from chromatin

In vitro and *in vivo* assays show that Fkbp39 binds both to chromatin and to nascent 60S subunits and can phase separate with both. This suggested that chromatin might load Fkbp39 to the emerging nascent 60S subunits during early steps of biogenesis. We used *in vitro* assays to test this hypothesis. Fkbp39 was initially incubated with nucleosomes, then increasing amount of nascent 60S subunits were added to mimic their emergence during ribosome biogenesis. The resulting complexes were visualized both on native acrylamide and agarose gels. The addition of nascent 60S subunits leads to the formation of Fkbp39:n60S (nascent 60S subunits) complexes and the disassembly of Fkbp39:nucleosome complexes, fig. 4.15(a). To determine if this process has a directionality, we tested whether nucleosomes could displace Fkbp39 from nascent 60S subunits. Fkbp39 was pre-bound to nascent 60S subunits and increasing amounts of nucleosomes were then added. Nucleosomes, however, can not displace Fkbp39 from nascent 60S subunits and instead form new Fkbp39:nucleosome complexes, fig. 4.15(b). These data show that nascent 60S subunits displace Fkbp39 from nucleosomes and that Fkbp39 would not dissociate from nascent 60S subunits to re-bind chromatin.

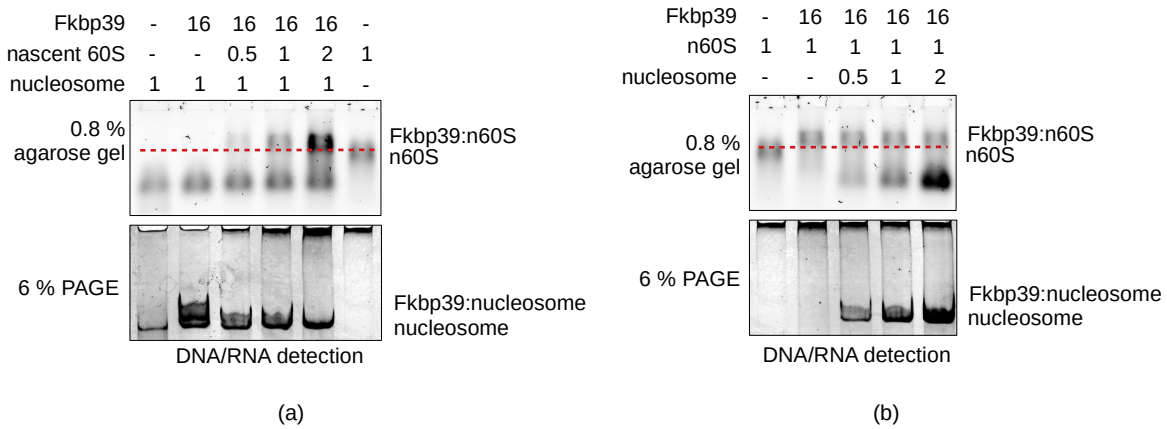

Figure 4.15: Fkbp39 dissociates from nucleosomes to bind emerging nascent 60S subunits *In vitro* binding assays. The relative molar ratio of each component is indicated with Fkbp39 functional unit being a pentamer. (a), Increasing amount of nascent 60S subunits were added to preformed Fkbp39:nucleosome complexes; (b) Increasing amount of nucleosomes were added to preformed Fkbp39:n60S complexes. Fkbp39:nucleosome complexes are visualized on 6% native PAGE gel, whereas Fkbp39:n60S on 0.8% TBE agarose gel. These are representative experiments of two independent assays. Nucleosomes were assembled by Dr. Silvija Bilokapic Halic.

To investigate the contribution of phase separation to this process, we pre-assembled Fkbp39:nucleosomes condensates, to which we then added nascent 60S subunits. Similar to fig. 4.15(a), nascent 60S subunits can enter these condensates and displace nucleosomes, fig. 4.16. In agreement with fig. 4.15(b), nucleosomes added to pre-formed Fkbp39:nascent 60S subunits condensates could not replace nascent 60S subunits and partition into these condensates only poorly, fig 4.17.

These data suggest that Fkbp39 initially bound to nucleosomes leaves chromatin to bind to the emerging nascent 60S subunits and together form assemblies that partition into a distinct compartment organized by Fkbp39 through liquid-liquid phase separation.

To test this model, Ytm1 ChIP-seq was performed to monitor nascent 60S subunits association with chromatin in wild type, *fkbp39*Δ, *fkbp41*Δ and double mutant cells. As the model predicts, in wild type cells Ytm1 is not detectable on chromatin. In *fkbp39*Δ and double mutant cells, on the contrary, Ytm1 is associated with the rDNA locus, mainly towards the 3' end of the rDNA repeat and the non transcribed spacer, fig. 4.18. This confirms that *in vivo* Fkbp39 dissociates nascent 60S subunits from chromatin.

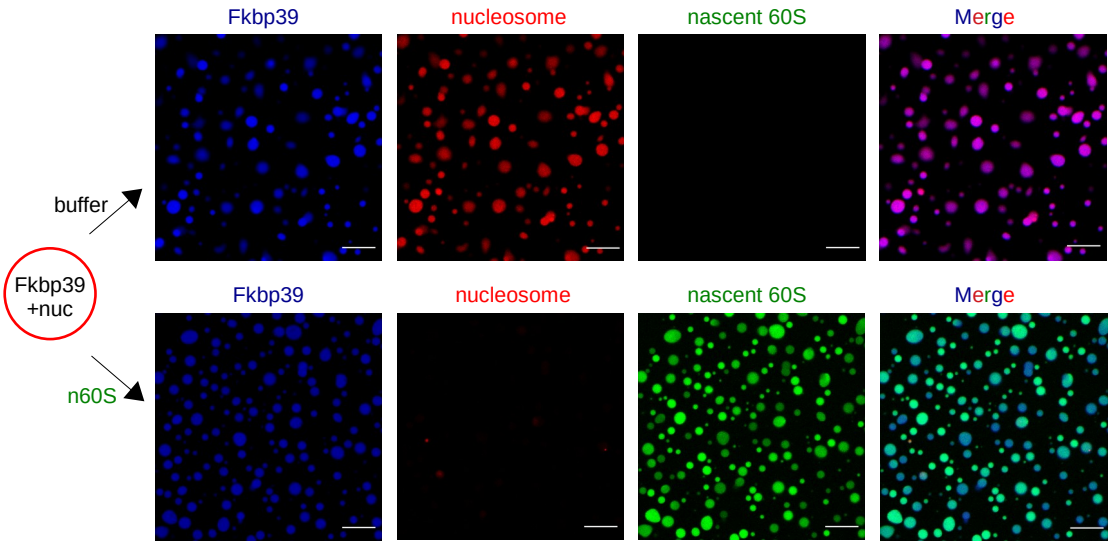

(a)

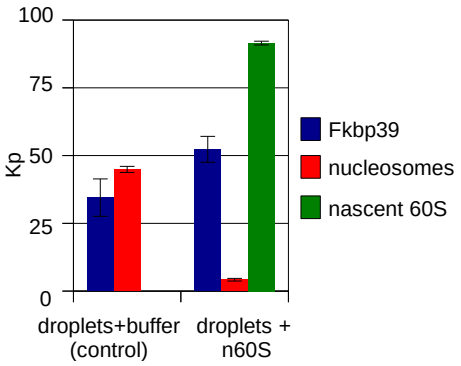

(b)

Figure 4.16: Nascent 60S subunits replace nucleosomes in Fkbp39-organized condensates Fluorescence microscopy experiments. (a), Fkbp39 labeled with alexa 405 was incubated with nucleosomes labeled with alexa 647 and condensates were let to settle. Then, nascent 60S subunits labeled with atto 488, in the lower row, or buffer, upper row, were added to the pre-formed condensates. Scale bars represents 10 μm. (b), Kps were calculated for the different components, error bars represent standard deviation. These are representative images from one of two independent experiments. These fluorescent microscopy experiments were performed in collaboration with Dr. Mylene Ferrolino and nucleosomes were assembled by Dr. Silvija Bilokapic Halic.

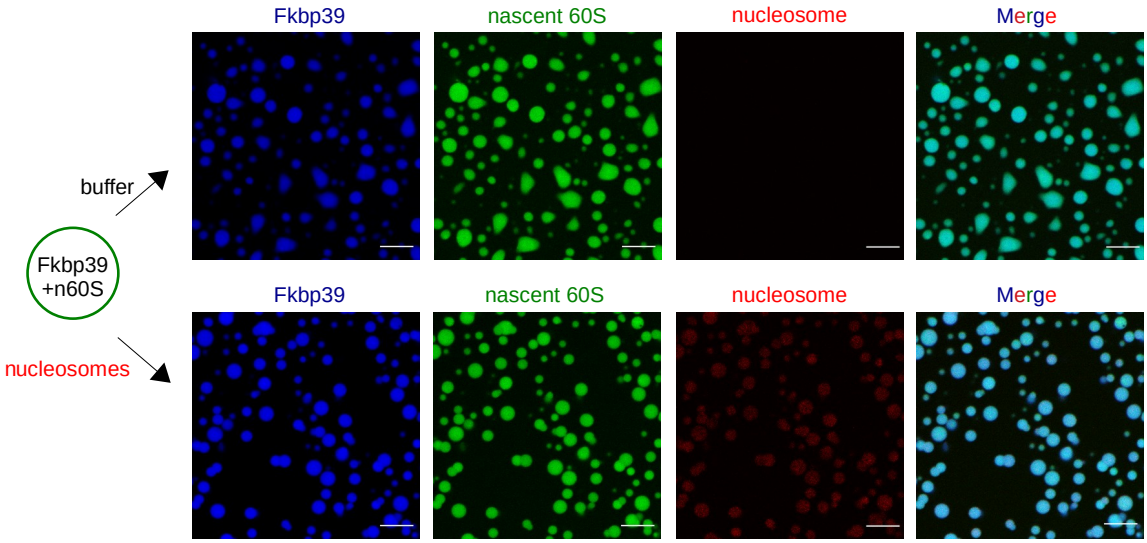

(a)

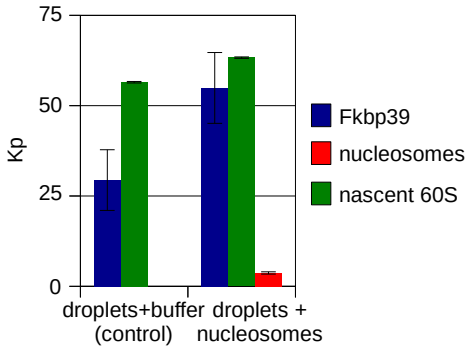

(b)

Figure 4.17: Nucleosomes enter Fkbp39:nascent 60S subunits condensates only poorly Fluorescence microscopy experiments. (a), Fkbp39 labeled with alexa 405 was incubated with nascent 60S subunits (n60S) labeled with atto 488 and condensates were let to settle. Then, nucleosomes labeled with alexa 647, in the lower row, or buffer, upper row, were added to the pre-formed condensates. Scale bars represents 10 μm. (b), Kps were calculated for the different components, error bars represent standard deviation. These are representative images from one of two independent experiments. These fluorescent microscopy experiments were performed in collaboration with Dr. Mylene Ferrolino and nucleosomes were assembled by Dr. Silvija Bilokapic Halic.

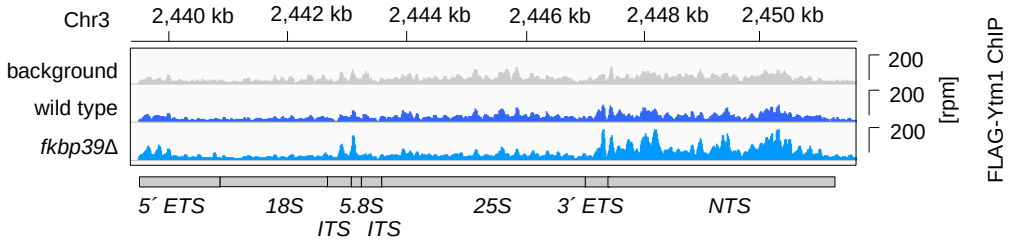

(a)

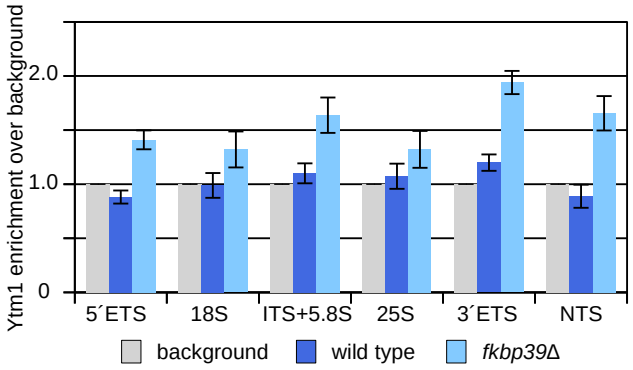

(b)

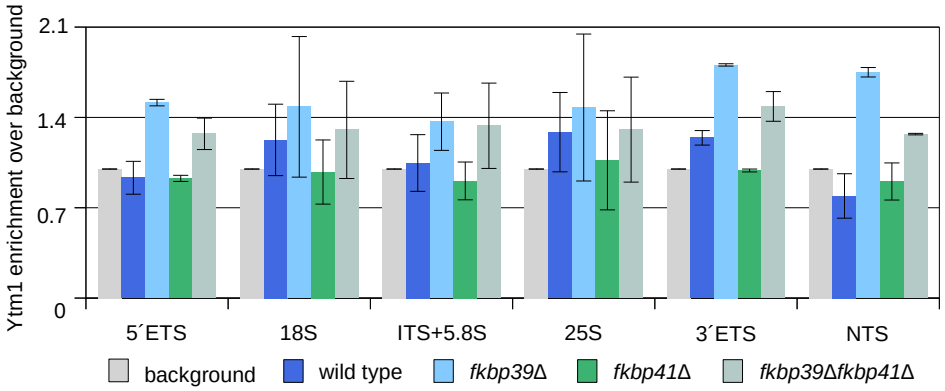

(c)

Figure 4.18: Nascent 60S subunits are retained on chromatin in *fkbp39Δ* cells Ytm1 ChIP-seq in wild type and *NPL-FKBP* deletion cells. (a), Ytm1 is detected on the rDNA locus only in *fkbp39Δ* cells, with a peak mainly over the 3'ETS and the non transcribed spacer (NTS). Scale bars on the right denote read numbers per million reads (rpm) normalized over background regions. The coordinates of the genomic location are indicated above the chart, the rDNA locus organization is depicted below in gray boxes. (b) and (c), Quantification of the reads mapping over the rDNA locus from Ytm1 ChIP-seq experiments in the indicated strains. Reads were normalized to background regions and plotted relative to background. Quantification is from seven (b) and two (c) independent ChIP-seq experiments, error bars represent standard error.

4.5 Consequences of *fkbp39* deletion on ribosome biogenesis

The previous experiments indicate that Fkbp39 separates nascent 60S subunits from chromatin and suggest it organizes them into a distinct compartment enriched in Fkbp39. In our hypothesis, this Fkbp39 enriched compartment corresponds to the granular component, where ribosome subunits maturation occurs. We investigated the role of this compartmentalization in ribosome biogenesis by deleting *fkbp39*. To investigate rRNA processing, we performed nascent RNA sequencing and compared these results to total RNA sequencing, which represents the steady state. 2' after RNA labeling, comparable levels of ribosomal RNAs accumulate in wild type and *fkbp39*Δ cells, indicating that Fkbp39 is not required for transcription. However, at 10' after RNA labeling, both the 18S and 25S RNA are reduced in *fkbp39*Δ cells, fig. 4.19(a). At steady state the 18S RNA reaches wild type level, whereas the 25S RNA is still reduced. Moreover, the amount of rRNA at steady state is reduced in *fkbp39*Δ cells compared to wild type, fig. 4.19(b). This suggests the presence of an rRNA processing defect. RNA sequencing also shows the accumulation of RNA corresponding to the 5'ETS and of RNA fragments spanning the 5'ETS and 18S junction, fig. 4.19(c).

We analyzed the cell ribosomes content through polysome profile. Compared to wild type, in *fkbp39*Δ cells, there is an increase of RNA signal from the void (RNA not engaged with ribosomes) and the 40S fractions, and a reduction from the 80S and polysome fractions, fig. 4.20.

To quantify these changes we performed the polysome profiles without cycloheximide because in this condition ribosomes runoff and the polysome peaks collapse into the 80S fraction. Quantification from independent polysome profile experiments confirms that in *fkbp39*Δ cells there is an increase of RNA not engaged with ribosomes and a corresponding decrease of RNA in the ribosomes fraction, fig. 4.21(a). This indicates that in *fkbp39*Δ cells there is a reduction of mature ribosomes. The imbalance between the 40S and 60S subunits, fig. 4.20(b), suggests the presence of a maturation defect specific for the 60S subunit. RNA sequencing from the fraction not engaged with ribosomes (void) confirms that in *fkbp39*Δ cells there is a reduction of rRNA, supporting the hypothesis of an rRNA processing defect, fig. 4.20(c).

It is surprising to observe that the change in the polysome profile distribution is specific to *fkbp39* deletion: the profile for *fkbp41*Δ cells overlaps with wild type, fig. 4.21(b). Even though these proteins share many common features, it seems they are not completely functionally redundant.

Cryo-EM structures of Ytm1-containing nascent 60S subunits purified from wild type and *fkbp39*Δ cells support these data (cryo-EM data were collected and analyzed by Dr. Silvija Bilokapic Halic and Dr. Mario Halic). The intermediates purified from these cells are almost identical, so neither Fkbp39 nor GC compart-

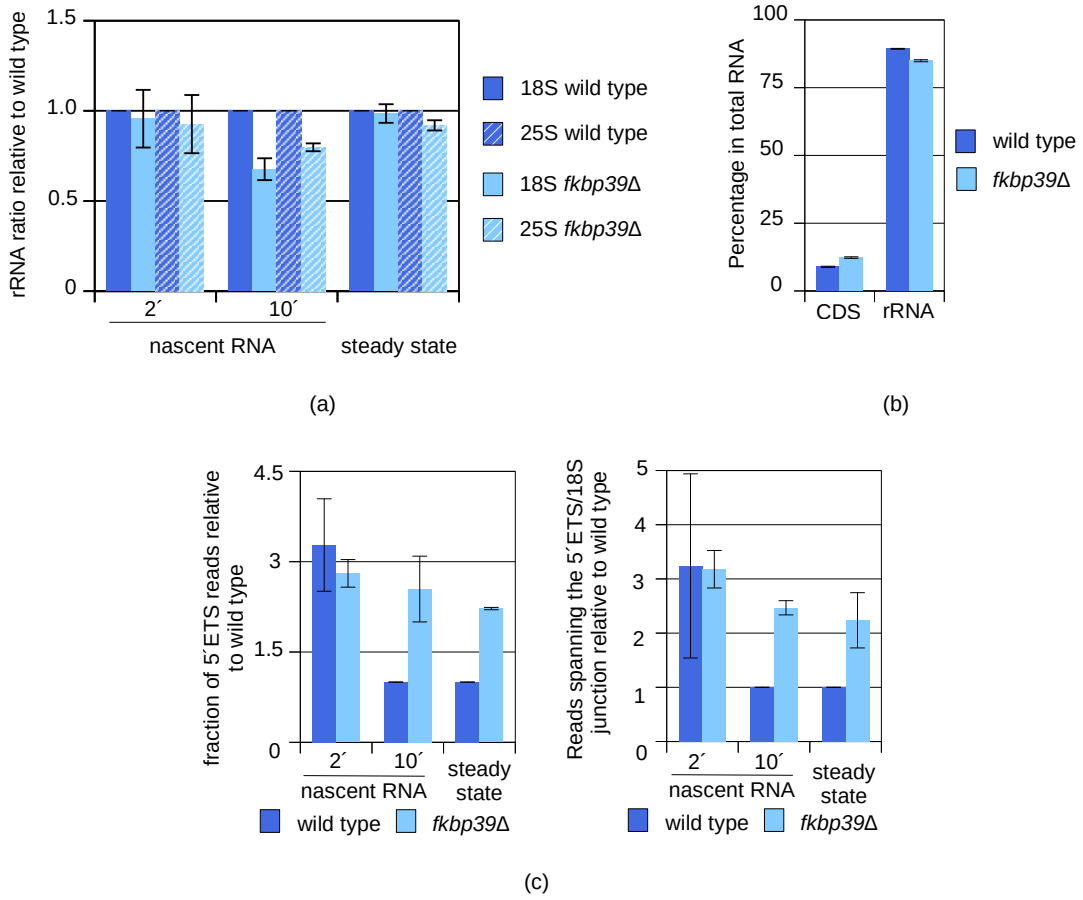

Figure 4.19: Defects in rRNA processing Nascent and total RNA sequencing quantification. (a), Sense reads mapping to the 18S and 25S RNA were extracted, quantified and normalized to the amount of total reads. Wild type values were set to 1. Quantification from three independent nascent RNA experiments, and two independent total RNA sequencing (steady state), error bars represent standard error. (b), Steady state (total) RNA sequencing quantification. Reads were classified into functional groups and the ones belonging to protein coding (CDS) and rRNA were plotted as percentage of total reads. Quantification from two independent total RNA sequencing, error bars represent standard error. (c), On the left sense reads mapping to the 5'ETS were extracted, quantified and normalized to the amount of total reads; on the right sense reads spanning the 5'ETS and 18S junctions were extracted, quantified and normalized to the amount of rRNA sense transcripts. For nascent RNA, wild type 10 minutes time point value was set to 1; for total RNA, wild type value was set to 1. Quantification from three independent nascent RNA experiments, and two independent total RNA sequencing, error bars represent standard error.

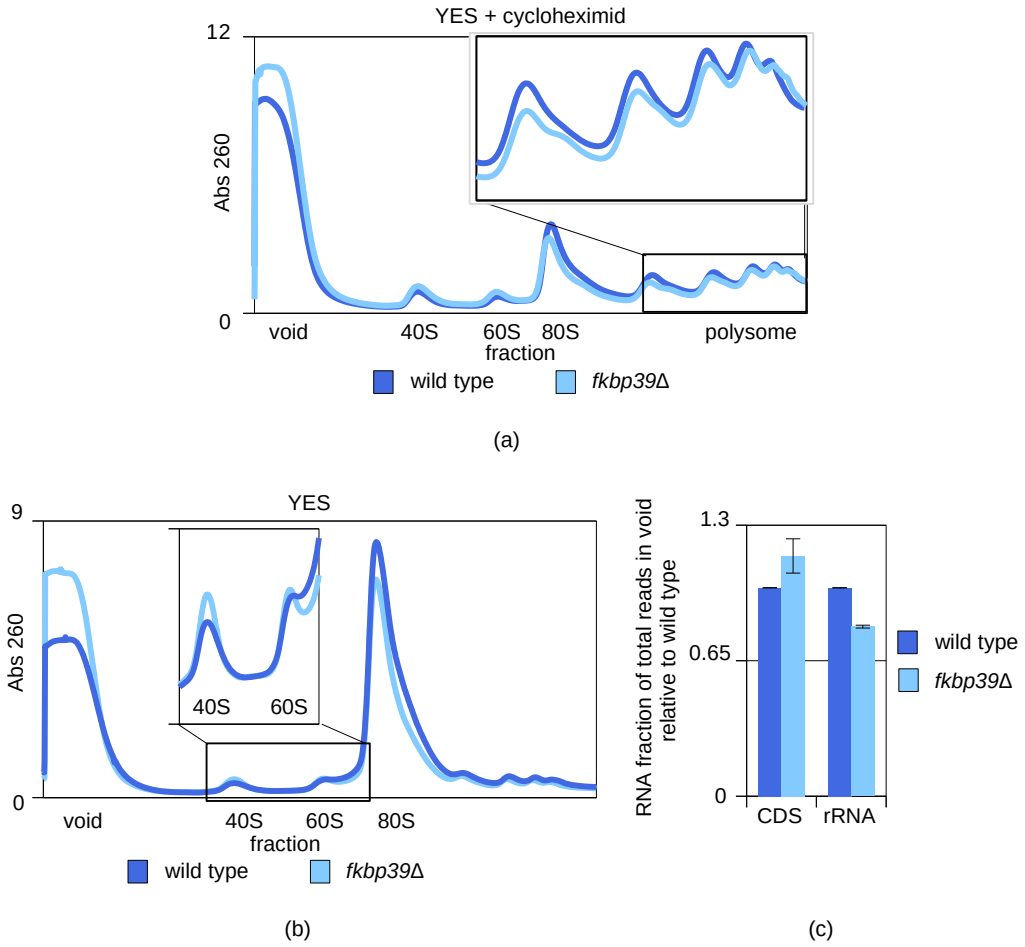

Figure 4.20: Ribosomes in *fkbp39*Δ cells (a), Polysome profile experiment in presence of cycloheximide. The polysome fraction is shown as zoomed in panel. The X axis represents the sucrose gradient, from 10% on the left to 50% on the right. The 260 nm absorbance signal is plotted on the Y axis. (b), Representative polysome profile experiment performed without cycloheximide. 40S and 60S subunits peaks are shown as zoomed in panel. The X axis represents the sucrose gradient, from 10% on the left to 50% on the right. The 260 nm absorbance signal is plotted on the Y axis. (c), RNA sequencing quantification from the void fraction of polysome profile experiments performed without cycloheximide. Reads mapping to protein coding sequences (CDS) and rRNA were quantified and plotted relative to wild type as fraction of total reads. Quantification from two independent experiments, error bars represent standard error.

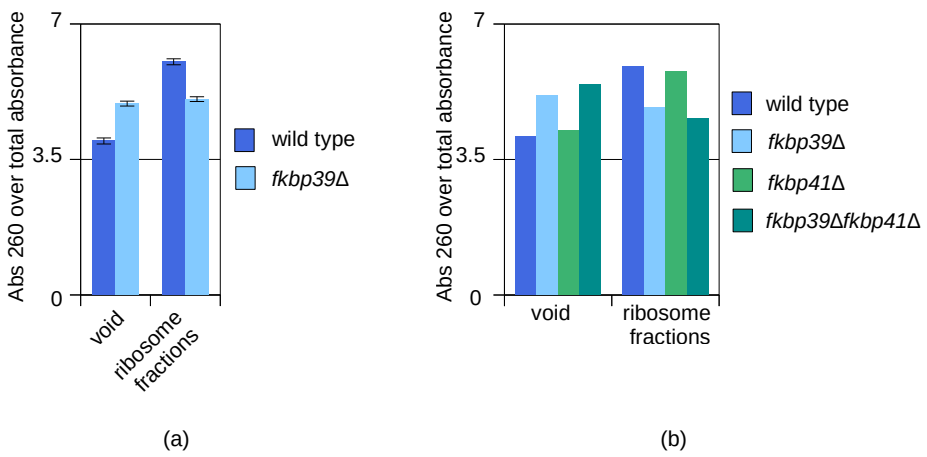

Figure 4.21: Polysome profile quantification (a) and (b), Quantification of the 260 nm signal from the polysome profile experiments performed without cycloheximide in the indicated strains (see methods for a detailed description). (a), Quantification from 5 independent polysome profiles, error bars represent standard error.

mentalization is essential for ribosome biogenesis. However, in *fkbp39*Δ cells, a smaller fraction of nascent 60S subunits have densities corresponding to Ppp1 (Nop7 in *S. cerevisiae*), the Ytm1-Erb1-Ppp1 complex, and 25S rRNA domain III. These findings show that Fkbp39 takes part in the maturation of 60S subunits, by assisting the incorporation of Ppp1 and 25S rRNA domain III.

4.6 Fkbp39 and RNAi

As mentioned previously, Fkbp39 and his *S. cerevisiae* orthologs were reported to target H3 [33, 126], and the H3 centromeric variant [34, 36]. H3 and H3 centromeric variant proline isomerization affects gene transcription [30, 33], and chromosome segregation [34, 36], respectively. Fkbp39 was also identified as a new factor involved in heterochromatic silencing [37], and according to *S. pombe* database,[38], it displays a negative genetic interaction with Ago1, Clr4 and Dcr1. A double-mutant organism that has a phenotype that differs from the pure combination of the single mutant phenotypes defines a genetic interaction between the respective gene products [127]. A more severe phenotype (defined as a negative genetic interaction) indicates compensatory pathways, whereas an alleviating phenotype (defined as positive genetic interaction) is due to gene products that operate in the same pathway.

Growth assays show that *fkbp39∆ago1∆* and *fkbp39∆clr4∆* cells grow slower compared to single mutants, fig. 4.22. This growth defect seems specific to Fkbp39 since *fkbp41∆ago1∆* cells growth is comparable to single mutants. *fkbp39∆fkbp41∆* cells do not display a growth defect.

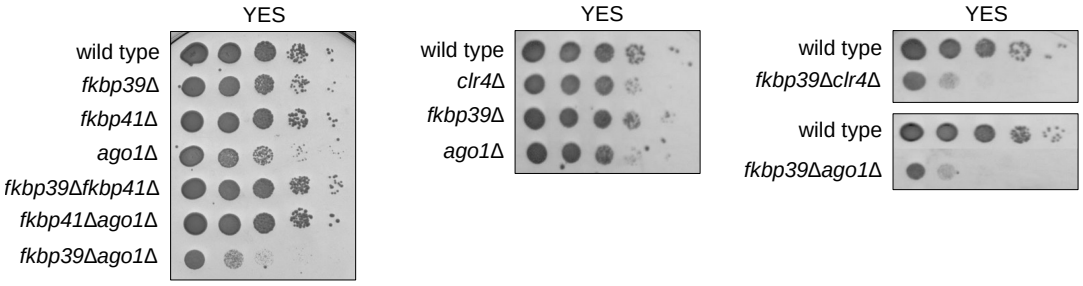

Figure 4.22: Negative genetic interaction between Fkbp39 and the RNAi pathway Growth assays on YES, rich media. Cells were plated in 10 fold dilutions and incubated for 2 days before imaging.

Since Fkbp39 and the RNAi pathway display a negative genetic interaction, we tested Fkbp39 contribution to the organization of centromeres, which is fundamental for proper chromosome segregation. RNAi is necessary for the establishment and maintenance of centromeric heterochromatin, essential for proper chromosomes segregation [87]. Anyway, it was recently reported that also the non-coding RNA binding protein Seb1 contributes to pericentromeric heterochromatin formation, independently of RNAi, by recruiting SHREC [128]. This suggests that alternative pathways to RNAi exist for centromeric heterochromatin regulation.

Through minichromosome loss assay it is possible to monitor *in vivo* chromosome segregation and to

quantify missegregation events. In RNAi mutants, due to the loss/reduction of centromeric heterochromatin, the number of missegregation events is higher than in wild type cells. *fkbp39*Δ cells do not display a segregation defect, and *fkbp39*Δ*ago1*Δ cells have a segregation phenotype similar to *ago1*Δ cells, fig. 4.23. This suggests that Fkbp39 does not contribute to the centromeres organization.

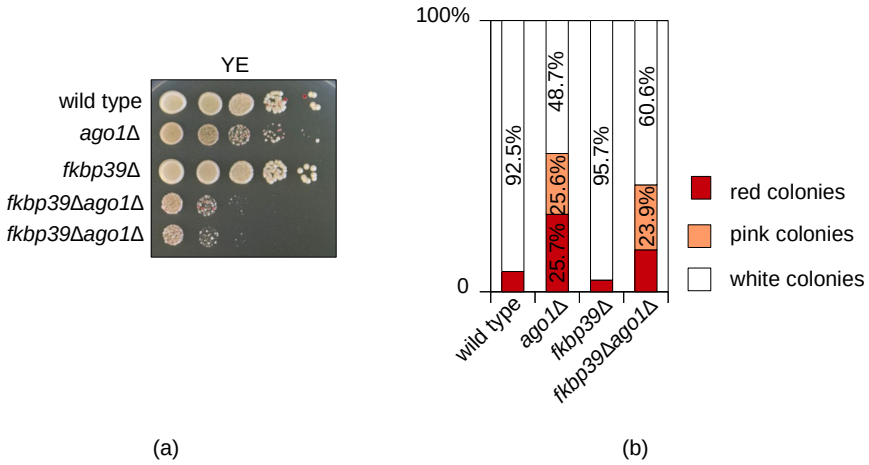

Figure 4.23: *fkbp39*Δ cells do not display a chromosome segregation defect Minichromosome loss assay. The minichromosome contains *S. pombe* centromeric structure, and can be used to follow chromosome segregation. The central core and inner most repeats from *cen3* are flanked on both sided by outer repeats, and the *sup3-5* reporter. Cells carrying the minichromosome turn white on low adenine media thanks to expression of the reporter gene, whereas cells, which lost the minichromosome are red [87]. Centromeric heterochromatin and H3 centromeric variant are normally assembled and deposited on the minichromosome, which behaves as *S. pombe* chromosomes at cell division. Cells carrying the minichromosome were grown in rich media and then plated in 10 fold dilutions on low adenine, YE, to monitor the *sup3-5* reporter expression (a). Two *fkbp39*Δ*ago1*Δ colonies were analyzed independently. (b), Quantification of white/red colonies, more than 600 colonies were screen for each genetic background.

To investigate directly the structure of heterochromatin and the activity of the RNAi pathway in *fkbp39*Δ cells, we performed H3K9me2 ChIP-seq and Ago1-bound sRNA sequencing. Because *in vitro* Fkbp39 has proved a histone chaperone activity [29], we also performed H3 ChIP-seq. H3K9me2 ChIP-seq confirms that centromeric heterochromatin in *fkbp39*Δ cells is alike wild type, fig. 4.24(a) and 4.24(b). Ago1-bound sRNA sequencing shows that in these cells sRNAs mapping to centromeric repeats have only non-relevant differences, such a very low level of spreading in between the repeats, fig. 4.25(b). Some differences are present at the subtelomeric regions, where in *fkbp39*Δ cells there is a reduction in H3K9me2, and sR-

NAs arise from the subtelomeric locus *tlh* (about 10 times more than in wild type cells), fig. 4.24(c), 4.24(d) and 4.25(a), 4.25(c). Despite differences in H3K9me2 level, H3 localization both at centromeres and subtelomeres is comparable in *fkbp39*Δ and wild type cells, fig. 4.24(b) and 4.24(d). Total RNA sequencing shows that in *fkbp39*Δ cells centromeric and subtelomeric transcripts are de-repressed, fig. 4.26. In *fkbp39*Δ*ago1*Δ cells, centromeric regions are transcribed at the same level as in *ago1*Δ cells, whereas at subtelomeres the de-repression is stronger.

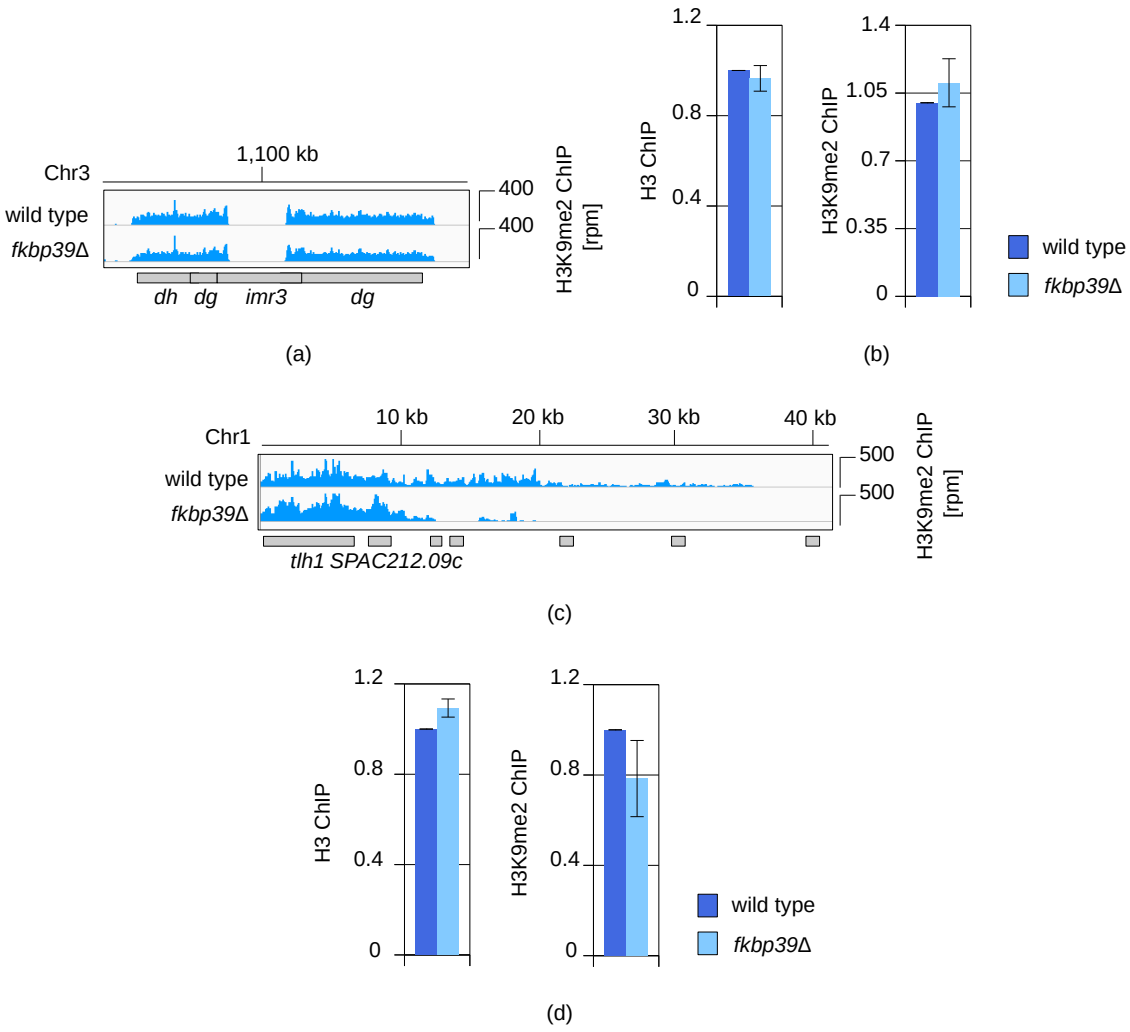

Figure 4.24: H3K9me2 in *fkbp39*Δ cells ChIP-seq results. (a) and (c), H3K9me2 at the centromere on chromosome 3 (a) and at the subtelomere on chromosome 1 (c) in *fkbp39*Δ and wild type cells. Scale bars on the right denote read numbers per million reads (rpm) normalized over background regions. The coordinates of the genomic location are indicated above the chart, the DNA organization is depicted below in gray boxes. (b) and (d), Quantification of the reads mapping over the centromere on chromosome 3 (b) and the subtelomeric region on chromosome 1 (d) from H3 and H3K9me2 ChIP-seq. Reads were normalized to background regions and plotted relative to wild type. Quantification from 4 independent H3K9me2 ChIP-seq and 3 H3 ChIP-seq experiments, error bars represent standard error.

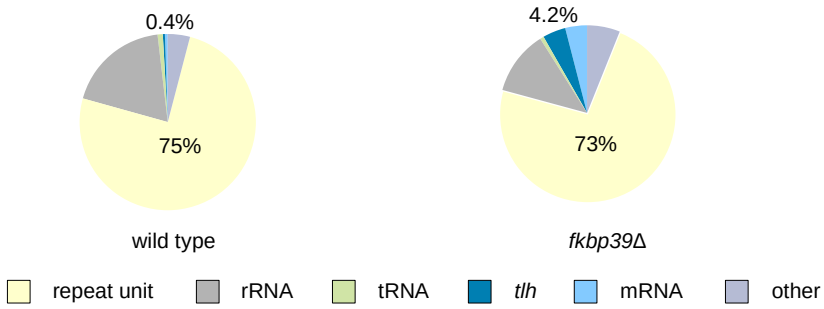

(a)

(b)

(c)

Figure 4.25: sRNA in *fkbp39*Δ cells Ago1-bound sRNA sequencing. Reads from the + and - strand are in light blue and gray respectively. Scale bars on the right denote read numbers per million reads (rpm). (a), sRNA classification in wild type and *fkbp39*Δ cells. Major small RNA classes are highlighted. (b), sRNA from the centromere on chromosome 3 (zoomed in panel on the right); (c), sRNA from the subtelomeric region *tlh*, on chromosome 1.

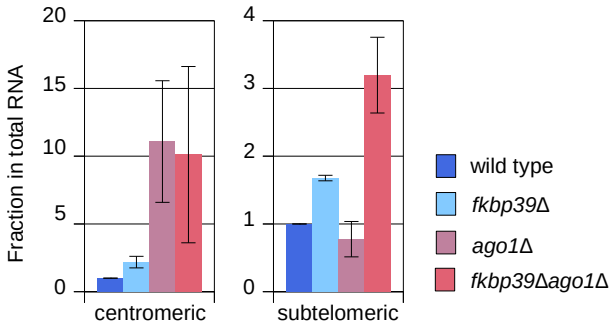

Figure 4.26: De-repression of heterochromatic regions in *fkbp39*Δ cells Total RNA sequencing quantification. Reads mapping to centromeric regions and the subtelomere on chromosome 1 were plotted as a fraction of total reads relative to wild type for the indicated strains. Quantification from two independent total RNA sequencing, error bars represent the standard error.

4.7 Argonaute and transcription

fkbp39Δ*ago1*Δ cells display a severe growth defect. Because cell growth is intimately connected to protein synthesis we decided to investigate the process of translation in these cells. As shown previously, Fkbp39 coordinates early steps of ribosome biogenesis and argonaute proteins are known to regulate translation via the microRNA pathway [129], though microRNAs have not been detected in *S. pombe*. To test the translation capability of *fkbp39*Δ*ago1*Δ cells, we established an *in vivo* translation assay, in which the accumulation of a reporter protein is monitored over time. The result was unexpected: not only double mutant cells but also *ago1*Δ cells have a very low protein accumulation compared to wild type, fig. 4.27(a). Using the same system, we analyzed the accumulation of the reporter mRNA. Both *fkbp39*Δ*ago1*Δ and *ago1*Δ cells have a reduced synthesis of the reporter mRNA, fig. 4.27(b). The reduction in protein accumulation observed with the *in vivo* translation assay is caused, at least partially, by a transcription defect.

The assessment of transcription and translation capacity *in vivo* through a reporter system presents several disadvantages: it is not possible to analyze these processes independently (they both influence and are influenced by cell growth, which results in the ”chicken-egg causality dilemma”), and the analysis is limited to one or few reporters at a time. We noticed that in our *in vivo* translation assay the use of minimal media (necessary for the maintenance of the plasmid carrying the reporter system) affects cell growth, increasing dramatically the doubling time of *ago1*Δ cells, table 4.3. In this condition, it is not possible to assess if the phenotype observed in *ago1*Δ cells cause or is the consequence of slow cell growth (”chicken-egg causality dilemma”). In rich media, only *fkbp39*Δ*ago1*Δ cells display a growth defect, so performing

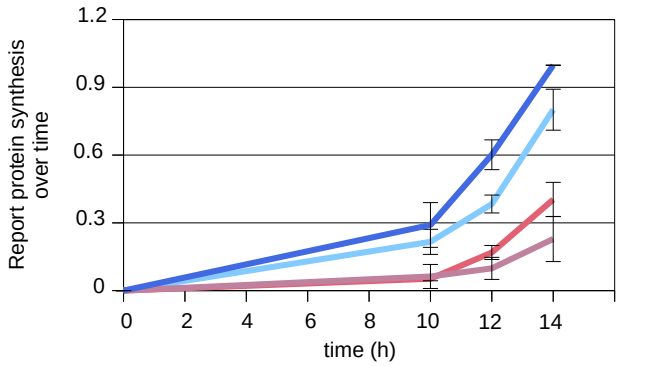

(a)

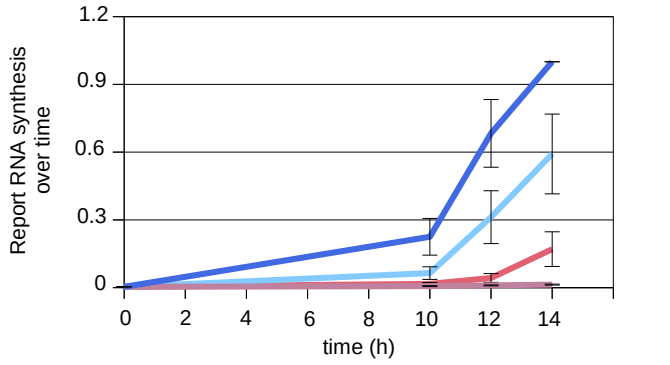

(b)

Figure 4.27: Impaired transcription of a reporter gene in *ago1*Δ cells *In vivo* translation assay. The FLAG-Triman reporter was expressed from a plasmid under the control of the thiamine-repressible *nmt1* promoter in the indicated strains. Cells were grown in presence of thiamine and aliquots were taken at the indicated time point after thiamine removal for protein (a) and mRNA reporter quantification (b). Quantification (from anti-FLAG western blot and RT-qPCR) is from three independent experiments and error bars represent standard errors.

experiments in this setting should simplify the data analysis for the other genetic backgrounds.

doubling time	wild type	*fkbp39Δ*	*ago1Δ*	*fkbp39Δago1Δ*
EMMC media	178'	193'	292'	255'
YES media	140'	150'	190'	300'

Table 4.3: Doubling time in minimal and rich media Doubling time in minimal media, EMMC, and rich media, YES. Doubling time was determined using Doubling *Time* [130].

Polysome profile, from cells grown in rich media, support our initial observation, fig. 4.28. *fkbp39Δ* cells display an increase of the RNA signal from the void fraction (RNA not engaged with ribosome) with a corresponding reduction in the signal from the 80S and polysome fractions, as discussed before. The polysome profile from *ago1Δ* cells is very similar to wild type, with only small differences, fig. 4.28(b). A reduction of the signal from the polysome fraction suggests some ribosomes redistribute to the 80S fraction, indicating their translation activity might be compromised. Double mutant cells display a reduction of the RNA signal from the polysome fraction, with a corresponding increase from the void, more pronounced than *fkbp39Δ* cells. Moreover, polysome profiles performed without cycloheximide suggest a reduction in the amount of ribosome both in *fkbp39Δ* and *fkbp39Δago1Δ* cells compared to wild type, though larger for the double mutant. A reduction in the number of ribosomes and translation results in a severe growth defect. Anyway, as mentioned before, reduced translation can also be the indirect consequence of defects in other fundamental processes, that affect cell growth. Because of the difficulty in assessing the causality between the observed phenotypes in *fkbp39Δago1Δ* cells, we decided to focus on the characterization of transcription in *ago1Δ* cells.

RNA-seq reveals no differences between the distribution of steady state RNA in *ago1Δ* cells relative to wild type, at the exception of repeats, which are de-repressed in RNAi mutant cells, fig.4.29. Repeats are de-repressed also in *fkbp39Δ* cells, though to a lower extent. Nascent RNA sequencing reveals that *ago1Δ* cells and other RNAi mutants have a reduced accumulation of nascent transcripts, fig. 4.30(a). Classification of nascent RNA into coding sequence transcripts (CDS), ribosomal RNA (rRNA) and heterochromatic transcripts (RNA generated from the transcription of genomic regions normally silenced through heterochromatin) reveals that the delay in transcript accumulation is unevenly distributed within these classes and that *ago1Δ* cells behave differently from other RNAi mutants. *ago1Δ* cells have a dramatic reduction in nascent CDS RNA at 2' time point, around 17% of wild type, whereas other RNAi mutants analyzed have a smaller reduction, around 75% of wild type, fig. 4.30(b). However, at a later time point, CDS transcripts in all mutants

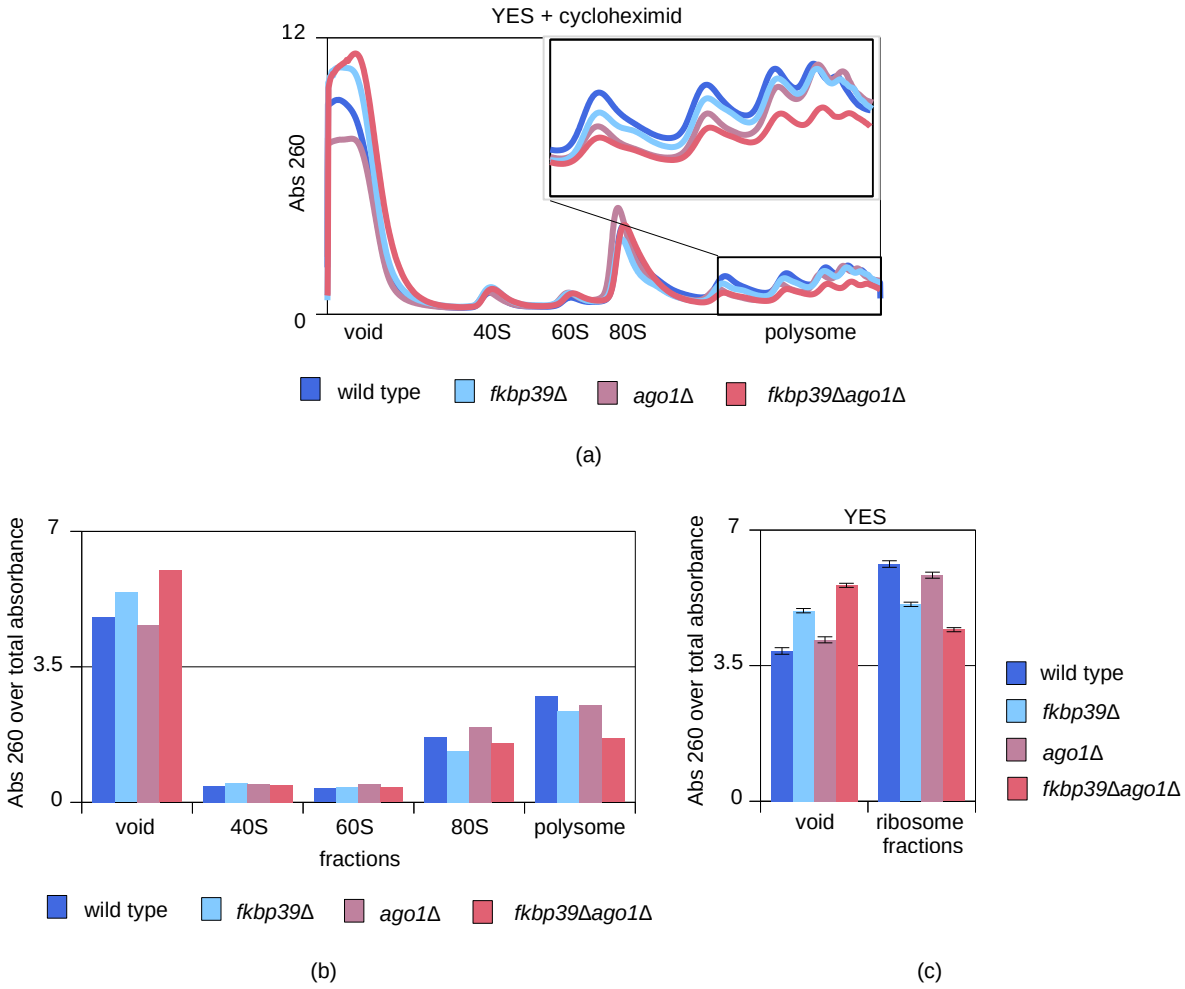

Figure 4.28: Polysome profile in different genetic backgrounds (a), Polysome profile experiment in presence of cycloheximide. The polysome fraction is shown as zoomed in panel. The X axis represents the sucrose gradient, from 10% on the left to 50% on the right. The 260 nm absorbance signal is plotted on the Y axis. (b), Quantification of the 260 nm signal from the polysome profile, related to fig. 4.28(a). (see methods for a detailed description). (c), Quantification of the 260 nm signal from the polysome profile experiments performed without cycloheximide in the indicated strains (see methods for a detailed description). Quantification from 3 independent polysome profiles, error bars represent standard error.

reach wild type levels. A similar trend can be observed for the accumulation of nascent heterochromatic transcripts, fig. 4.30(d): *ago1Δ* cells have a slower accumulation compared to other RNAi mutants, which is greater than wild type due to the de-repression of these loci. The situation is different for rRNA transcripts, on average the RNAi mutant strains have a reduction at 2' time point, which persist at 10' (on average rRNA transcripts are 75% of wild type), fig. 4.30(c). In these settings all the strains analyzed have comparable doubling times, table 4.4, so the difference in nascent transcripts accumulation can not be ascribed to an indirect effect of slow cell growth. Since RNA Polymerase II (Pol II) transcripts are the most affected, we performed Pol II ChIP-seq in wild type, *fkbp39Δ* and *ago1Δ* cells, fig. 4.31. Even though these cells have a reduction in nascent transcripts, Pol II localization at CDS is comparable to wild type. On the other hand, *ago1Δ* cells have a greater Pol II localization at heterochromatic loci, in agreement with their de-repression. *fkbp39Δ* cells also show an increase of Pol II localization at heterochromatic loci compared to wild type, fig. 4.31.

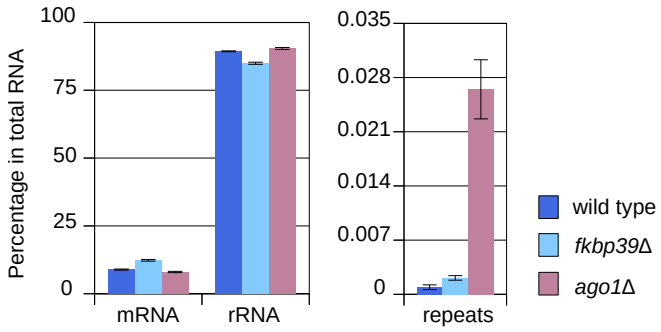

Figure 4.29: Steady state RNA in *ago1Δ* cells Steady state (total) RNA sequencing quantification. Reads were classified into functional groups and the ones belonging to protein coding (CDS), rRNA and repeats were plotted as percentage of total reads. Quantification from two independent total RNA sequencing, error bars represent standard error.

YEA media	wild type	*fkbp39Δ*	*ago1Δ*	*clr4Δ*	*chp1Δ*	*swi6Δ*
doubling time	160'	170'	192'	170'	193'	158'

Table 4.4: Doubling time in YEA media (low adenine media). Doubling time was determined using Doubling *Time* [130].

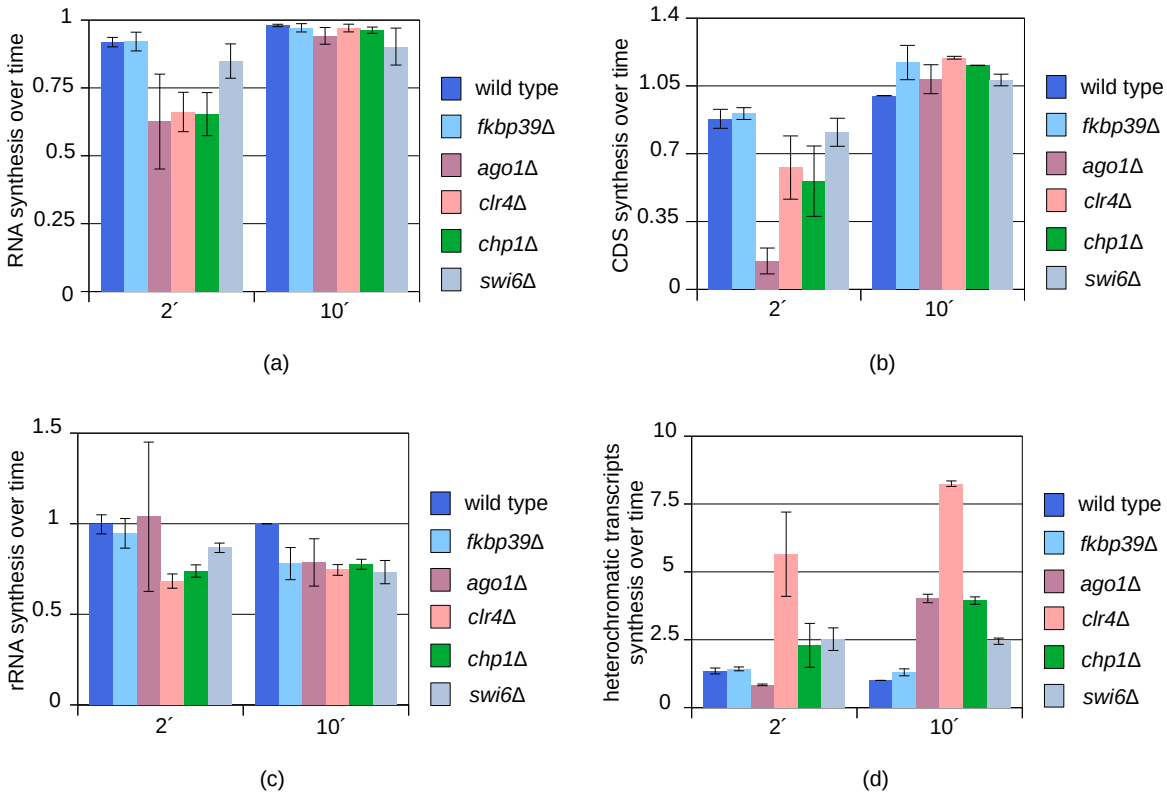

Figure 4.30: Nascent RNA sequencing Nascent RNA sequencing quantification at 2 and 10 minutes time points. Reads were normalized to the signal/background ratio factor (see methods) to show the amount of nascent RNA in the indicated strains over time, and normalized to wild type 10 minutes time point value, which was set to 1 (a). Reads where further classified into functional groups: coding sequence transcripts (CDS) (b), rRNA (c) and heterochromatic transcripts(d). Quantification from two independent nascent RNA experiments, error bars represent standard error.

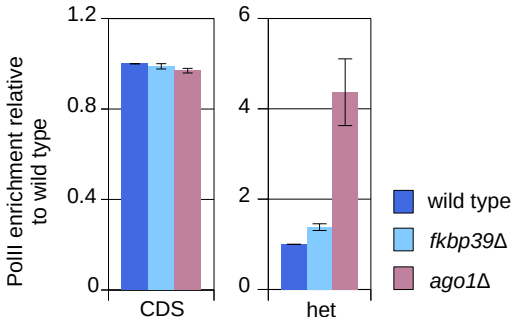

Figure 4.31: Pol II localization Pol II ChIP-seq quantification. Reads from coding sequences (CDS) and heterochromatic loci (het) were normalized to total reads and plotted relative to wild type. Quantification from two independent Pol II ChIP-seq experiments, error bars represent standard error.

Chapter 5

Discussion

5.1 NPL-FKBP proteins and rDNA localization

In vitro binding assays confirmed what previously reported for other NPL-FKBP proteins: Fkbp39 binds nucleosomes, fig. 4.2 [31]. The properties of this interaction are also conserved, as the linker DNA is required for binding and the prolyl-isomerase domain contributes as well [31]. Considering Fkbp39 domain organization, the contribution of the prolyl-isomerase domain to nucleosomes binding may be surprising, as the intrinsically disordered region (highly charged) seems to be the best candidate for non-specific electrostatic interactions. The FKBP domain within NPL-FKBP proteins is peculiar being characterized by an additional stretch of basic residues. Considering Fkbp39, the residues 257-361 represent the canonical FKBP domain, which is very poorly expressed and/or very unstable inside cells (data not shown), while the extended FKBP domain starts at position 199, fig. 4.1. These additional residues face outward and are important for the interaction with the negative charges of the DNA [31]. Previously, the stretch of residues 199-256 has been considered part of the IDR domain, resulting in partially contradictory, or at least confusing results. Indeed, the chaperone domain, responsible for the *in vitro* chaperone activity stretches up to the amino acid 256 [29]. Independently of the contribution of residues 199-256 to nucleosome binding, they seem to be essential for the stability of the FKBP domain. On top of these considerations, it was proposed that in absence of the C-terminal RRM domain, non-specific interactions may take place between the acidic and basic tracts within the NPM1 IDR [125]. This could hide the importance of this domain in the interactions with the endogenous partners when performing *in vitro* experiments using a C-terminal truncated version of the protein, such as the Fkbp39_1-199 mutant.

Both Fkbp39 and Fkbp41 bind chromatin *in vivo* and localize to the rDNA locus, as other NPL-FKBP proteins and NPM1, fig. 4.4 [19, 22, 20, 29]. In particular, they localize over the 25S and 3'ETS rDNA. ChIP-qPCR experiments showed that Fkbp39 residues 1-256 allow 50% binding compared to the full-length protein similar to Fkbp39_activity*. Anyway, Fkbp39_1-256 is very abundant (more than the full length protein), whereas Fkbp39_activity* is barely detectable (data not shown). This does affect the ChIP-qPCR result and complicates the interpretation of the data. It is currently not clear why Fkbp39_activity*, which contains only 3 point mutations, is poorly expressed or very unstable, being cloned at *fkbp39* endogenous locus as *fkbp39_1-256*. Overall both the IDR and the FKBP domain contribute to nucleosome binding but it is difficult to assess the relative importance of the single domains. Fkbp41 localization to the rDNA locus is also reduced in different *fkbp39* background, mirroring Fkbp39 trend, fig. 4.5. Both in *fkbp39_1-256* and *fkbp39_activity** Fkbp41 recruitment is 50% than in the wild type, as these Fkbp39 mutants have 50% binding. In *fkbp39*Δcells, Fkbp41 has a similar reduction. This suggests that the two proteins interact and that Fkbp39 influences Fkbp41 localization to the rDNA locus, which can still bind independently of Fkbp39, although to a reduced extent.

5.2 NPL-FKBP proteins interact with nascent 60S subunits

Endogenous Fkbp39 purification followed by mass spectrometry analysis identified mainly ribosomal proteins and 60S subunit biogenesis factors, table 4.1. Fkbp39 interaction with assembly ribosomes is not surprising considering its localization to the nucleolus [35], and it was already previously reported [32]. The mass spectrometry results also prove that Fkbp39 and Fkbp41 interact: Fkbp41 is constantly the second most abundant identified protein. Co-IP experiments were used to confirm and characterize some of these interactions, fig. 4.7. It emerged that Fkbp39 and Fkbp41 not only interact but probably form heteropentamers through the N terminal oligomerization domain. Fkbp41 interacts with nascent 60S subunits as well, represented by the biogenesis factor Ytm1, although this binding is lost upon *fkbp39* deletion. The contrary is not true, as the endogenous Fkbp39 and Ytm1 interact even in absence of Fkbp41. Surprisingly, even if Fkbp39 first 256 residues (Fkbp39_1-256) are sufficient for Ytm1 binding in presence of Fkbp41, they are not in *fkbp41*Δ cells. This shows that the interaction with nascent 60S subunits is through the FKBP domain, as confirmed by *in vitro* binding assays, fig. 4.8(c). Similarly, NPM1 RRM domain is fundamental for the interaction with rRNA and NPM1 nucleolar localization [56]. It is possible that NPL-FKBP protein's FKBP domain shares some functions with NPM1 RRM, as the interaction with assembling ribosomes. Overall these exper-

iments suggest a model for the interaction within these proteins: Fkbp39 interacts with Fkbp41, is important for its localization to the rDNA locus and it bridges Fkbp41 to the nascent 60S subunit. In absence of Fkbp39, the interaction Fkbp41-Ytm1 is lost, but not the opposite, so in *fkbp41*Δ cells, the interaction Fkbp39-Ytm1 still occurs. As a consequence, in *fkbp39*Δ cells any interaction NPL-FKBP proteins-nascent 60S subunit is lost. Even though the interaction with the nascent 60S subunits happens through the FKBP domain, Fkbp39 residues 1-256 play an additional non characterized function *in vivo*. Indeed, Fkbp41 FKBP domain can interact with Ytm1 in *fkbp39_1-256* but not in *fkbp39*Δ cells, despite a similar Fkbp41 localization to the rDNA locus in these genetic backgrounds, fig. 4.8(c) and fig. 4.5(b).

From the mass spectrometry results, it appears that Fkbp39 interacts specifically with nascent 60S subunits. This is surprising because according to the current model of ribosome biogenesis, even though the two subunits go through independent maturation, both move from the internal DFC towards the external GC as maturation proceeds [52, 70]. *In vitro* binding assays show that Fkbp39 binds equally well both to nascent 60S and 40S subunits, fig. 4.10. Fkbp39 binding to nascent ribosomes is probably mediated by non-specific interactions rather than by the recognition of a binding partner, in agreement with previous data showing that NPM1 establishes only weak, transient and non-specific electrostatic interactions with nascent ribosomes [56, 55]. NPM1 partitions twenty folds or more within the human nucleolus,[72] specifically in the GC, so probably Fkbp39 does the same. As a consequence, the complexes interacting with Fkbp39, and identified by mass spectrometry, probably localize to the GC. This suggests that nascent 40S subunits are mainly excluded from the Fkbp39 organized GC.

5.3 Fkbp39-mediated phase separation in ribosome biogenesis

NPM1 plays a fundamental role in the organization of the nucleolus through LLPS [54]. Its phase separation properties have been extensively characterized *in vitro*: both the homotypic and heterotypic phase transition with rRNA and ribosomal proteins depend on electrostatic interactions between charged residues [55]. Similarly, Fkbp39 undergoes both homotypic phase separation, facilitated by the addition of a crowder such as PEG, and heterotypic phase transition with DNA and rRNA, fig. 4.11 and 4.13. Much more interesting, both nucleosomes and nascent 60S subunits partition into Fkbp39 condensates, fig. 4.14. Recently, chromatin condensation into phase-separated sub-compartments was reported by several publications. Two different mechanisms were proposed to explain this phenomenon: LLPS or polymer-polymer phase separation (PPPS, based on the binding of bridging factors that create a connected chromatin scaffold) [131]. Reconsti-

tuted chromatin undergoes LLPS in physiological condition, driven by histone tail interactions, promoted by H1 and regulated by histone modification, so that regions with different modifications organize into distinct sub-domains [132]. Histone modifications seem particularly important in this process since *readers* of these modifications can associate through LLPS, and organize functional sub-domains, such as silent heterochromatin [133, 134]. Although Fkbp39 can arrange nucleosomes into a phase-separated compartment *in vitro*, it is extremely unlikely that it organizes chromatin into a phase-separated sub-compartment *in vivo*. This because LLPS only starts when the amount of a key molecule exceeds its critical concentration, which for NPM1 happens far from the chromatin environment. In other words, of all the NPM1 proteins present inside the nucleolus only a small fraction localizes to chromatin and so it is extremely unlikely that this fraction reaches the threshold concentration required to drive phase separation.

In vivo Fkbp39 localizes to chromatin and interacts with nascent 60S subunits and *in vitro* phase separates with nucleosomes and nascent 60S subunits. To recapitulate the physiological situation and test the relevance of these interactions, we performed *in vitro* binding assays with Fkbp39 initially bound to nucleosomes, to which nascent 60S subunits were later added, fig. 4.15(a). This should roughly recapitulate Fkbp39 bound to the 25S rDNA in presence of emerging nascent 60S subunits, which are being co-transcriptionally assembled. This shows that Fkbp39:nucleosome complexes gradually disassemble and Fkbp39 binds to nascent 60S subunits. To prove that this process has a directionality, we performed the same *in vitro* binding assays adding the components in the reverse order: nucleosomes were added to Fkbp39:nascent 60S subunit complexes, fig. 4.15(b). In this case, Fkbp39:nascent 60S subunits complexes do not disassemble but instead Fkbp39 forms new complexes with nucleosomes. Similar experiments were performed with Fkbp39-organized condensates to assess the contribution of phase separation to these interactions, fig. 4.16 and 4.17, with similar results. This prompted us to build a model, which describes the first steps of nascent 60S subunits biogenesis, fig. 5.1. In wild type cells, Fkbp39 localizes to the rDNA locus, mainly at the 25S and 3'ETS rDNA. As Pol I transcribes, the pre-25S rRNA is processed and co-transcriptionally assembled into nascent 60S subunits. As nascent 60S subunits emerge, Fkbp39 dissociates from chromatin to bind them, leaving the chromatin environment (the central fibrillar strand, with characteristics of both FC and DFC). Indeed, fluorescence microscopy experiments suggest that Fkbp39 organizes condensates with either nascent 60S subunits or nucleosomes, even though the latter could enter very poorly into Fkbp39:nascent 60S subunit condensates, fig. 4.17. This phase contains Fkbp39, nascent 60S subunits and few nucleosomes. We tested for the formation of a three-component complex (with Fkbp39 binding at the same time to nucleosomes and nascent 60S subunits) but did not detect it (data not shown).

In our hypothesis, this three-component complex either does not form or is very transient and rare, being under the limit of detection. The *in vitro* binding assays support this model since there is no super-shift corresponding to this complex. It is possible, however, that the two complexes Fkbp39:nascent 60S subunits and Fkbp39:nucleosomes can coexist in one phase, especially if the latter is present in small amount, as microscopy suggests. As Fkbp39 binds to emerging nascent 60S subunits, it causes their partition away from chromatin through LLPS. The directionality of the process assures that nascent 60S subunits move from the internal compartments towards the external GC. We speculate that progressively, Fkbp39 proteins interact to organize the Fkbp39-enriched GC via LLPS. The Fkbp39-mediated nascent 60S subunits movement away from chromatin resembles the 5'ETS rRNA translocation to the DFC carried out by fibrillarin [71]. Our data are in agreement with a model, in which the nascent 40S and 60S subunits are moved away from chromatin and guided towards the processing compartments by the different key organizers of the nucleolus.

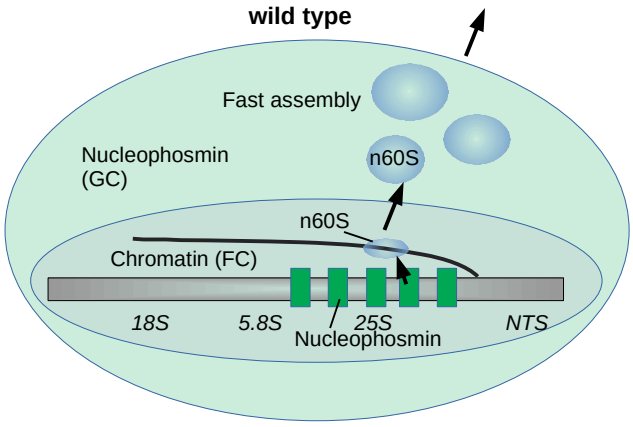

Figure 5.1: Model of Fkbp39 role in early 60S subunit biogenesis Fkbp39 binds the 25S and 3'ETS rDNA sites. As nascent 60S subunits emerge, Fkbp39 dissociates from chromatin to bind them, causing their partitioning away from chromatin through LLPS. This leads to the formation of the GC.

We also propose a different organization of ribosome biogenesis within the nucleolar compartments. Fibrillarin localization to both 18S and 25S rDNA sites, fig. 4.9, suggests that 2'-*O*-ribose methylation happens co-transcriptionally, when pre-rRNA is still associated with chromatin, thus earlier than what predicted by the current model, which places it in the DFC [135]. More significantly, we propose that both rRNA processing and co-transcriptional ribosome assembly take place within the DFC (F, in yeast), whereas in the current model ribosomal proteins associate with rRNA only within the GC [135]. Indeed, this is in partial contradiction with the co-transcriptional assembly model of ribosome biogenesis, valid both for yeasts

and higher eukaryotes, and with our mass spectrometry results, which portray a GC devoid of nascent 40S subunits [64] and table 4.1. We suggest that nascent 40S subunit maturation takes place within the DFC, together with rRNA processing and early assembly of the nascent 60S subunit. Then Fkbp39 mediates nascent 60S subunits partition into the GC, where later maturation occurs. In our model, Fkbp39 separates nascent 60S subunits from chromatin and nascent 40S subunits. We propose that Fkbp39 specificity for nascent 60S subunits is due to its chromatin localization over the 25S and 3'ETS rDNA, which provides the right position for partitioning onto emerging nascent 60S subunits.

This model allows prediction of the consequences of NPL-FKBP proteins deletion (such as the absence of the GC and retention of nascent 60S subunits on chromatin), which can be used to test it. Due to *S. pombe* dimension, a structural analysis of the nucleolus is very complex, so we tested nascent 60S subunits retention on chromatin. Nascent 60S subunits indeed accumulate towards the end of the rDNA transcriptional unit in *fkbp39*Δ and *fkbp39*Δ*fkbp41*Δ cells, but not in wild type nor *fkbp41*Δ cells, fig. 4.18. This result supports both the model and the hypothesis that Fkbp41 exerts its role in this process through Fkbp39. In absence of Fkbp39, cells exhibit defects in rRNA processing, which results in a reduced amount of rRNA and mature ribosomes, fig. 4.19 and 4.20. The rRNA processing defect seems compatible with a switch from NTC to RTC, which causes a retarded release of the mature rRNA when performing kinetic studies, fig. 4.19 [65]. This would suggest that *fkbp39*Δ cells are under stress. Anyway, *fkbp39*Δ cells grow similar to wild type, so ribosome production is only slightly affected. Moreover, cryo-EM data show that *fkbp39* deletion mainly results in a delayed assembly of 60S subunits. All these observations prompted us to conclude that the main role of compartmentalization is to increase the efficiency and kinetics of ribosome biogenesis, as previously predicted [46].

5.4 Negative genetic interaction between Fkbp39 and the RNAi pathway

Fkbp39 and the RNAi pathway display a negative genetic interaction: double mutant cells have a phenotype more severe than the combination of single mutants, fig. 4.22. This suggests that Fkbp39 and RNAi are component of different pathways that carry on the same function. In this case, when one of the two pathways is compromised, the other one can take over without, or with minor, consequences on cell growth, whereas in absence of both, defects become visible. On the contrary, Fkbp41 does not show a negative genetic

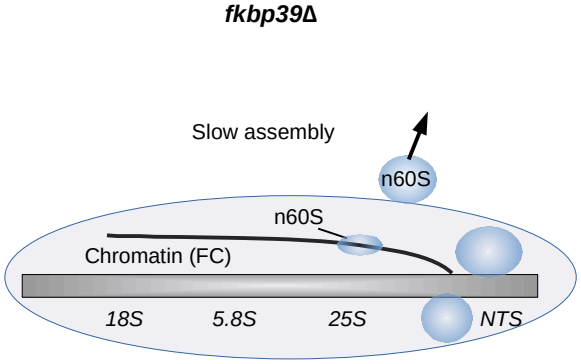

Figure 5.2: Impact of *fkbp39* deletion on early steps of 60S subunit biogenesis Model describing the main consequences of *fkbp39* deletion on 60S subunit biogenesis. In *fkbp39*Δ cells, nascent 60S subunits accumulate towards the end of the rDNA transcriptional unit, which results in a delay in rRNA processing and 60S subunit assembly.

interaction with RNAi. The different phenotype of the two NPL-FKBP proteins suggests that Fkbp39 and Fkbp41 have different roles or, as previously mentioned, that Fkbp39 is necessary for Fkbp41 functions, so in *fkbp39*Δ cells both activities are compromised while in *fkbp41*Δ cells Fkbp39 is fully functional.

S. pombe is a model organism for the study of RNAi mediated transcriptional silencing and, as a consequence, RNAi is very well characterized. This silencing pathway is mainly involved in transcriptional silencing of repetitive elements, is necessary for establishment and maintenance of centromeric heterochromatin, and supports heterochromatin formation at subtelomeres and the mating-type locus together with other pathways [86]. Defects in chromosome segregation and genome instability could be responsible for the severe growth defects observed in double mutant cells. Anyway, the minichromosome-loss assay shows that *fkbp39*Δ cells do not have a segregation defect, and, more relevant, *fkbp39*Δ*ago1*Δ double mutant cells have a similar phenotype as *ago1*Δ, fig. 4.23. This suggests that the double mutant severe growth defect is not due to a worsen chromosome segregation defect.

H3K9me2 ChIP-seq, Ago1-bound sRNA and total RNA sequencing support the idea of a role for Fkbp39 in heterochromatin formation. Indeed in *fkbp39*Δ cells, centromeric and subtelomeric transcripts are derepressed, there is a decrease in subtelomeric H3K9me2 and sRNAs arise from the subtelomeric locus *tlh*, fig. 4.24, 4.25 and 4.26. How Fkbp39 regulates heterochromatin is unclear. Fkbp39 has *in vitro* histone chaperone activity, so *in vivo* it might regulate histone incorporation at heterochromatic loci. However, H3 ChIP-seq shows that *fkbp39* deletion does not alter H3 localization at these loci, fig. 4.24. Fkbp39 localizes to rDNA, fig. 4.4, but in *S. pombe*, differently from other organisms, heterochromatin does not cluster in

proximity to the nucleolus, where rDNA is located [136].

Another possible explanation for the severe growth defect of double mutant cells exists. It is possible that in addition to Fkbp39 unknown role in heterochromatin, Fkbp39 and RNAi work in non-related important processes and that cell fitness is profoundly impaired when both are compromised. In support of this, even though RNAi compensates *fkbp39* deletion effects at subtelomeres, it is difficult to imagine that the little de-repression of heterochromatin transcripts in *fkbp39*Δ*ago1*Δ cells is responsible for their dramatic growth defect.

5.5 Argonaute proteins, not only silencing

Unexpectedly, *in vivo* translation assays suggest that *ago1*Δ cells have a compromised RNA transcription, which seems to be confirmed by nascent RNA sequencings, fig. 4.27 and 4.30. Since genome wide sequencing experiments, like nascent RNA, are sensitive to normalization, especially in case of a global change, this is not a clear-cut result. However, the RNA transcription defect was confirmed by different methods, *in vivo* translation assays and nascent RNA sequencing, and different normalizations. Total RNA sequencing from *ago1*Δ cells is very similar to wild type, at the exception of the de-repression of heterochromatin transcripts, in agreement with published data. The 10 minutes time point of nascent RNA sequencing, which can be already considered very close to steady state, does not display significant differences as well. This suggests that RNA transcription is slower but it is balanced by compensatory mechanisms, possibly by a reduced RNA turnover. Not all RNA classes are uniformly slowed down, with coding sequence transcripts being the most affected. Moreover, such a drastic reduction in RNA synthesis is not shared by all RNAi mutants. Pol II is normally located at coding sequences in *ago1*Δ cells, with higher enrichment at heterochromatic loci as expected, fig. 4.31. These data do not allow the presentation of a model but suggest that Ago1 is involved rather than the process of heterochromatin establishment (as H3K9me deposition and recognition).

Argonaute proteins are widely-know for their role in silencing pathways together with guiding small RNAs. However, several observations suggest that they might act also as transcriptional activators, although the mechanism is still debated. In cultured human cells, some argonaute bound-small RNAs targeting the promoter region can induce a long-lasting transcription activation of the corresponding locus, a phenomenon initially named dsRNA-induced gene activation (RNAa) [137, 138]. These small RNAs complementary to promoter regions target non-coding antisense transcripts originated from the corresponding locus, and in-

duce deposition of activating post-translational modification at the target promoter [139]. This led to the formulation of two opposite possible mechanisms of action. The *trans*-acting RNAa model suggests that transcription activation is the result of an off-target post-transcriptional gene silencing: the non-coding RNA is down-regulated by RNAi and this leads to de-repression of the corresponding transcript [140]. Opposite to this, in the *cis*-acting RNAa model, the argonaute-small RNA complex is targeted to the promoter region by base-pairing interactions with the promoter-associated antisense non-coding RNA, which acts as a scaffold for the recruitment of chromatin-modifying complexes that activate transcription (not so different from the ”nascent transcript model” of heterochromatin assembly described previously) [141]. More possibilities for argonaute proteins recruitment to the promoter region have been postulated, which differ in the target used for base-pairing interactions with the small activating RNA (sense or antisense non-coding RNAs, single-strand promoter DNA or double-strand promoter DNA) [142]. The complexes recruited at the promoter region were suggested to stimulate transcription initiation and elongation also by interacting with Pol II [143]. In agreement with this, in the nucleus of human cancer cells, Ago1 is associated with chromatin, interacts with Pol II and seems to activate transcription [144]. Also in *Arabidopsis thaliana*, AGO1 was detected on chromatin, where it positively regulates gene transcription [145]. AGO1 site-specific recruitment to chromatin depends on sRNAs, and it probably promotes transcription by facilitating Pol II localization. Pol II occupancy at AGO1 regulated genes is indeed reduced in AGO1 depleted cells [145].

Despite all these observations support the idea that argonaute proteins could positively regulate gene transcriptions, there are profound differences with the *S. pombe* defect in RNA transcription here reported. Indeed in all the mentioned studies, argonaute proteins were detected on chromatin and regulate the transcription of a set of defined genes, to which they are recruited by small RNAs. On the contrary, in *S. pombe*, Ago1 seems to regulate the whole Pol II transcription, without being guided to specific targets by small RNAs. It is possible, that *ago1* deletion impact on RNA transcription is due to an indirect effect. Despite being a direct or indirect effect, it seems that in *ago1*Δ cells, Pol II is normally recruited to coding sequences, suggesting that there might be a problem during early steps of transcription or during elongation (around 28% of *S. pombe* genes exhibit a Pol II promoter-proximal pause-like distributions in wild type cells [146]).

It is possible that *fkbp39*Δ*ago1*Δ cells growth defect might be due to Fkbp39 and Ago1 non-overlapping role (or indirect effect in case of *ago1*Δ) in ribosome biogenesis and transcription, respectively. Indeed *fkbp39*Δ*ago1*Δ cells have reduced transcription and translation, fig. 4.27 and 4.28, which seem the cumulative effect of *fkbp39* and *ago1* deletion. Even though it is difficult to assess the causality relation between slow cell growth and compromised transcription and translation due to the intrinsic connection of these pro-

cesses (”chicken-egg causality dilemma”), despite all the efforts, these were the only phenotypes observed for *fkbp39*Δ*ago1*Δ cells.

5.6 Conclusion and future perspective

Phase separation is a fundamental strategy used within cells to organize macromolecules and processes efficiently. Nowadays it is widely accepted that membrane-less organelles organize thanks to the presence of different non-miscible phases, and experimental data match very well the physical implication of this model [47, 46]. It seems that phase separation not only explains the characteristic of these organelles but also supports the organization of other structures such as chromatin domains [131, 134]. However, relative few studies concentrate on the biological implications of this type of interactions.

This thesis focused on the role of yeast nucleophosmin like proteins in ribosome biogenesis, and investigated the causes of their negative genetic interaction with the RNAi pathway in *S. pombe*.

NPM1 is the main structural element of the granular component and its role in nucleolar architecture organization through phase separation is very well characterized [54, 55]. Due to this localization, it is considered to interact with late nucleolar assembling ribosomes, and to assist their escort to the nucleus [72]. However, NPM1 was detected on rDNA [19, 22, 20], as well as one of its *S. cerevisiae* homologous [29]. Both Fkbp39 and Fkbp41 localize to the rDNA chromatin, especially over the 25S and 3’ ETS rDNA, fig. 4.4. In agreement with published data and their cellular localization, these proteins interact with nascent ribosomes [21, 32], table 4.1 and fig. 4.7. Moreover, Fkbp39 phase separation properties are similar to NPM1, fig. 4.11 and 4.13. All of these observations suggest that *S. pombe* NPL-FKBP proteins have similar functions as human NPM1. We were particularly interested in investigating the role of Fkbp39 localization to rDNA in ribosome biogenesis. Data from *in vitro* binding assays and fluorescence microscopy experiments, led us towards a model describing Fkbp39 early role in ribosome biogenesis and nascent subunits segregation, fig. 5.1. According to our model, Fkbp39 separates nascent 60S subunits from chromatin and, while doing so, thanks to the interaction with surrounding Fkbp39 molecules, organizes via liquid-liquid phase separation the compartment where their maturation occurs. Mass spectrometry data show that nascent 40S subunits are mostly excluded from this compartment, so we suggest that 40S subunit nucleolar processing happens almost exclusively in the dense fibrillar component. Absence of the granular component indeed mainly affects 60S subunit biogenesis, fig. 4.18, 4.19 and 4.20. Our data suggest that phase separation is required for efficient processing, as in absence of the granular component 60S subunit biogenesis slows down. Fkbp39

chromatin localization is fundamental for its early role in ribosome biogenesis, being responsible for the *in vivo* nascent 60S subunit specificity, fig. 4.10. Because of this, it would be very interesting to investigate which factors restrict Fkbp39 localization mainly over the 25S and 3' ETS rDNA.

Despite being less characterized, NPL-FKBP proteins have additional functions within yeasts cells [30, 33, 34, 36, 37]. By investigating the cause of the negative genetic interaction between Fkbp39 and the RNAi pathway in *S. pombe* we made interesting findings: Fkbp39 contributes to heterochromatin silencing and Ago1 seems to regulate transcription. For both these processes, the mechanism is unknown. Further studies are required to confirm these observations and to clarify if these phenotypes are due to direct or indirect consequences of deletion of *fkbp39* and *ago1* genes, respectively.

Bibliography

[1] L. J. Frehlick, J. M. Eirin-Lopez, and J. Ausio, “New insights into the nucleophosmin/nucleoplasmin family of nuclear chaperones,” *Bioessays*, vol. 29, pp. 49–59, Jan 2007.

[2] J. Ellis, “Proteins as molecular chaperones,” *Nature*, vol. 328, no. 6129, pp. 378–379, 1987.

[3] R. A. Laskey, B. M. Honda, A. D. Mills, and J. T. Finch, “Nucleosomes are assembled by an acidic protein which binds histones and transfers them to DNA,” *Nature*, vol. 275, pp. 416–420, Oct 1978.

[4] A. Philpott, T. Krude, and R. A. Laskey, “Nuclear chaperones,” *Semin. Cell Dev. Biol.*, vol. 11, pp. 7–14, Feb 2000.

[5] M. S. Lindstrom, “NPM1/B23: A Multifunctional Chaperone in Ribosome Biogenesis and Chromatin Remodeling,” *Biochem Res Int*, vol. 2011, p. 195209, 2011.

[6] S. Dutta, I. V. Akey, C. Dingwall, K. L. Hartman, T. Laue, R. T. Nolte, J. F. Head, and C. W. Akey, “The crystal structure of nucleoplasmin-core: Implications for histone binding and nucleosome assembly,” *Molecular Cell*, vol. 8, no. 4, pp. 841 – 853, 2001.

[7] V. M. Namboodiri, I. V. Akey, M. S. Schmidt-Zachmann, J. F. Head, and C. W. Akey, “The structure and function of Xenopus NO38-core, a histone chaperone in the nucleolus,” *Structure*, vol. 12, pp. 2149–2160, Dec 2004.

[8] C. Warren, T. Matsui, J. M. Karp, T. Onikubo, S. Cahill, M. Brenowitz, D. Cowburn, M. Girvin, and D. Shechter, “Dynamic intramolecular regulation of the histone chaperone nucleoplasmin controls histone binding and release,” *Nat Commun*, vol. 8, p. 2215, 12 2017.

[9] D. Wang, A. Baumann, A. Szebeni, and M. O. Olson, “The nucleic acid binding activity of nucleolar protein B23.1 resides in its carboxyl-terminal end,” *J. Biol. Chem.*, vol. 269, pp. 30994–30998, Dec 1994.

[10] I. Ramos, N. Fernandez-Rivero, R. Arranz, K. Aloria, R. Finn, J. M. Arizmendi, J. Ausio, J. M. Valpuesta, A. Muga, and A. Prado, “The intrinsically disordered distal face of nucleoplasmin recognizes distinct oligomerization states of histones,” *Nucleic Acids Res.*, vol. 42, pp. 1311–1325, Jan 2014.

[11] A. Franco, R. Arranz, N. Fernandez-Rivero, A. Velazquez-Campoy, J. Martin-Benito, J. Segura, A. Prado, J. M. Valpuesta, and A. Muga, “Structural insights into the ability of nucleoplasmin to assemble and chaperone histone octamers for DNA deposition,” *Sci Rep*, vol. 9, p. 9487, 07 2019.

[12] M. Okuwaki, K. Matsumoto, M. Tsujimoto, and K. Nagata, “Function of nucleophosmin/B23, a nucleolar acidic protein, as a histone chaperone,” *FEBS Lett.*, vol. 506, pp. 272–276, Oct 2001.

[13] S. S. Gadad, J. Shandilya, A. H. Kishore, and T. K. Kundu, “NPM3, a member of the nucleophosmin/nucleoplasmin family, enhances activator-dependent transcription,” *Biochemistry*, vol. 49, pp. 1355–1357, Feb 2010.

[14] M. Okuwaki, A. Sumi, M. Hisaoka, A. Saotome-Nakamura, S. Akashi, Y. Nishimura, and K. Nagata, “Function of homo- and hetero-oligomers of human nucleoplasmin/nucleophosmin family proteins NPM1, NPM2 and NPM3 during sperm chromatin remodeling,” *Nucleic Acids Res.*, vol. 40, pp. 4861–4878, Jun 2012.

[15] R. J. Burgess and Z. Zhang, “Histone chaperones in nucleosome assembly and human disease,” *Nat. Struct. Mol. Biol.*, vol. 20, pp. 14–22, Jan 2013.

[16] J. K. Box, N. Paquet, M. N. Adams, D. Boucher, E. Bolderson, K. J. O’Byrne, and D. J. Richard, “Nucleophosmin: from structure and function to disease development,” *BMC Mol. Biol.*, vol. 17, p. 19, 08 2016.

[17] D. M. Mitrea, C. R. Grace, M. Buljan, M. K. Yun, N. J. Pytel, J. Satumba, A. Nourse, C. G. Park, M. Madan Babu, S. W. White, and R. W. Kriwacki, “Structural polymorphism in the N-terminal oligomerization domain of NPM1,” *Proc. Natl. Acad. Sci. U.S.A.*, vol. 111, pp. 4466–4471, Mar 2014.

[18] M. A. Amin, S. Matsunaga, S. Uchiyama, and K. Fukui, “Depletion of nucleophosmin leads to distortion of nucleolar and nuclear structures in HeLa cells,” *Biochem. J.*, vol. 415, pp. 345–351, Nov 2008.

[19] S. Chiarella, A. De Cola, G. L. Scaglione, E. Carletti, V. Graziano, D. Barcaroli, C. Lo Sterzo, A. Di Matteo, C. Di Ilio, B. Falini, A. Arcovito, V. De Laurenzi, and L. Federici, “Nucleophosmin mutations alter its nucleolar localization by impairing G-quadruplex binding at ribosomal DNA,” *Nucleic Acids Res.*, vol. 41, pp. 3228–3239, Mar 2013.

[20] D. Papaioannou, A. Petri, O. M. Dovey, S. Terreri, E. Wang, F. A. Collins, L. A. Woodward, A. E. Walker, D. Nicolet, F. Pepe, P. Kumchala, M. Bill, C. J. Walker, M. Karunasiri, K. Mrozek, M. L. Gardner, V. Camilotto, N. Zitzer, J. L. Cooper, X. Cai, X. Rong-Mullins, J. Kohlschmidt, K. J. Archer, M. A. Freitas, Y. Zheng, R. J. Lee, I. Aifantis, G. Vassiliou, G. Singh, S. Kauppinen, C. D. Bloomfield, A. M. Dorrance, and R. Garzon, “The long non-coding RNA HOXB-AS3 regulates ribosomal RNA transcription in NPM1-mutated acute myeloid leukemia,” *Nat Commun*, vol. 10, p. 5351, 11 2019.

[21] A. Darracq, H. Pak, V. Bourgoin, F. Zmiri, G. Dellaire, E. B. Affar, and E. Milot, “NPM and NPM-MLF1 interact with chromatin remodeling complexes and influence their recruitment to specific genes,” *PLoS Genet.*, vol. 15, p. e1008463, 11 2019.

[22] K. Murano, M. Okuwaki, M. Hisaoka, and K. Nagata, “Transcription regulation of the rRNA gene by a multifunctional nucleolar protein, B23/nucleophosmin, through its histone chaperone activity,” *Mol. Cell. Biol.*, vol. 28, pp. 3114–3126, May 2008.

[23] Y. Yu, L. B. Maggi, S. N. Brady, A. J. Apicelli, M. S. Dai, H. Lu, and J. D. Weber, “Nucleophosmin is essential for ribosomal protein L5 nuclear export,” *Mol. Cell. Biol.*, vol. 26, pp. 3798–3809, May 2006.

[24] K. Itahana, K. P. Bhat, A. Jin, Y. Itahana, D. Hawke, R. Kobayashi, and Y. Zhang, “Tumor suppressor ARF degrades B23, a nucleolar protein involved in ribosome biogenesis and cell proliferation,” *Mol. Cell*, vol. 12, pp. 1151–1164, Nov 2003.

[25] L. B. Maggi, M. Kuchenruether, D. Y. Dadey, R. M. Schwope, S. Grisendi, R. R. Townsend, P. P. Pandolfi, and J. D. Weber, “Nucleophosmin serves as a rate-limiting nuclear export chaperone for the Mammalian ribosome,” *Mol. Cell. Biol.*, vol. 28, pp. 7050–7065, Dec 2008.

[26] C. Edlich-Muth, J. B. Artero, P. Callow, M. R. Przewloka, A. A. Watson, W. Zhang, D. M. Glover, J. Debski, M. Dadlez, A. R. Round, V. T. Forsyth, and E. D. Laue, “The pentameric nucleoplasmin fold is present in Drosophila FKBP39 and a large number of chromatin-related proteins,” *J. Mol. Biol.*, vol. 427, pp. 1949–1963, May 2015.

[27] K. P. Lu, G. Finn, T. H. Lee, and L. K. Nicholson, “Prolyl cis-trans isomerization as a molecular timer,” *Nat. Chem. Biol.*, vol. 3, pp. 619–629, Oct 2007.

[28] J. M. Bonner and G. L. Boulianne, “Diverse structures, functions and uses of FK506 binding proteins,” *Cell. Signal.*, vol. 38, pp. 97–105, 10 2017.

[29] T. Kuzuhara and M. Horikoshi, “A nuclear FK506-binding protein is a histone chaperone regulating rDNA silencing,” *Nat. Struct. Mol. Biol.*, vol. 11, pp. 275–283, Mar 2004.

[30] S. K. Park, H. Xiao, and M. Lei, “Nuclear FKBPs, Fpr3 and Fpr4 affect genome-wide genes transcription,” *Mol. Genet. Genomics*, vol. 289, pp. 125–136, Apr 2014.

[31] A. Leung, F. P. Jardim, N. Savic, Y. R. Monneau, R. Gonzàlez-Romero, G. Gudavicius, J. M. Eirin-Lopez, T. Bartke, C. D. Mackereth, J. Ausiò, and C. J. Nelson, “Basic surface features of nuclear FKBPs facilitate chromatin binding,” *Sci Rep*, vol. 7, p. 3795, 06 2017.

[32] L. Kater, M. Thoms, C. Barrio-Garcia, J. Cheng, S. Ismail, Y. L. Ahmed, G. Bange, D. Kressler, O. Berninghausen, I. Sinning, E. Hurt, and R. Beckmann, “Visualizing the Assembly Pathway of Nucleolar Pre-60S Ribosomes,” *Cell*, vol. 171, pp. 1599–1610, Dec 2017.

[33] C. J. Nelson, H. Santos-Rosa, and T. Kouzarides, “Proline isomerization of histone H3 regulates lysine methylation and gene expression,” *Cell*, vol. 126, pp. 905–916, Sep 2006.

[34] K. Ohkuni, R. Abdulle, and K. Kitagawa, “Degradation of centromeric histone H3 variant Cse4 requires the Fpr3 peptidyl-prolyl Cis-Trans isomerase,” *Genetics*, vol. 196, pp. 1041–1045, Apr 2014.

[35] A. Matsuyama, R. Arai, Y. Yashiroda, A. Shirai, A. Kamata, S. Sekido, Y. Kobayashi, A. Hashimoto, M. Hamamoto, Y. Hiraoka, S. Horinouchi, and M. Yoshida, “ORFeome cloning and global analysis of protein localization in the fission yeast Schizosaccharomyces pombe,” *Nat. Biotechnol.*, vol. 24, pp. 841–847, Jul 2006.

[36] H. L. Tan, K. K. Lim, Q. Yang, J. S. Fan, A. M. M. Sayed, L. S. Low, B. Ren, T. K. Lim, Q. Lin, Y. K. Mok, Y. C. Liou, and E. S. Chen, "Prolyl isomerization of the CENP-A N-terminus regulates centromeric integrity in fission yeast," *Nucleic Acids Res.*, vol. 46, pp. 1167–1179, 02 2018.

[37] L. J. Jahn, B. Mason, P. Brogger, T. Toteva, D. K. Nielsen, and G. Thon, "Dependency of Heterochromatin Domains on Replication Factors," *G3 (Bethesda)*, vol. 8, pp. 477–489, 02 2018.

[38] "PomBase." `https://www.pombase.org/`. Accessed: 2020-04-20.

[39] S. F. Banani, H. O. Lee, A. A. Hyman, and M. K. Rosen, "Biomolecular condensates: organizers of cellular biochemistry," *Nat. Rev. Mol. Cell Biol.*, vol. 18, pp. 285–298, 05 2017.

[40] C. P. Brangwynne, C. R. Eckmann, D. S. Courson, A. Rybarska, C. Hoege, J. Gharakhani, F. Julicher, and A. A. Hyman, "Germline P granules are liquid droplets that localize by controlled dissolution/condensation," *Science*, vol. 324, pp. 1729–1732, Jun 2009.

[41] C. P. Brangwynne, T. J. Mitchison, and A. A. Hyman, "Active liquid-like behavior of nucleoli determines their size and shape in Xenopus laevis oocytes," *Proc. Natl. Acad. Sci. U.S.A.*, vol. 108, pp. 4334–4339, Mar 2011.

[42] C. C. Correll, J. Bartek, and M. Dundr, "The Nucleolus: A Multiphase Condensate Balancing Ribosome Synthesis and Translational Capacity in Health, Aging and Ribosomopathies," *Cells*, vol. 8, 08 2019.

[43] R. Somjee, D. M. Mitrea, and R. W. Kriwacki, "Exploring Relationships between the Density of Charged Tracts within Disordered Regions and Phase Separation," *Pac Symp Biocomput*, vol. 25, pp. 207–218, 2020.

[44] P. Li, S. Banjade, H. C. Cheng, S. Kim, B. Chen, L. Guo, M. Llaguno, J. V. Hollingsworth, D. S. King, S. F. Banani, P. S. Russo, Q. X. Jiang, B. T. Nixon, and M. K. Rosen, "Phase transitions in the assembly of multivalent signalling proteins," *Nature*, vol. 483, pp. 336–340, Mar 2012.

[45] S. C. Weber and C. P. Brangwynne, "Getting RNA and protein in phase," *Cell*, vol. 149, pp. 1188–1191, Jun 2012.

[46] D. M. Mitrea and R. W. Kriwacki, "Phase separation in biology; functional organization of a higher order," *Cell Commun. Signal*, vol. 14, p. 1, Jan 2016.

[47] S. F. Banani, A. M. Rice, W. B. Peeples, Y. Lin, S. Jain, R. Parker, and M. K. Rosen, “Compositional Control of Phase-Separated Cellular Bodies,” *Cell*, vol. 166, pp. 651–663, Jul 2016.

[48] E. Matos-Perdomo and F. Machin, “Nucleolar and Ribosomal DNA Structure under Stress: Yeast Lessons for Aging and Cancer,” *Cells*, vol. 8, 07 2019.

[49] T. Pederson, “The nucleolus,” *Cold Spring Harb Perspect Biol*, vol. 3, Mar 2011.

[50] F. M. Boisvert, S. van Koningsbruggen, J. Navascues, and A. I. Lamond, “The multifunctional nucleolus,” *Nat. Rev. Mol. Cell Biol.*, vol. 8, pp. 574–585, Jul 2007.

[51] F. Frottin, F. Schueder, S. Tiwary, R. Gupta, R. Korner, T. Schlichthaerle, J. Cox, R. Jungmann, F. U. Hartl, and M. S. Hipp, “The nucleolus functions as a phase-separated protein quality control compartment,” *Science*, vol. 365, pp. 342–347, 07 2019.

[52] M. Thiry and D. L. Lafontaine, “Birth of a nucleolus: the evolution of nucleolar compartments,” *Trends Cell Biol.*, vol. 15, pp. 194–199, Apr 2005.

[53] M. Thiry, F. Lamaye, and D. L. Lafontaine, “The nucleolus: when 2 became 3,” *Nucleus*, vol. 2, no. 4, pp. 289–293, 2011.

[54] M. Feric, N. Vaidya, T. S. Harmon, D. M. Mitrea, L. Zhu, T. M. Richardson, R. W. Kriwacki, R. V. Pappu, and C. P. Brangwynne, “Coexisting Liquid Phases Underlie Nucleolar Subcompartments,” *Cell*, vol. 165, pp. 1686–1697, Jun 2016.

[55] D. M. Mitrea, J. A. Cika, C. B. Stanley, A. Nourse, P. L. Onuchic, P. R. Banerjee, A. H. Phillips, C. G. Park, A. A. Deniz, and R. W. Kriwacki, “Self-interaction of NPM1 modulates multiple mechanisms of liquid-liquid phase separation,” *Nat Commun*, vol. 9, p. 842, 02 2018.

[56] D. M. Mitrea, J. A. Cika, C. S. Guy, D. Ban, P. R. Banerjee, C. B. Stanley, A. Nourse, A. A. Deniz, and R. W. Kriwacki, “Nucleophosmin integrates within the nucleolus via multi-modal interactions with proteins displaying R-rich linear motifs and rRNA,” *Elife*, vol. 5, Feb 2016.

[57] M. C. Ferrolino, D. M. Mitrea, J. R. Michael, and R. W. Kriwacki, “Compositional adaptability in NPM1-SURF6 scaffolding networks enabled by dynamic switching of phase separation mechanisms,” *Nat Commun*, vol. 9, p. 5064, 11 2018.

[58] R. J. Jackson, C. U. Hellen, and T. V. Pestova, “The mechanism of eukaryotic translation initiation and principles of its regulation,” *Nat. Rev. Mol. Cell Biol.*, vol. 11, pp. 113–127, Feb 2010.

[59] T. E. Dever and R. Green, “The elongation, termination, and recycling phases of translation in eukaryotes,” *Cold Spring Harb Perspect Biol*, vol. 4, p. a013706, Jul 2012.

[60] J. Bassler and E. Hurt, “Eukaryotic Ribosome Assembly,” *Annu. Rev. Biochem.*, vol. 88, pp. 281–306, 06 2019.

[61] J. Venema and D. Tollervey, “Processing of pre-ribosomal RNA in Saccharomyces cerevisiae,” *Yeast*, vol. 11, pp. 1629–1650, Dec 1995.

[62] M. Ciganda and N. Williams, “Eukaryotic 5S rRNA biogenesis,” *Wiley Interdiscip Rev RNA*, vol. 2, no. 4, pp. 523–533, 2011.

[63] R. Tomecki, P. J. Sikorski, and M. Zakrzewska-Placzek, “Comparison of preribosomal RNA processing pathways in yeast, plant and human cells - focus on coordinated action of endo- and exoribonucleases,” *FEBS Lett.*, vol. 591, pp. 1801–1850, 07 2017.

[64] Y. N. Osheim, S. L. French, K. M. Keck, E. A. Champion, K. Spasov, F. Dragon, S. J. Baserga, and A. L. Beyer, “Pre-18S ribosomal RNA is structurally compacted into the SSU processome prior to being cleaved from nascent transcripts in Saccharomyces cerevisiae,” *Mol. Cell*, vol. 16, pp. 943–954, Dec 2004.

[65] M. Kos and D. Tollervey, “Yeast pre-rRNA processing and modification occur cotranscriptionally,” *Mol. Cell*, vol. 37, pp. 809–820, Mar 2010.

[66] T. W. Turowski and D. Tollervey, “Cotranscriptional events in eukaryotic ribosome synthesis,” *Wiley Interdiscip Rev RNA*, vol. 6, no. 1, pp. 129–139, 2015.

[67] M. Kornprobst, M. Turk, N. Kellner, J. Cheng, D. Flemming, I. Kos-Braun, M. Kos, M. Thoms, O. Berninghausen, R. Beckmann, and E. Hurt, “Architecture of the 90S Pre-ribosome: A Structural View on the Birth of the Eukaryotic Ribosome,” *Cell*, vol. 166, pp. 380–393, Jul 2016.

[68] K. Axt, S. L. French, A. L. Beyer, and D. Tollervey, “Kinetic analysis demonstrates a requirement for the Rat1 exonuclease in cotranscriptional pre-rRNA cleavage,” *PLoS ONE*, vol. 9, no. 2, p. e85703, 2014.

[69] Y. Du, W. An, X. Zhu, Q. Sun, J. Qi, and K. Ye, “Cryo-EM structure of 90S small ribosomal subunit precursors in transition states,” *Science.*, vol. 369, pp. 1477–1481, Sep 2020.

[70] S. Klinge and J. L. Woolford, “Ribosome assembly coming into focus,” *Nat. Rev. Mol. Cell Biol.*, vol. 20, pp. 116–131, 02 2019.

[71] R. W. Yao, G. Xu, Y. Wang, L. Shan, P. F. Luan, Y. Wang, M. Wu, L. Z. Yang, Y. H. Xing, L. Yang, and L. L. Chen, “Nascent Pre-rRNA Sorting via Phase Separation Drives the Assembly of Dense Fibrillar Components in the Human Nucleolus,” *Mol. Cell*, vol. 76, pp. 767–783, 12 2019.

[72] J. A. Riback, L. Zhu, M. C. Ferrolino, M. Tolbert, D. M. Mitrea, D. W. Sanders, M. T. Wei, R. W. Kriwacki, and C. P. Brangwynne, “Composition-dependent thermodynamics of intracellular phase separation,” *Nature*, vol. 581, pp. 209–214, 05 2020.

[73] M. Thanbichler, S. C. Wang, and L. Shapiro, “The bacterial nucleoid: a highly organized and dynamic structure,” *J. Cell. Biochem.*, vol. 96, pp. 506–521, Oct 2005.

[74] K. Luger, A. W. Mader, R. K. Richmond, D. F. Sargent, and T. J. Richmond, “Crystal structure of the nucleosome core particle at 2.8 A resolution,” *Nature*, vol. 389, pp. 251–260, Sep 1997.

[75] E. Prieto, K. Hizume, T. Kobori, S. H. Yoshimura, and K. Takeyasu, “Core histone charge and linker histone H1 effects on the chromatin structure of Schizosaccharomyces pombe,” *Biosci. Biotechnol. Biochem.*, vol. 76, no. 12, pp. 2261–2266, 2012.

[76] A. Vaquero, A. Loyola, and D. Reinberg, “The constantly changing face of chromatin,” *Sci Aging Knowledge Environ*, vol. 2003, p. RE4, Apr 2003.

[77] K. Luger, M. L. Dechassa, and D. J. Tremethick, “New insights into nucleosome and chromatin structure: an ordered state or a disordered affair?,” *Nat. Rev. Mol. Cell Biol.*, vol. 13, pp. 436–447, Jun 2012.

[78] R. Margueron and D. Reinberg, “Chromatin structure and the inheritance of epigenetic information,” *Nat. Rev. Genet.*, vol. 11, pp. 285–296, Apr 2010.

[79] J. Gayon, “From Mendel to epigenetics: History of genetics,” *C. R. Biol.*, vol. 339, no. 7-8, pp. 225–230, 2016.

[80] E. Heitz, *Das heterochromatin der moose*. Bornträger, 1928.

[81] T. Straub, “Heterochromatin dynamics,” *PLoS Biol.*, vol. 1, p. E14, Oct 2003.

[82] J. Liu, M. Ali, and Q. Zhou, “Establishment and evolution of heterochromatin,” *Ann. N. Y. Acad. Sci.*, Feb 2020.

[83] R. C. Allshire and H. D. Madhani, “Ten principles of heterochromatin formation and function,” *Nat. Rev. Mol. Cell Biol.*, vol. 19, pp. 229–244, 04 2018.

[84] Y. Huang, “Transcriptional silencing in Saccharomyces cerevisiae and Schizosaccharomyces pombe,” *Nucleic Acids Res.*, vol. 30, pp. 1465–1482, Apr 2002.

[85] V. Wood, R. Gwilliam, M. A. Rajandream, M. Lyne, R. Lyne, A. Stewart, J. Sgouros, N. Peat, J. Hayles, S. Baker, D. Basham, S. Bowman, K. Brooks, D. Brown, S. Brown, T. Chillingworth, C. Churcher, M. Collins, R. Connor, A. Cronin, P. Davis, T. Feltwell, A. Fraser, S. Gentles, A. Goble, N. Hamlin, D. Harris, J. Hidalgo, G. Hodgson, S. Holroyd, T. Hornsby, S. Howarth, E. J. Huckle, S. Hunt, K. Jagels, K. James, L. Jones, M. Jones, S. Leather, S. McDonald, J. McLean, P. Mooney, S. Moule, K. Mungall, L. Murphy, D. Niblett, C. Odell, K. Oliver, S. O’Neil, D. Pearson, M. A. Quail, E. Rabbinowitsch, K. Rutherford, S. Rutter, D. Saunders, K. Seeger, S. Sharp, J. Skelton, M. Simmonds, R. Squares, S. Squares, K. Stevens, K. Taylor, R. G. Taylor, A. Tivey, S. Walsh, T. Warren, S. Whitehead, J. Woodward, G. Volckaert, R. Aert, J. Robben, B. Grymonprez, I. Weltjens, E. Vanstreels, M. Rieger, M. Schafer, S. Muller-Auer, C. Gabel, M. Fuchs, A. Dusterhoft, C. Fritzc, E. Holzer, D. Moestl, H. Hilbert, K. Borzym, I. Langer, A. Beck, H. Lehrach, R. Reinhardt, T. M. Pohl, P. Eger, W. Zimmermann, H. Wedler, R. Wambutt, B. Purnelle, A. Goffeau, E. Cadieu, S. Dreano, S. Gloux, V. Lelaure, S. Mottier, F. Galibert, S. J. Aves, Z. Xiang, C. Hunt, K. Moore, S. M. Hurst, M. Lucas, M. Rochet, C. Gaillardin, V. A. Tallada, A. Garzon, G. Thode, R. R. Daga, L. Cruzado, J. Jimenez, M. Sanchez, F. del Rey, J. Benito, A. Dominguez, J. L. Revuelta, S. Moreno, J. Armstrong, S. L. Forsburg, L. Cerutti, T. Lowe, W. R. McCombie, I. Paulsen, J. Potashkin, G. V. Shpakovski, D. Ussery, B. G. Barrell, P. Nurse, and L. Cerrutti, “The genome sequence of Schizosaccharomyces pombe,” *Nature*, vol. 415, pp. 871–880, Feb 2002.

[86] R. Martienssen and D. Moazed, “RNAi and heterochromatin assembly,” *Cold Spring Harb Perspect Biol*, vol. 7, p. a019323, Aug 2015.

[87] H. D. Folco, A. L. Pidoux, T. Urano, and R. C. Allshire, “Heterochromatin and RNAi are required to establish CENP-A chromatin at centromeres,” *Science*, vol. 319, pp. 94–97, Jan 2008.

[88] S. Tashiro, Y. Nishihara, K. Kugou, K. Ohta, and J. Kanoh, “Subtelomeres constitute a safeguard for gene expression and chromosome homeostasis,” *Nucleic Acids Res.*, vol. 45, pp. 10333–10349, Oct 2017.

[89] I. Hall, G. Shankaranarayana, K. Noma, N. Ayoub, A. Cohen, and S. Grewal, “Establishment and maintenance of a heterochromatin domain,” *Science.*, vol. 297, pp. 2232–2237, Sep 2002.

[90] H. Cam, T. Sugiyama, E. Chen, X. Chen, P. FitzGerald, and S. Grewal, “Comprehensive analysis of heterochromatin- and RNAi-mediated epigenetic control of the fission yeast genome.,” *Nat Genet.*, vol. 37, pp. 809–819, Aug 2005.

[91] D. Holoch and D. Moazed, “RNA-mediated epigenetic regulation of gene expression,” *Nat. Rev. Genet.*, vol. 16, pp. 71–84, Feb 2015.

[92] J. J. Ipsaro and L. Joshua-Tor, “From guide to target: molecular insights into eukaryotic RNA-interference machinery,” *Nat. Struct. Mol. Biol.*, vol. 22, pp. 20–28, Jan 2015.

[93] M. Halic and D. Moazed, “Dicer-independent primal RNAs trigger RNAi and heterochromatin formation,” *Cell*, vol. 140, pp. 504–516, Feb 2010.

[94] M. Marasovic, M. Zocco, and M. Halic, “Argonaute and Triman generate dicer-independent priRNAs and mature siRNAs to initiate heterochromatin formation,” *Mol. Cell*, vol. 52, pp. 173–183, Oct 2013.

[95] A. Verdel, S. Jia, S. Gerber, T. Sugiyama, S. Gygi, S. I. Grewal, and D. Moazed, “RNAi-mediated targeting of heterochromatin by the RITS complex,” *Science*, vol. 303, pp. 672–676, Jan 2004.

[96] E. H. Bayne, S. A. White, A. Kagansky, D. A. Bijos, L. Sanchez-Pulido, K. L. Hoe, D. U. Kim, H. O. Park, C. P. Ponting, J. Rappsilber, and R. C. Allshire, “Stc1: a critical link between RNAi and chromatin modification required for heterochromatin integrity,” *Cell*, vol. 140, pp. 666–677, Mar 2010.

[97] M. R. Motamedi, A. Verdel, S. U. Colmenares, S. A. Gerber, S. P. Gygi, and D. Moazed, “Two RNAi complexes, RITS and RDRC, physically interact and localize to noncoding centromeric RNAs,” *Cell*, vol. 119, pp. 789–802, Dec 2004.

[98] G. Jih, N. Iglesias, M. A. Currie, N. V. Bhanu, J. A. Paulo, S. P. Gygi, B. A. Garcia, and D. Moazed, "Unique roles for histone H3K9me states in RNAi and heritable silencing of transcription," *Nature*, vol. 547, pp. 463–467, 07 2017.

[99] M. R. Motamedi, E. J. Hong, X. Li, S. Gerber, C. Denison, S. Gygi, and D. Moazed, "HP1 proteins form distinct complexes and mediate heterochromatic gene silencing by nonoverlapping mechanisms," *Mol. Cell*, vol. 32, pp. 778–790, Dec 2008.

[100] T. Sugiyama, H. P. Cam, R. Sugiyama, K. Noma, M. Zofall, R. Kobayashi, and S. I. Grewal, "SHREC, an effector complex for heterochromatic transcriptional silencing," *Cell*, vol. 128, pp. 491–504, Feb 2007.

[101] J. F. Partridge, K. S. Scott, A. J. Bannister, T. Kouzarides, and R. C. Allshire, "cis-acting DNA from fission yeast centromeres mediates histone H3 methylation and recruitment of silencing factors and cohesin to an ectopic site," *Curr. Biol.*, vol. 12, pp. 1652–1660, Oct 2002.

[102] S. U. Colmenares, S. M. Buker, M. Buhler, M. Dlakic, and D. Moazed, "Coupling of double-stranded RNA synthesis and siRNA generation in fission yeast RNAi," *Mol. Cell*, vol. 27, pp. 449–461, Aug 2007.

[103] R. Jain, N. Iglesias, and D. Moazed, "Distinct Functions of Argonaute Slicer in siRNA Maturation and Heterochromatin Formation," *Mol. Cell*, vol. 63, pp. 191–205, 07 2016.

[104] M. Buhler, W. Haas, S. P. Gygi, and D. Moazed, "RNAi-dependent and -independent RNA turnover mechanisms contribute to heterochromatic gene silencing," *Cell*, vol. 129, pp. 707–721, May 2007.

[105] A. S. Henderson, D. Warburton, and K. C. Atwood, "Location of ribosomal DNA in the human chromosome complement," *Proc. Natl. Acad. Sci. U.S.A.*, vol. 69, pp. 3394–3398, Nov 1972.

[106] S. Hamperl, M. Wittner, V. Babl, J. Perez-Fernandez, H. Tschochner, and J. Griesenbeck, "Chromatin states at ribosomal DNA loci," *Biochim. Biophys. Acta*, vol. 1829, no. 3-4, pp. 405–417, 2013.

[107] K. Merz, M. Hondele, H. Goetze, K. Gmelch, U. Stoeckl, and J. Griesenbeck, "Actively transcribed rRNA genes in S. cerevisiae are organized in a specialized chromatin associated with the high-mobility group protein Hmo1 and are largely devoid of histone molecules," *Genes Dev.*, vol. 22, pp. 1190–1204, May 2008.

[108] P. Tongaonkar, S. L. French, M. L. Oakes, L. Vu, D. A. Schneider, A. L. Beyer, and M. Nomura, "Histones are required for transcription of yeast rRNA genes by RNA polymerase I," *Proc. Natl. Acad. Sci. U.S.A.*, vol. 102, pp. 10129–10134, Jul 2005.

[109] C. P. Prior, C. R. Cantor, E. M. Johnson, V. C. Littau, and V. G. Allfrey, "Reversible changes in nucleosome structure and histone H3 accessibility in transcriptionally active and inactive states of rDNA chromatin," *Cell*, vol. 34, pp. 1033–1042, Oct 1983.

[110] S. L. French, Y. N. Osheim, F. Cioci, M. Nomura, and A. L. Beyer, "In exponentially growing Saccharomyces cerevisiae cells, rRNA synthesis is determined by the summed RNA polymerase I loading rate rather than by the number of active genes," *Mol. Cell. Biol.*, vol. 23, pp. 1558–1568, Mar 2003.

[111] I. Grummt and C. S. Pikaard, "Epigenetic silencing of RNA polymerase I transcription," *Nat. Rev. Mol. Cell Biol.*, vol. 4, pp. 641–649, Aug 2003.

[112] I. Grummt and A. G. Ladurner, "A metabolic throttle regulates the epigenetic state of rDNA," *Cell*, vol. 133, pp. 577–580, May 2008.

[113] G. Thon and J. Verhein-Hansen, "Four chromo-domain proteins of Schizosaccharomyces pombe differentially repress transcription at various chromosomal locations," *Genetics*, vol. 155, pp. 551–568, Jun 2000.

[114] B. A. M. Bouwman and N. Crosetto, "Endogenous DNA Double-Strand Breaks during DNA Transactions: Emerging Insights and Methods for Genome-Wide Profiling," *Genes (Basel)*, vol. 9, Dec 2018.

[115] T. Kobayashi, "Ribosomal RNA gene repeats, their stability and cellular senescence," *Proc. Jpn. Acad., Ser. B, Phys. Biol. Sci.*, vol. 90, no. 4, pp. 119–129, 2014.

[116] R. Srivastava, R. Srivastava, and S. H. Ahn, "The Epigenetic Pathways to Ribosomal DNA Silencing," *Microbiol. Mol. Biol. Rev.*, vol. 80, pp. 545–563, 09 2016.

[117] S. Ide, T. Miyazaki, H. Maki, and T. Kobayashi, "Abundance of ribosomal RNA gene copies maintains genome integrity," *Science*, vol. 327, pp. 693–696, Feb 2010.

[118] T. Ikura and N. Ito, "Requirements for peptidyl-prolyl isomerization activity: a comprehensive mutational analysis of the substrate-binding cavity of FK506-binding protein 12," *Protein Sci.*, vol. 16, pp. 2618–2625, Dec 2007.

[119] A. Ulrich, K. R. Andersen, and T. U. Schwartz, "Exponential megapriming PCR (EMP) cloning–seamless DNA insertion into any target plasmid without sequence constraints," *PLoS ONE*, vol. 7, no. 12, p. e53360, 2012.

[120] S. Bilokapic, M. Strauss, and M. Halic, "Structural rearrangements of the histone octamer translocate DNA," *Nat Commun*, vol. 9, p. 1330, 04 2018.

[121] J. Goecks, A. Nekrutenko, J. Taylor, E. Afgan, G. Ananda, D. Baker, D. Blankenberg, R. Chakrabarty, N. Coraor, J. Goecks, G. Von Kuster, R. Lazarus, K. Li, A. Nekrutenko, J. Taylor, and K. Vincent, "Galaxy: a comprehensive approach for supporting accessible, reproducible, and transparent computational research in the life sciences," *Genome Biol.*, vol. 11, no. 8, p. R86, 2010.

[122] H. Thorvaldsdottir, J. T. Robinson, and J. P. Mesirov, "Integrative Genomics Viewer (IGV): high-performance genomics data visualization and exploration," *Brief. Bioinformatics*, vol. 14, pp. 178–192, Mar 2013.

[123] "ESPript." `http://espript.ibcp.fr/`. Accessed: 2020-04-20.

[124] T. D. Miles, J. Jakovljevic, E. W. Horsey, P. Harnpicharnchai, L. Tang, and J. L. Woolford, "Ytm1, Nop7, and Erb1 form a complex necessary for maturation of yeast 66S preribosomes," *Mol. Cell. Biol.*, vol. 25, pp. 10419–10432, Dec 2005.

[125] M. Hisaoka, K. Nagata, and M. Okuwaki, "Intrinsically disordered regions of nucleophosmin/B23 regulate its RNA binding activity through their inter- and intra-molecular association," *Nucleic Acids Res.*, vol. 42, pp. 1180–1195, Jan 2014.

[126] Y. R. Monneau, H. Soufari, C. J. Nelson, and C. D. Mackereth, "Structure and activity of the peptidyl-prolyl isomerase domain from the histone chaperone Fpr4 toward histone H3 proline isomerization," *J. Biol. Chem.*, vol. 288, pp. 25826–25837, Sep 2013.

[127] R. Mani, R. St Onge, J. t. Hartman, G. Giaever, and F. Roth, "Defining genetic interaction," *Proc Natl Acad Sci U S A.*, vol. 105, pp. 3461–6, Feb 2008.

[128] D. B. Marina, S. Shankar, P. Natarajan, K. J. Finn, and H. D. Madhani, "A conserved ncRNA-binding protein recruits silencing factors to heterochromatin through an RNAi-independent mechanism," *Genes Dev.*, vol. 27, pp. 1851–1856, Sep 2013.

[129] H. O. Iwakawa and Y. Tomari, “The Functions of MicroRNAs: mRNA Decay and Translational Repression,” *Trends Cell Biol.*, vol. 25, pp. 651–665, Nov 2015.

[130] “Roth V. 2006 Doubling Time Computing.” `http://www.doubling-time.com/compute.php`. Accessed: 2020-04-20.

[131] F. Erdel and K. Rippe, “Formation of Chromatin Subcompartments by Phase Separation,” *Biophys. J.*, vol. 114, pp. 2262–2270, 05 2018.

[132] B. A. Gibson, L. K. Doolittle, M. W. G. Schneider, L. E. Jensen, N. Gamarra, L. Henry, D. W. Gerlich, S. Redding, and M. K. Rosen, “Organization of Chromatin by Intrinsic and Regulated Phase Separation,” *Cell*, vol. 179, pp. 470–484, 10 2019.

[133] L. Wang, Y. Gao, X. Zheng, C. Liu, S. Dong, R. Li, G. Zhang, Y. Wei, H. Qu, Y. Li, C. D. Allis, G. Li, H. Li, and P. Li, “Histone Modifications Regulate Chromatin Compartmentalization by Contributing to a Phase Separation Mechanism,” *Mol. Cell*, vol. 76, pp. 646–659, 11 2019.

[134] S. Sanulli, M. J. Trnka, V. Dharmarajan, R. W. Tibble, B. D. Pascal, A. L. Burlingame, P. R. Griffin, J. D. Gross, and G. J. Narlikar, “HP1 reshapes nucleosome core to promote phase separation of heterochromatin,” *Nature*, vol. 575, pp. 390–394, 11 2019.

[135] D. L. J. Lafontaine, J. A. Riback, R. Bascetin, and C. P. Brangwynne, “The nucleolus as a multiphase liquid condensate,” *Nat. Rev. Mol. Cell Biol.*, Sep 2020.

[136] T. Mizuguchi, G. Fudenberg, S. Mehta, J. M. Belton, N. Taneja, H. D. Folco, P. FitzGerald, J. Dekker, L. Mirny, J. Barrowman, and S. Grewal, “Cohesin-dependent globules and heterochromatin shape 3D genome architecture in S. pombe.,” *Nature.*, vol. 516, pp. 432–435, Dec 2014.

[137] L. C. Li, S. T. Okino, H. Zhao, D. Pookot, R. F. Place, S. Urakami, H. Enokida, and R. Dahiya, “Small dsRNAs induce transcriptional activation in human cells,” *Proc. Natl. Acad. Sci. U.S.A.*, vol. 103, pp. 17337–17342, Nov 2006.

[138] B. A. Janowski, S. T. Younger, D. B. Hardy, R. Ram, K. E. Huffman, and D. R. Corey, “Activating gene expression in mammalian cells with promoter-targeted duplex RNAs,” *Nat. Chem. Biol.*, vol. 3, pp. 166–173, Mar 2007.

[139] J. C. Schwartz, S. T. Younger, N. B. Nguyen, D. B. Hardy, B. P. Monia, D. R. Corey, and B. A. Janowski, “Antisense transcripts are targets for activating small RNAs,” *Nat. Struct. Mol. Biol.*, vol. 15, pp. 842–848, Aug 2008.

[140] M. S. Weinberg and K. V. Morris, “Long non-coding RNA targeting and transcriptional de-repression,” *Nucleic Acid Ther*, vol. 23, pp. 9–14, Feb 2013.

[141] X. Zhang, H. Li, J. C. Burnett, and J. J. Rossi, “The role of antisense long noncoding RNA in small RNA-triggered gene activation,” *RNA*, vol. 20, pp. 1916–1928, Dec 2014.

[142] L. C. Li, “Small RNA-Guided Transcriptional Gene Activation (RNAa) in Mammalian Cells,” *Adv. Exp. Med. Biol.*, vol. 983, pp. 1–20, 2017.

[143] V. Portnoy, S. H. Lin, K. H. Li, A. Burlingame, Z. H. Hu, H. Li, and L. C. Li, “saRNA-guided Ago2 targets the RITA complex to promoters to stimulate transcription,” *Cell Res.*, vol. 26, pp. 320–335, Mar 2016.

[144] V. Huang, J. Zheng, Z. Qi, J. Wang, R. F. Place, J. Yu, H. Li, and L. C. Li, “Ago1 Interacts with RNA polymerase II and binds to the promoters of actively transcribed genes in human cancer cells,” *PLoS Genet.*, vol. 9, no. 9, p. e1003821, 2013.

[145] C. Liu, Y. Xin, L. Xu, Z. Cai, Y. Xue, Y. Liu, D. Xie, Y. Liu, and Y. Qi, “Arabidopsis ARGONAUTE 1 Binds Chromatin to Promote Gene Transcription in Response to Hormones and Stresses,” *Dev. Cell*, vol. 44, pp. 348–361, 02 2018.

[146] G. T. Booth, I. X. Wang, V. G. Cheung, and J. T. Lis, “Divergence of a conserved elongation factor and transcription regulation in budding and fission yeast,” *Genome Res.*, vol. 26, pp. 799–811, 06 2016.

Acknowledgments

First of all, I would like to thank Dr. Mario Halic for giving me the chance to carry out my PhD in his group, for his constant supervision and support and his contribution to this work. Moreover, I would like to thank him for the opportunities he gave me, from the possibility to teach and attend conferences, to my experience as visiting student at the St. Jude Children's Research Hospital.

I also would like to thank all the people, who directly contributed to this work. Thank you very much Dr. Silvija Bilokapic Halic, without you this would have been impossible. You taught me a lot, and I am really thankful for this. Thank you Dr. Michael White and Dr. Mylene Ferrolino for your help with microscopy and for the discussions about phase separation.

I also would like to thank all the other members of the Halic group, who helped me throughout my PhD and from whom I learned a lot. In particular thank you very much Dr. Nives Ivic, you have been my first supervisor and a valuable friend. Thank you Dr. Mirela Marasovic, Dr. Manuel Zocco, Dr. Cornelia Brönner, Dr. Paola Pisacane, Guoli Ma, Magdalena Olszak, Segolene Demolin, Dr. Elias Akoury, Dr. Saed Mohebi, Dr. Petr Tesina, Dr. Joseph Bartho and Sigrun Jaklin, for all the nice moments we spent together. And thank you Luca Salvi. It was (is) not easy but despite everything we are still pipetting and (hopefully) moving forward. I also would like to thank the students I had the chance to supervise, Bernadette and Maximilian, because thank to you I learned a lot about myself and who I would like to be.

I would like to thank my TAC committee, Dr. Sigurd Braun and Prof. Dr. Klaus Förstermann, for their support through my PhD. I am very thankful to Prof. Dr. Klaus Förstermann, for being my second evaluator and chair of my examination board, and all the other members of my examination board. I also thank Dr. Stefan Krebs and the LAFUGA facility at the Gene Center Munich, for the assistance with high-throughput sequencing.

Un grazie infinito va ai miei genitori, che mi sono stati accanto sempre durante questi anni. Il vostro supporto è stato fondamentale, senza avrei rischiato di perdermi.

Davide, senza di te non ce l’avrei fatta. Grazie per il tuo supporto incondizionato, per la tua pazienza, per il sorriso che riesci a regalarmi sempre e per le mille altre cose che compongono le nostre giornate.